Friction in deep drawing

R.J.J.M. Sniekers

Friction in deep drawing

FRICTION IN DEEP DRAWING

PROEFSCHRIFT

ter verkrijging van de graad van doctor aan de Technische Universiteit Eindhoven, op gezag van de Rector Magnificus, prof.dr. J.H. van Lint, voor een commissie aangewezen door het College van Dekanen in het openbaar te verdedigen op donderdag 18 april 1996 om 16.00 uur.

door

Roland Johannes Joseph Marie Sniekers

geboren te Maasbracht

Dit proefschrift is goedgekeurd door de promotoren:
prof.ir. J.A.G. Kals
en
prof.dr.ir. M.J.W. Schouten

copromotor: dr.ir. J.A.H. Ramaekers

CIP-DATA KONINKLIJKE BIBLIOTHEEK, DEN HAAG

Sniekers, Roland Johannes Joseph Marie

Friction in deep drawing / Roland Johannes Joseph Marie Sniekers.
[S.1. : s.n.]. I11.
Thesis Technische Universiteit Eindhoven. -With ref. -
With summary in Dutch.
ISBN 90-386-0417-3
Subject headings: friction / metal forming / deep drawing

Druk: Universitaire Drukkerij
TU Eindhoven

Summary

This thesis reports on a study in the field of metal forming. The subject of the study is formed by the frictional phenomena observed in deep drawing.

Deep drawing is a sheet metal working process, in which products or half products are manufactured from a flat sheet of metal. This process is called drawing, because the material is drawn into a die by a punch. Typical products are in the automobile industry (doors, floor panels), consumer electronics (electron guns in televisions, shaver heads) and the packaging industry (food packages) etc. etc.

The deep drawing process involves a great deal of sliding of the sheet material along the tools. Under certain conditions, this sliding will cause friction between the tools and the material. Of course, this friction influences the process. This thesis *Friction in deep drawing* considers some aspects of friction on the deep drawing process. These aspects include the manufacturability of the product, the resulting product appearance, wear and galling. Wear and galling are so-called long-term effects of friction and they reduce the life time of the tools. The main objective of the present study is to improve the prediction of the manufacturability of the product, by improving the description of the friction as present in the process. Product appearance is not investigated. Long-term effects are researched briefly.

In common sheet metal working practice, science is increasingly replacing the art; craftsmanship in tool and process design is less and less available, and is beoing increasingly replaced by preproduction simulations of processes. These preproduction simulations consist of mathematical formulations, analytical or numerical, by which the process is described (by approximation). To obtain a correct simulation, input is necessary for a number of parameters, i.e. geometry, material behaviour and friction.

While geometry and material behaviour are determined by geometrical design and material testing, the input for friction is mostly chosen on the basis of arbitrary reasons. This thesis aims at developing a suitable method for obtaining valid input values for the description of friction.

First, an introduction is given on friction, on deep drawing and the effect of friction on deep drawing. Then, a literature review is made. From this, it appears that many, many parameters influence friction in deep drawing operations. As a result, it will be necessary to use experimental conditions which simulate actual practice as closely as possible. With this in mind, Chapter 3 gives an overview of the most frequently used testing devices for the measurement of friction for sheet metal forming operations.

In Chapter 4, the experimental set-ups used for the current research are evaluated, not only for the technical construction, but also the method of data processing. The test conditions for each of these tests are simulated by means of the Finite Element Method.

The transition from a certain experimentally obtained value into a process simulation still suffers from some incompatibilities between the experiment and the actual process. In

Chapter 5, a method is described in which the friction coefficient is seen as a function of one or more parameters. This then makes it possible to calculate a friction coefficient from experimentally obtained values at each point in the process, as long as all the factors of influence have been included in the experimental set-up. At the end of this part, the values of the friction coefficient obtained from one test, the flat die simulator, are used as input for the simulation of another test, the radial strip drawing simulator. It appears that the calculated friction coefficient for the radial strip drawing simulator is then quite low, compared with the experimentally obtained value for this test.

In the sixth Chapter, the Finite Element Method is used to make an analysis of a simple axisymmetric product. In this analysis, various friction coefficients are used for the various contact conditions, as well as a description of the friction coefficient, obtained from flat die simulator experiments. Here, the friction coefficient is seen as a function of both sliding speed and contact pressure. It appears that the best simulation is achieved when each contact region's own friction coefficient in the deep drawing process is determined by means of a test which is as similar to the process as possible.

Chapter 7 deals with the development and first results of a new test-device. This test-device is aimed at the measurement of the evolution of the friction coefficient because of wear and galling.

The last Chapter discusses and reviews the work. One of the major conclusions is that, in friction testing for deep drawing, the omission of the subsurface deformation probably limits the application of the flat die simulator. It is proposed to extend the flat die simulator, or to alter the radial strip drawing test.

In conclusion, the interaction between the friction and deep drawing is investigated, and methods to achieve valid data for simulation purposes, or rankings for first impressions are proposed.

Samenvatting

Deze studie is verricht op het gebied van metaal omvormen. Onderwerp van de studie zijn de wrijvingsverschijnselen zoals die bij dieptrekken waargenomen kunnen worden.

Dieptrekken is een plaatbewerkingsproces waarbij uitgaande van een plaat, producten worden gemaakt. Het wordt een trek-proces genoemd omdat de stempel het materiaal de matrijs in moet trekken. Typische producten worden gevonden in de automobiel industrie, (deuren, vloerpaneel), consumer electronics, (onderdelen elektronen kanon in een beeldbuis, scheerkopjes Philishave) de verpakkingsindustrie (blik).

Bij het dieptrekken moet het materiaal relatief veel langs het gereedschap glijden. In het contactvlak zal wrijving heersen. Deze wrijving heeft onder bepaalde condities invloed op het dieptrekproces. Deze dissertatie, -Friction in deep drawing-, behandeld een aantal aspecten van wrijving op het dieptrekproces. Deze aspecten zijn onder meer maakbaarheid van het product, uiterlijk van het product, slijtage en aanladen. Slijtage en aanladen zijn zogenaamde lange termijn effecten. Deze effecten bepalen voor een groot deel de levensduur van het gereedschap. Hoofdonderwerp van deze studie is de verbetering van de voorspelling van de maakbaarheid van het product, door verbetring van de beschrijving van de wrijving welke in het proces heerst.

Algemeen geldt in de plaatbewerkingspraktijk dat wetenschap meer en meer de kunst vervangt. Het vakmanschap in proces en gereedschapontwerp is minder beschikbaar, en wordt vervangen door simulatie technieken in de fabricage voorbereiding. Deze simulatie technieken bestaan uit mathematische formuleringen, analytisch of numeriek, waardoor het proces (benaderender wijs) beschreven wordt. Om een accurate simulatie uit te voeren is invoer nodig voor een groot aantal parameters zoals geometrie, materiaalgedrag en wrijving.

Terwijl geometrie en materiaalgedrag worden gekozen op basis van het ontwerp en materiaaltests, worden wrijvingsparameters gekozen meestal op arbitraire gronden gekozen. Deze dissertatie richt zich op het ontwikkelen van passende methoden voor het verkrijgen van invoergegevens welke wrijving beschrijven.

Hiervoor wordt allereerst een inleiding gepresenteerd ten aanzien van wrijving, dieptrekken, en het effect van wrijving op dieptrekken. Vervolgens wordt een literatuurstudie gemaakt. Uit deze literatuurstudie blijkt dat vele parameters van invloed zijn op het wrijving bij dieptrekken. Hieruit kan dan geconcludeerd worden dat testcondities de dieptrekpraktijk zo dicht mogelijk moeten naderen. In hoofdstuk 3 worden de meest gebruikte test apparaten met elkaar vergeleken.

In hoofdstuk 4 worden de meetopstellingen welke in dit onderzoek gebruikt worden besproken, niet alleen de constructie maar ook de dataverwerking. De condities waaronder een test wordt uitgevoerd worden bepaald middels de eindige elementen methode.

De overdracht van een experimenteel bepaalde waarde in een proces simulatie wordt nog beperkt door incompatibiliteit tussen het experiment en het eigenlijk process. In hoofdstuk

5 wordt een methode beschreven waarin de wrijvingscoefficient wordt gezien als een functie van een of meer parameters. Hiermee kan dan met een aantal experimenteel verkregen waarden in de simulatie van het process in elk punt de wrijvingscoefficient berekend worden, mits alle invloedsfactoren in het experimenten schema zijn opgenomen. Ten slotte wordt in dit hoofdstuk op basis van waarden voor de wrijvingscoefficient, verkregen uit experimenten met de flat die simulator, de wrijvingscoefficient als functie van alleen de druk beschreven. Deze functie wordt geimplementeerd in een simulatie van een andere test, de radial strip drawing simulator. Het blijkt dat berekende wrijvingscoefficient laag is vergeleken met de experimenteel verkregen waarde.

In hoofdstuk 6 wordt een analyse gepresenteerd welke is uitgevoerd middels de eindige elementen methode, voor een eenvoudig, axisymmetrisch product. In deze analyse worden verscheidene wrijvingscoefficienten gebruikt voor de verschillende contactgebieden. Ook wordt een beschrijving van de wrijvingscoefficient, welke weer gebaseerd is op flat die simulator experimenten gebruikt. De wrijvingscoefficient wordt beschreven als functie van contactdruk en glijsnelheid. Het blijkt dat het beste resultaat bereikt wordt indien voor elke regio in het proces een aparte wrijvingscoefficient wordt bepaald middels de wrijvingstest die het meest overeenkomt met het desbetreffende deformatieproces.

Hoofdstuk 7 beschrijft de ontwikkeling van en de eerste resultaten verkregen met een nieuwe testopsteling. Deze testopstelling is geschikt voor het meten van de ontwikkeling van de wrijvingscoefficient ten gevolge van slijtage en aanladen.

In het laatste hoofdstuk, wordt het werk besproken. Één van de belangrijkste conclusies is dat het meten van wrijvingscoefficienten voor dieptrekken met de flat die simulator beperkt wordt door de afwezigheid van substraat-deformatie. Bij de aanbevelingen voor verder onderzoek wordt voorgesteld om deze test uit te breiden, of om de radial strip drawing test te modificeren.

Samenvattend, de interactie tussen proces en wrijving is onderzocht, en methoden zijn ontwikkeld waarmee accurate invoer voor simulatie doeleinden kan worden verkregen. Ook kunnen met deze tests rankings worden gemaakt.

Notation

General

τ	Shear stress, induced by friction
μ	Coulomb friction coefficient
p	Normal pressure
p_{bh}	Blank holder pressure
v	Sliding speed
η	Dynamic viscosity
D_0	Initial blank diameter
s_0	Initial blank (sheet) thickness
D	Current blank diameter
s	Current (local) blank (sheet) thickness
β_o	Initial deep drawing ratio
β	Current deep drawing ratio
ρ_D	Radius of curvature of die shoulder
r_D	Radius of die cavity
ρ_P	Radius of curvature of punch nose
r_P	Radius of punch
D_P	Diameter of punch ($D_P = 2\ r_P$)
D_{Hi}	Inner diameter of blank holder
D_{Hu}	Outer diameter of blank holder
$\mathring{u}_o$	Punch velocity
σ_f	Flow stress
σ_{fo}	Constant flow stress
C	Characteristic deformation resistance
n	Strainhardening exponent
ε_0	Pre-strain
E	Youngs modulus
ν	Poisson constant
x, y, z	Cartesian co-ordinates
r, ϕ, z	Cylindrical co-ordinates

Chapter 1

τ_{max}	Maximum shear stress induced by friction
m	Von Mises friction coefficient
f	Wanheim-Bay friction coefficient
α	Proportionality factor
A_r	Real contact area
A_a	Apparent contact area
F_n	Normal force
F_s	Shear force
v_o	Relative sliding speed
F_{fl}	Force to draw in the flange

Chapter 2

η_0	Initial value of the dynamic viscosity
α	Pressure coefficient of Burns equation
β	Temperature coefficient of Burns equation
$\Delta\theta$	Temperature difference
h	Oil film thickness
R_a	Roughness value, central line average

Chapter 3

R	Radius of tooling curvature
$\mathring{u}$	Testing velocity
F_N	Normal force
F_P	Process force
F_{BP}	Back-pull force

Chapter 4

F_{Bp}	Back-pull force
F_P	Process force
F_o	Kistler force, induced by friction
F_C	Generalised normal force
F_ρ	Resulting force by the strip on the radius
F_{Fr}	Generalised friction force
M_{Fr}	Torque induced by friction
b	Width of strip
s	Thickness of strip
R	Radius of curvature of tooling
D	Rocker arm length
θ	Contact angle
u	Displacement
σ_0	Back-pull stress
L_1	Length of leg, back-pull side
L_2	Length of leg, pull side
s	Co-ordinate along tool surface
l_i	Length of ith FEM element along tool
F_N	Normal force
F_{Nm}	Measured normal force
F_{Na}	Actual normal force
μ_T	Friction coefficient between two tooling parts
e	Eccentricity of middle of strip-middle of test platens
L	Sliding length in flat die simulator
d	Distance from sliding surface to point of rotation
Δp	Pressure difference

Chapter 5

γ	Slip
$\Delta\gamma$	Slip increment
γ_{crit}	Critical slip
β	Parameter, physical meaning as critical slip
ϕ	Co-ordinate, describing position on tool surface

Chapter 6

D_{Di}	Inner diameter of die cavity
D_{Du}	Outer diameter of die

Chapter 7

F_2, F_3, F_4	Measured forces in test
L_1, L_2, L_3	Dimensions in test equipment
F_P	Process force
F_{Bp}	Back-pull force
F_{Fr}	Friction force
F_N	Normal force
R	Radius of tool
v_o	Sliding velocity
σ_o	Back-pull stress

Chapter 8

u	Displacement of moving head tensile tester
w	Displacement of test platens flat die simulator
F_N	Normal force
l	Sliding length
ρ	Radius of test platen
R	Smallest radius

Table Of Contents

Chapter 1 General introduction

1.1 Background

The use of numerical modelling is rapidly gaining importance in the pre-production stage of tooling for metal forming operations. With the use of these models (mostly finite element simulations), the time consuming and costly trial and error process can be reduced to a certain extent. To obtain a valid model, the required input should be as accurate as possible. The input basically consists of geometrical quantities of the tools and pre-shape of the workpiece, material behaviour for both the elastic-plastic workpiece and the elastic tools, contact conditions at the interface between tool and workpiece and, finally, some process conditions such as punch velocity.

In the present study, the attention is focused on the deep drawing metal forming process aimed at improving the description of the contact conditions because friction in deep drawing has a major influence on the process, and frictional conditions are relatively difficult to predict. As an illustration, one of the major conclusions at the VDI conference "Simulation of 3-D sheet metal forming processes in automotive industry" [1.1] was that the accuracy of the description of contact conditions is one of the greatest restrictions in obtaining accurate descriptions of deep drawing processes.

1.2 Deep drawing

Within the wide range of metal forming processes, a distinction is made between solid forging and sheet metal forming. The first group contains elements such as forging and extrusion, while the second group consists mainly of bending and deep drawing. This latter process forms the basis of the present study.

Figure 1 shows the principle of the axisymmetrical deep drawing process. Starting with a circular disc (left), placed on a die and clamped by a blank holder, this blank is then forced to flow into the cavity formed by the die and punch (right).

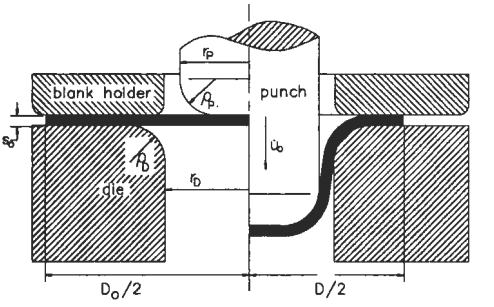

Fig. 1 : Axisymmetric deep drawing

In the process, two active tools can be identified: the punch and the blank holder. The latter plays an important role in the process. When loaded moderately, the material between the die and the blank holder is allowed to flow towards the die cavity. Otherwise, when a higher load is exerted on the blank holder, the material is not allowed to flow from the flange region towards the die cavity, and the process becomes stretching, which is actually seen as a sub-class of the deep drawing process.

The process as described is the simplest form of deep drawing, as a result, the product left in Figure 2 is manufactured. As an example for more complex products, the cross section of a product can be modified in subsequent redrawing steps.

Fig. 2 : Various pre-shapes of a deep drawn product

1.3 Friction

Friction is the resistance to sliding that occurs along the interface between two surfaces of substances. At first, two basic observations of friction were made: Friction force is proportional to the normal force; and friction force is independent of the apparent contact area. These observations were made by Leonardo da Vinci, Amonton and Coulomb [1.2]. In the theory of plasticity, this is usually known as Coulomb friction rule in the form:

$$\tau_{max} \leq \mu p \qquad (1.1)$$

Where τ_{max} represents the maximum frictionally induced shear stress, μ is the Coulomb friction coefficient and p is the normal contact pressure.
Additionally, it has to be mentioned that the frictionally induced stress has a direction opposite to the sliding direction.

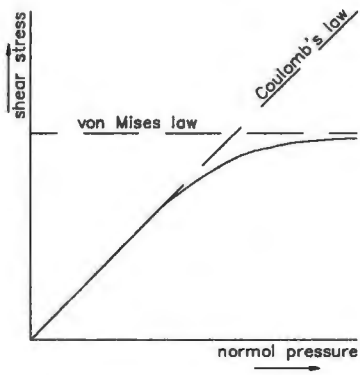

Fig. 3 : Friction stress vs. contact pressure

This linear relationship serves very well for relatively low contact pressures, but at higher contact pressures, it is well known that the linearity is lost, see Figure 3. The slope of the curve diminishes and asymptotically reaches a finite value. This latter behaviour is quite well represented in the von Mises friction rule, which states that there is a ratio between the shear stress of the workpiece material, and the strength of the interface layer in pure shear:

$$\tau_{max} \leq m\frac{\sigma_f}{\sqrt{3}} \qquad (1.2)$$

Again, τ_{max} represents the maximum frictionally induced shear stress, while m is the von Mises or constant friction factor, and σ_f the flow stress of the material.

In general, the following rule applies in forming process analysis techniques: "At low contact pressures, use the Coulomb friction rule; at high contact pressures, use the von Mises rule".

Bay and Wanheim [1.3] combine these two friction rules, and arrive at:

$$\tau = f\alpha\frac{\sigma_f}{\sqrt{3}} \tag{1.3}$$

Where f is a friction factor valued in the range 0 to 1, while α represents the ratio between the real and apparent contact areas, which is a function of the contact pressure and friction factor.

The physical background of this analysis is firstly that asperities start to influence each other at higher normal loads; secondly, that the frictionally induced stress also has an influence on the size of the real contact area. By using this relationship, the actual frictional behaviour is better approximated. However, problems arise in the estimation of the values of f and α.

In simulation packages, the use of the Coulomb friction rule appears to be a de facto standard, but a large amount of research is being done to refine the Coulomb model, i.e. presenting the friction coefficient μ as a function of various quantities.

1.4 Lubrication regime and the nature of friction

The description of the lubrication situation in the following four different regions is widely accepted:

- Dry friction
- Boundary lubrication
- Mixed lubrication
- Hydrodynamic lubrication.

In metal forming practice, it is common to apply lubrication which specifically aims at reducing friction and wear. Figure 4 identifies the latter three different lubrication regimes, and their friction coefficients by means of a "Stribeck curve". The horizontal axis is divided into logarithmic units of the Sommerfeld number:

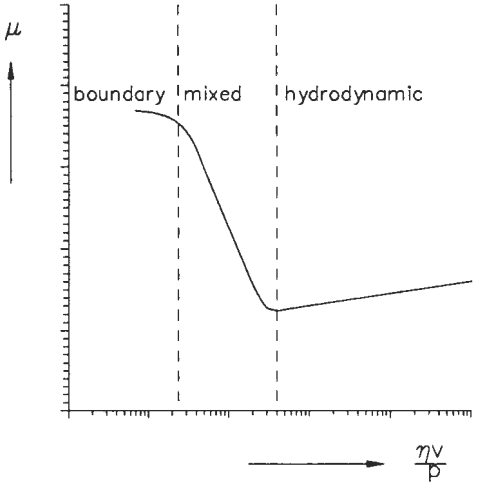

Fig. 4 : The Stribeck curve

$$\frac{\eta v}{p} \tag{1.4}$$

(η is the dynamic viscosity, v the relative speed, and p the contact pressure), and the friction coefficient μ is plotted on the vertical axis.
Each of these lubrication regimes is described in detail in the following paragraphs.

1.4.1 Dry friction

When no additional lubricant is supplied, all the force is guided through from one body to another by contact at the asperities. In principle, this can lead to pure intermetallic contact, but this is only likely to occur in an ultra-high vacuum. Generally, this requirement is not fulfilled during deep drawing. In a normal environment, the surfaces of both the tool and the workpiece absorb gases from the air, resulting in the formation of various oxides and hydroxides. These will significantly reduce the friction. Various models have been suggested in literature to describe qualitively and quantitively what happens when two bodies are brought into contact with each other.

True contact between two bodies in contact is only made at the tips of the asperities. It is widely accepted that the resulting high local stresses lead to plastic deformation of the asperities.

Also, agreement has been reached that this deformation of asperities is caused by adhesion, ploughing, and actual asperity deformation. Although some agreement has been reached about the mechanisms that form the basis of friction, no fully acceptable model is available yet.

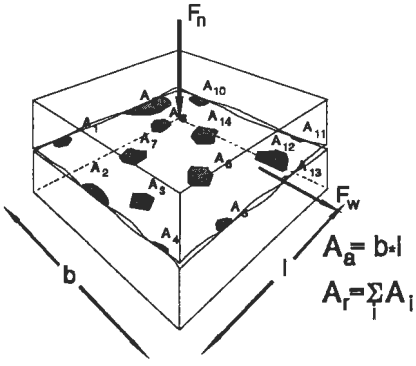

Fig. 5 : Real vs. apparent contact area

1.4.1.1 Cold welding and junctions

The theory, developed independently by Bowden and Tabor [1.4] (mostly referred to), Holm [1.5] and Merchant and Ernst [1.6] is based on the fact that no matter what surface finish is applied, there will always be roughness. As a result, two contacting bodies will only have real contact over a part A_r from the apparent contact area A_a, see Figure 5. Locally, the contact pressure p can reach the hardness value of the softer material, which, roughly approximated, is three times the yield stress σ_f, and the asperities of the metals will deform plastically. Thus, for the normal force F_n, one can derive:

$$F_n = 3\sigma_f A_r \tag{1.5}$$

It is postulated that cold welding occurs for dry, clean surfaces. As a result, junctions are created with a shear strength that might reach the shear strength of the softer material. If a tangential displacement is now applied, the shear force F_s will be:

$$F_s = \frac{\sigma_f}{\sqrt{3}} A_r \tag{1.6}$$

Combination of the previously-mentioned equations yields:

$$\mu = \frac{F_s}{F_n} = \frac{\frac{\sigma_f}{\sqrt{3}} A_r}{3\sigma_f A_r} = \frac{1}{3\sqrt{3}} = 0.19 \tag{1.7}$$

Of course, this is not the entire truth in most cases, which is one reason why various authors have proposed modifications of the welding theory. One important modification is the junction growth theory. Because the effective (von Mises) stress can never exceed the yield stress of a material, it follows that if an asperity is loaded to the yield stress by a normal pressure, and then an additional tangential force (caused by relative tangential sliding, which leads to an additional shear stress) is applied, the normal pressure has to decrease. This must be done by increasing the cross-sectional area of the junction. Also, when the bulk material deforms plastically, the indentation hardness will decrease.

1.4.1.2 Ploughing model

Bowden, Tabor and Moore [1.7] published a model in which a single asperity of the tool is assumed to plough through the softer workpiece material, see Figure 6. However, in the same article, they showed that the calculated friction force is much smaller than the values obtained from experiments.

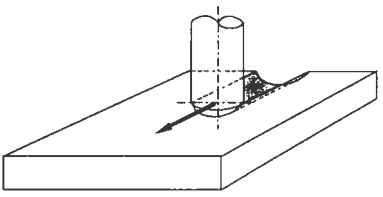

Fig. 6 : Ploughing according to Bowden and Tabor

Starting from the point of view that friction is caused by plastic deformation in the contact area, Dautzenberg [1.8] suggested a friction model in which a variation of the ploughing model is presented. Central in his approach is the view that an asperity pierced into a softer metal will shear out a chip of softer metal. By strain hardening the workpiece material, the workpiece material gains a strength similar to the tool material asperity, after which the workpiece chip and the tool asperity are both deformed plastically. A strong point of this model is that it is able to predict wear phenomena. Good agreement between theory and experimental data is found for pin-on-disc tests.

1.4.1.3 Asperity deformation

A central idea in this approach is that asperities from opposing surfaces deform each other. These deformations can consist of the following (see Figure 7):

- Flattening, whereby the asperities of the softer material are squashed.
- Shearing a chip off the base material.
- Smearing an asperity of the softer material over the base material.

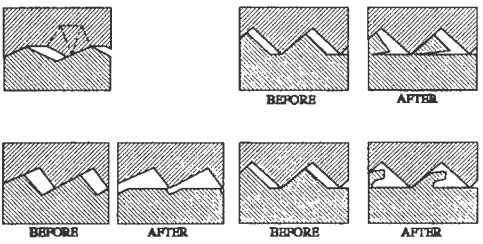

Fig. 7 : Asperity deformation

A mathematical description of this kind of behaviour has been made by Wanheim et al. [1.9, 1.10] with the aid of the slip-line field method, while Avitzur et al. [1.11, 1.12, 1.13, 1.14] used the Upper Bound method. Wilson et al. [1.15, 1.16, 1.17] performed analysis on workpiece conformation to the tooling.

1.4.2 Hydrodynamic lubrication

The two surfaces are fully separated by a lubricant film. Relative tangential displacements lead to shear in the lubricant film only. The resisting force is now caused by this shear in the lubricant. In actual hydrodynamic lubrication, the lubricant is dragged into a lubricant film by the relative velocity of the surfaces and the shape of these surfaces. A good example of this is a bearing.

There is also hydrostatic lubrication, in which the lubricant is pressurised to form a lubricant film.

In the hydrodynamic case, another two sub-cases can be mentioned, the first is elasto-hydrodynamic lubrication, in which the elastic deformation of the workpiece or tooling changes or initiates the gap in which the lubricant is pressurised by the relative motion of the opposing surfaces; the second is plastohydrodynamic lubrication, which basically uses the same idea as the former, except that now only the workpiece deforms plastically.

Figure 8 shows the shearing process. Two flat plates are separated by a lubricant film of thickness h (possibly a function of the x co-ordinate). The lubricant is considered as being an ideal Newtonian fluid. For such a fluid, the shear stress is proportional to the shear rate:

$$\frac{\partial v}{\partial y} \tag{1.8}$$

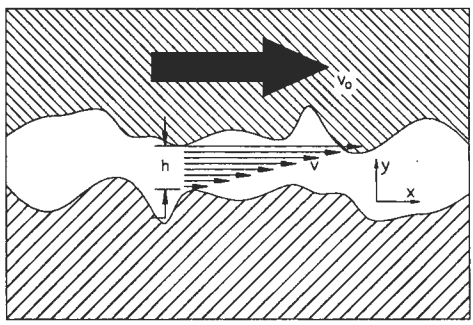

Fig. 8 : Hydrodynamic lubrication

The lower plate is fixed, while the upper plate moves at a constant speed v_o. The constant of proportionality is η, the dynamic viscosity. Thus, for the shear stress τ, it yields:

$$\tau = \eta \frac{\partial v}{\partial y} \tag{1.9}$$

Relating the shear stress to the normal pressure p, we obtain:

$$\mu = \frac{\tau}{p} = \frac{\eta}{p}\frac{\partial v}{\partial y} \tag{1.10}$$

Assuming the velocity to be linear in the y-direction, for sufficiently large h the previous function can be simplified to:

$$\mu = \frac{\tau}{p} = \frac{\eta}{p}\frac{v_o}{h} \tag{1.11}$$

With full hydrodynamic lubrication, the flow of the lubricant can be described using Reynolds equations, see for instance Wilson [1.18].

1.4.3 Boundary lubrication

Here, a very thin film, a few molecules thick, covers the surfaces, see Figure 9. The force is transmitted through this molecular layer. The formation of this layer depends on two different mechanisms. The first is physical adsorption of the lubricant molecules caused by, for instance, polarities in the lubricant. The second depends on chemical reaction of the lubricant with the metal or metal oxides. This latter type gives stronger bonds, which improves the load carrying capacity. The latter mechanism is often called extreme pressure lubrication.

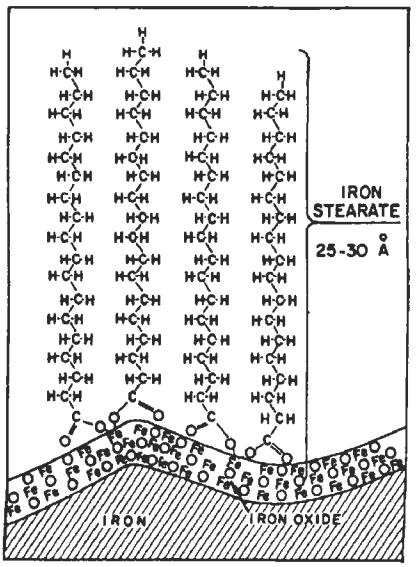

Fig. 9 : Boundary lubrication

While the shear stress in hydrodynamic lubrication is determined by the viscosity and the shear rate, the viscosity now plays only a minor part in the determination of the lubricant properties. These are mainly determined by the other chemical and physical properties of the lubricant and the metals in use.

In the ideal situation, when such boundary layers are formed, and the underlying surfaces subsequently start to slide along each other, molecules of the lubricant are sheared off or pulled off the surfaces, and are then replaced by a new lubricant molecule. With chemical reactions between lubricant and metals etc., this can lead to "chemical wear", because metal atoms are also pulled out of the surface.

If the applied lubricant contains fatty acids and the surfaces to be lubricated are reactive, the acid reacts with the metal or metal oxide, and a metal soap is formed. Metal soap, built by chemical reaction or supplied externally, is effective up to its melting point if the thickness of this layer is only one molecule. This point is also called the transition point. Another important point for boundary lubrication is that the longer the chain length of the molecule, the lower the friction coefficient. With increasing load, the lubricant film becomes thinner and thinner, but as long as there is only one mono-layer of lubricant present, friction remains relatively low.

1.4.4 Mixed lubrication

As the name suggests, this situation is a mix of boundary and hydrodynamic lubrication. At some parts of the surfaces, the load is carried by the boundary layer, while at other parts a full lubricant film is built up.

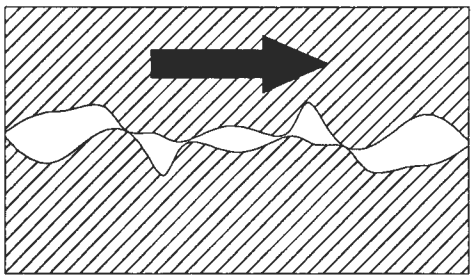

Fig. 10 : Mixed lubrication

In Figure 10, the different lubrication regimes can be identified. The valleys contain some entrapped lubricant; at the peaks, the surfaces are separated by a mono-layer.

1.5 Friction effects in deep drawing

In recent times, metal forming research has paid increasing attention to frictional characteristics. The appearance of friction in forming operations has a major influence on product quality (geometry, surface finish), tool wear, and manufacturability of products. At present, with numerical modelling of deep drawing processes in the design stage of the product gaining importance, an accurate prediction of the frictional behaviour becomes of great interest, see Durham et al. [1.19, 1.20] and Jackson [1.21].

In deep drawing, the material is clamped with a certain blank holder force between blank holder and die. This is necessary because there is a compressive circumferential stress in the flange (and die shoulder). The material will buckle if the circumferential stress reaches a certain critical level. The blank holder affects this buckling in two ways: When a buckle appears, the blank holder force will concentrate on the buckle as soon as it starts to form. Furthermore, before any buckle arises, the blank holder already has a buckle preventing effect, caused by the frictionally induced shear stress, which enlarges the radial stress. As a result, the tangential stress has to decrease because the effective (von Mises) stress can never exceed the yield stress, see Fukui [1.22].

As known from research by von Finckenstein [1.23], the blank holder exhibits its force only at the outer third part of the remaining flange because of the thickening behaviour of the flange material, which is most pronounced at the outer rim.

Thus, in conclusion: part of the flange is not directly influenced by the blank holder. This inner part of the flange is only affected by the increase in radial stress in the outer part caused by the frictional shear stresses induced by the blank holder. Therefore, a certain amount of friction stress might be necessary to conserve the buckle preventive action of the blank holder.

In the die shoulder region, contact pressures between die and workpiece material can achieve high values, so even a low friction coefficient will lead to relatively high shear

stresses. The impact of the contact pressure can easily be seen on a simple product drawn halfway: the material appears to be shiny at the point where the die curvature starts.

At the punch nose, however, material flow should be suppressed, so the friction coefficient should be as high as possible. As a result, the material flow is suppressed, and the friction stresses help to transfer the punch force to the material.

The effect of friction can be more clearly observed with large deep drawings, i.e. a large D_P/s_0 ratio. As a first estimation, according to Ramaekers [1.24], the force required to draw the flange inwards is:

$$F_{fl} = 1.1\sqrt{\frac{\beta_0}{\beta}}\ln\beta + \mu\frac{p_{bh}}{\sigma_{fo}}\frac{D_P}{s_0}(\beta-1) \tag{1.12}$$

Where F_{fl} denotes the dimensionless force required to draw the flange inward. β_0 and β represent the initial and momentary drawing ratio, p_{bh} is the blank holder pressure, σ_{fo} the constant flow stress, D_P the punch diameter, and s_0 the initial sheet thickness.

Two parts can be recognised in the formula. One describes the deformation part of the force, the other describes a friction induced part. In the frictionally induced term, the "size" of the product turns out to be a kind of multiplier of the friction coefficient.

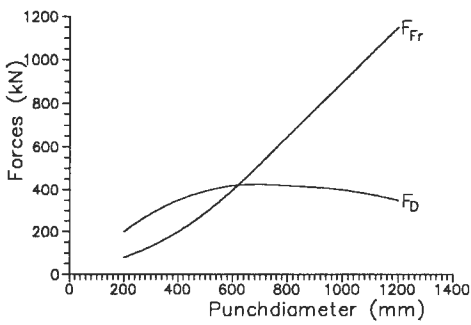

Fig. 11 : Friction and deformation forces in deep drawing, after Doege [1.25]

Similar work has been carried out by Doege and Hesberg [1.25]. Figure 11 shows that the power consumption resulting from friction can be a multiple of the value of the deformation power. The increasing power consumption caused by friction for large products leads to decreasing maximum deep drawing ratios.

An increase in the value of the friction coefficient can lead to a dramatic increase of the necessary force, which subsequently can lead to strain localisation, and failure of the deep drawing operation.

1.6 Discussion, scope of the work

The original aim of the "Development and experimental verification of friction models" PhD project was the development of a parameter-lean friction model, suitable for implementation in analyses in the field of metal forming processes. By parameter-lean, the author means that as few parameters as possible are introduced into the formulation.

The entire field of metal forming is far too large to be covered in one single PhD project, which is why the current research is limited to one process. As has already become clear, the process that was chosen was the deep drawing process, which can be seen as a representative of the work of the sheet metal forming group. The methods and techniques presented will also be applicable to similar processes (for instance, collar drawing).

Even when the limitation towards deep drawing is made, various types of research can be made, from studying micro-mechanics at the tips of asperities to the characterisation of frictional behaviour as a function of a large number of variables. In this study, an intermediate level has been chosen, aiming at directly improving the predictability of deep drawing operations. This means that this project will work out tools and methods to measure friction, its development in time for reasons of wear and galling, and methods for improving the description of friction in simulation techniques.

For practical reasons, e.g. in the pre-production engineering phase, it is important to have an estimation of the friction coefficient for calculation and simulation purposes. For solving production problems, it will also be necessary to rank different materials and lubricants etc., considering their frictional behaviour.

However, problems arise when the frictional behaviour is characterised by one or more "constants". In each of these constants, compound effects of the surface chemistry, surface morphology, mechanical behaviour, and so on, are included.

The scope of the work is now formed by: The study and determination of the influencing factors on friction in deep drawing, and means to measure "friction" for sufficiently described circumstances. This is done to achieve valid values of friction coefficients for use in analysing techniques.

References

1.1 FE-simulation of 3-D sheet metal forming processes in automotive industry.
VDI Berichte 894,
VDI Verlag GmbH, Dusseldorf 1991

1.2 Coulomb, M.
Sur une application des règles de maximis & minimis à quelques problèmes de statique, relatifs à l'architecture.
Mémoires Mathematique et Physique
7 (1774) p.343-382

1.3 Wanheim, T., Bay, N.
A model for friction in metal forming processes.
Annals of the CIRP, 27 (1978) 1

1.4 Bowden, F.P., Tabor, D.
The theory of metallic friction and the role of shearing and ploughing.
Bull. 145, Comm. of Australia, Council Sci. and Ind. Res. 1942

1.5 Holm, R.
Über die auf die wirklichen Berührungsfläche bezogene Reibungskraft.
Veröff., Siemenswerk, 17 (1938) 38

1.6 Ernst, H., Merchant, M.E.
Surface friction between metals - a basic factor in the metal cutting process.
Proc. Special Summer Conf. on Friction and surface finish, M.I.T., 76 (1940)

1.7 Bowden, F.P., Moore, A.J., Tabor, D.
The ploughing and adhesion of sliding metals.
Journal of Applied Physics 11 (1943) 80

1.8 Dautzenberg, J.H.
Reibung und Gleitverschleiss bei Trockenreibung.
PhD. dissertation, Eindhoven University of Technology, 1977

1.9 Abilgaard, T., Wanheim, T.
An investigation into the mechanisms of abrasive wear and processing of metals.
Proc. 2nd Cairo Univ., Mech. Design and Prod. Conf., Cairo, (1982), p.521-529.

1.10 Abilgaard, T., Wanheim, T.
A mechanism for metallic friction.
ICPE Conf., Tokyo, Aug. 1980

1.11 Avitzur, B.
Effect of surface irregularities, subsurface layers, pressure, lubrication and sliding speed on friction resistance to sliding in metals.
Key Engineering Materials, 33 (1989), p.1-16

1.12 Avitzur, B., Zhu, Y.D.
A friction model based on the upper bound approach to the ridge and sublayer deformations update.
Proc. 13th NAMRC, Berkeley, CA, May 19-22, 1985, SME, Dearborn, MI, USA, p.103-109

1.13 Avitzur, B., Huang, C.K., Zhu, Y.D.
A friction model based on the upper bound approach to the ridge and sublayer deformations update.
Wear, 95 (1984), p.59-77

1.14 Avitzur, B., Nakamura, Y.
Analytical determination of friction resistance as a function of normal load and geometry of surface irregularities.
Wear, 107 (1986), p.367-383.

1.15 Wilson, W.R.D.
Friction models for metal forming in the boundary lubrication regime.
Trans. ASME
Journal of Engineering Materials and Technology, 113 (1991) 1, p.60-68

1.16 Wilson, W.R.D., Sheu, S.
Real area of contact and boundary friction in metal forming.
International Journal of Mechanical Sciences,
30 (1988) 7, p.475-488

1.17 Sheu, S., Wilson, W.R.D.
Flattening of workpiece surface asperities in metal-forming.
Proc. North American Metal Working Research Conf. XI 1983, p.172-178

1.18 Wilson, W.R.D.
Friction and lubrication in bulk metal forming processes.
Journal of Applied Metalworking,
6 (1979), p.1-19

1.19 Durham, D.R., Turkovich, B.F. von
Modelling the frictional boundary condition in material deformation.
41 General assembly of CIRP
Palo Alto, CA, USA, 18-24 aug. 1991
Annals of Manufacturing Technology CIRP,
40 (1991) 1, p.235-238

1.20 Durham, D.R., Assempoor, A.
Comparison of friction models in material forming processes.
Winter annual meeting of the ASME
Dallas, TX, USA 25-30 Nov. (1990)
Computer modelling and simulation of manufacturing processes.
ASME, Materials Division
MD V 20, New York, NY, USA, p.293-301

1.21 Jackson, J.E., Gangjee, T., Haque, I.
Lubricant modeling and its effect on simulation of material forming.
Trans. ASME
Journal of Engineering Materials and Technology, 111 (1989) 1, p.74-80

1.22 Fukui, S., Yoshida, K.
Measurement of mean friction coefficient in sheet drawing.
Int. Journal of Machine Tool Design,
2 (1962), p.19-26

1.23 Finckenstein, E. von, Lawrenz, K.J.
Beschichtete bleche umformen.
Bänder Bleche Rohre, 19 (1978) 3, p.130-136

1.24 Ramaekers, J.A.H., Houtackers, L.J.A.,
Peeters, P.B.G.
Plastisch bewerken van metalen. Procesbeheersing in de onderdelen fabricage.
Omtec Stichting voor Mechanische
Omvormtechnologie 1987

1.25 Doege, E., Hesberg, U.
Eigenschaften und Umformverhalten oberflachen-veredelten feinblechhes beim tiefziehen.
Blech Rohre Profile, 39 (1992) 1

Chapter 2 Literature review

2.1 Introduction

The friction characteristics in sheet metal forming are influenced by many parameters. The aim of this chapter is to summarise and weigh the findings reported in literature. By means of such an overview, it will become clearer how experiments have to be carried out to achieve valid friction coefficients. Secondly, such an overview can help in solving practical production problems, as a checklist when determining the source of the problem, and in some cases as a guideline for taking counteractive measures.

While surveying the literature, one has to find a way to summarise the items of interest. The following subdivision appeared to the author to be a valid means of presenting the parameters that influence the friction coefficient:

- Stribeck curve-related quantities
  - pressure
  - sliding speed
  - viscosity
  - temperature
- Morphology of the opposing surfaces
  - function
  - description
  - evolution of roughness
- Materials and lubricant effects in the contact zone
  - tool material
  - workpiece material
  - coatings
  - lubricant
- Others
  - tool geometry
  - blank holder

It must be remarked that the uniformity of the friction coefficient during various production batches in the press shop is also of major importance. Die sets are finally tuned to a given frictional condition at the beginning of the first production batch. In the following production batches, the process has to be robust, so that it is not sensitive to (small) deviations in the input. The quest therefore is to select combinations of parameters that lead to a friction coefficient which is as stable as possible.

2.2 Stribeck curve-related quantities

2.2.1 Introduction

In Paragraph 1.3, the basic idea of the Stribeck curve has been explained. Generally, it has been recognised that most deep drawing operations are performed in the boundary and the mixed lubrication regime. In Figure 12, the window shows the range in which deep

drawing is performed. As can be seen, the friction coefficient in the boundary lubrication regime is independent of the Sommerfeld number, while a dependence can be observed in the mixed lubrication regime.

As a rule of thumb, the following subdivision is made: When the film thickness is approximately three times the combined roughness of tool and workpiece, hydrodynamic lubrication governs. Below this value, mixed lubrication is present, and, finally, at values towards zero, boundary lubrication and even intermetallic contact take place, see also Paragraph 2.2.5, Figure 13.

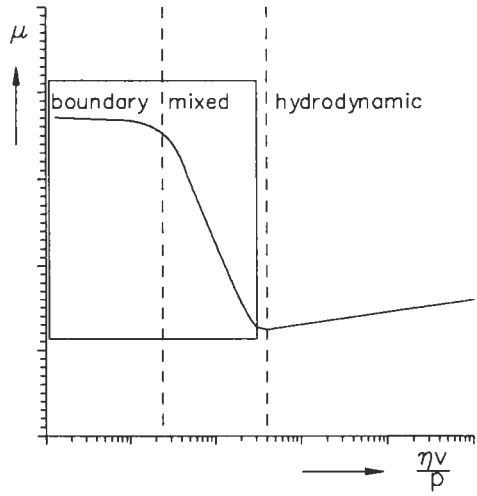

Fig. 12: Deep drawing window in the Stribeck curve

Efforts to estimate the contributions of the various regimes in a given situation have been made by Hsu [2.1]. For the hydrodynamic part, as present in the flange, an analytical relation can be deduced. With mixed or boundary lubrication, the analysis becomes increasingly empirical.

The following sections highlight quantities which affect the Sommerfeld number.

2.2.2 Velocity

The (sliding) velocity is one of the components of the Sommerfeld number, and thus one of the determining factors in creating a certain lubrication regime. The sliding velocity in deep drawing is largely based on the punch velocity. This especially holds for the material sliding over the die shoulder and between the blank holder and die. Here, the sliding speed is approximately of the same order as the punch velocity.

At the punch nose, the situation is different. Whether sliding occurs or not is determined by the force necessary to draw in the flange, the strength of the workpiece material on the punch nose, and the friction coefficient at the punch nose, as shown by the work of Bongaerts [2.2]. If sliding is present, the sliding speed is dependent on the punch velocity, but generally in magnitude at least one order smaller. Besides its magnitude, the variation of the punch force is important, as a function of the punch stroke.

Furthermore, since metal forming is an irreversible process, all the deformation energy eventually transforms to heat. If a deep drawing process is now performed at higher speed, this means that the same amount of heat is generated in a shorter time. As a result, the temperature of the workpiece has to increase. The effect of this on the viscosity of the oil is described in Paragraph 2.2.4. Following this, as a result of an increase of a higher

punch velocity, the effective strain rate will increase. With this increase of the effective strain rate, Wilson et al. [2.3, 2.4] state that the indentation resistance of the workpiece material decreases, which results in increasing friction.

2.2.3 Pressure

In general, three different contact regions can be identified in normal cupping. The first is the zone where the sheet material is clamped between the die and the blank holder. For a rigid blank holder, the contact region is limited to the outer third of the flange. For a flexible blank holder, the contact pressure is distributed over a larger area. More details are given in Paragraph 2.5.1.4.

A second region where contact pressure between tooling and workpiece is present is in the vicinity of the die shoulder. Globally speaking, the punch force is largely counteracted here. Additionally, the material has to be bent/unbent while entering/leaving the die shoulder. This leads to peaks in the contact pressure distribution.

A third region can be identified at the punch nose. Here, similar effects are present as at the die shoulder region.

In general, the contact pressure can only be influenced by controlling the blank holder force, but the largest share of the contact pressure distribution is determined by the geometry of the process and the material behaviour of the sheet material.

2.2.4 Viscosity

In the Sommerfeld number, a lubricant is characterised by the viscosity only, which is a property that mainly influences the hydrodynamic (hydrostatic) lubrication of the frictional conditions. The boundary lubrication part is, to a large extent, based on the properties of the lubricant to form a chemical or physical bond with the workpiece and tool material. When a lubricant does not have this characteristic, circumstances which fulfill the requirements for hydrodynamic lubrication will immediately lead to asperity peaks breaking through the lubricant film, leading to metallic contact. This will at least lead to an increased friction coefficient, which might be followed by product failure or even tooling breakdown.

The influence of temperature and pressure on viscosity can be given by means of a VPT (viscosity, pressure, temperature) diagram, see for instance Siegert and Thomas [2.5]. The so-called Burns equation for pressure and temperature dependence of the viscosity clearly shows that straight oils have decreasing viscosity η at higher temperatures:

$$\eta = \eta_o e^{\alpha p - \beta \Delta\theta} \tag{2.1}$$

In this equation, η_o is the reference viscosity, determined at the reference temperature. $\Delta\theta$ gives the temperature difference. p is the pressure, while α and β give the pressure and temperature dependency coefficients, respectively.

The straightforward temperature dependence of viscosity is only valid if there are no chemically active compounds in the lubricant. Heating accelerates chemical reactions between these additives and the sliding surfaces, causing the lubricant to adhere, see Kumpulainen [2.6, 2.7]. Eventually it is possible that friction first rises, reaches a maximum, and then decreases by this effect. This latter temperature effect has already been mentioned by Lenard [2.8] but it is not clear in his work if this is solely due to lubrication. On the other hand, reactivity in the boundary lubrication regime is improved when the temperature increases. However, when the temperature is high, boundary layers can break down, resulting in loss of lubrication functionality, resulting first in decreasing friction and then by increasing friction.

2.2.5 Film thickness

In the classical view on lubrication regimes, ideas have often been formed on the basis of a sliding bearing. With such a bearing, film thickness h builds up with increasing speed of rotation, see Figure 13. One can identify some reservoir from which lubricant is dragged into the deformation zone.

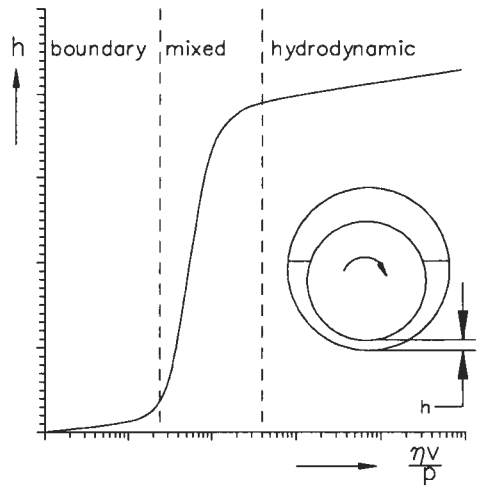

Fig. 13: Film thickness in case of sliding bearing

In deep drawing, however, film thickness depends on the amount of lubricant supplied on the sheet at the start. When the flange is clamped between blank holder and die, the oil flows sideways, partly through the micro-channels in the roughness structure, partly as film.

When the actual deep drawing subsequently starts, oil partly becomes trapped between sheet and die, and will thus supply lubrication in drawing the sheet over the die radius.

2.3 Morphology of the contacting surfaces, roughness

2.3.1 Introduction

As already stated, lubrication in deep drawing is mainly of the mixed type. The balance between boundary and hydrodynamic lubrication is largely based on the roughness of the opposing surfaces.

In general, a larger roughness shifts the Stribeck curve to the right. For instance, Emmens [2.9] found that the transition point from boundary lubrication to mixed lubrication will be reached sooner with low roughness.

At spots where contact is present, a situation as shown in Figure 14 is likely to occur.

The smooth upper part represents the tooling, the lower part represents the rougher workpiece. The tool is designed to be smoother than the workpiece material, but wear and build-up during its life time can change this.

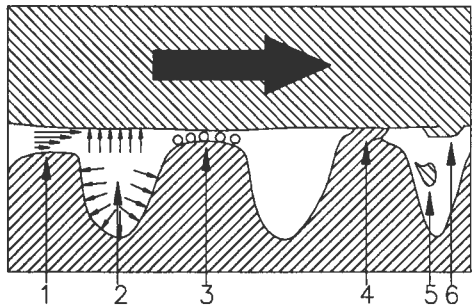

Fig. 14: Micro geometrical conditions

At the moderately high peaks (1), hydrodynamic lubrication separates the two surfaces. The higher peaks suffer from too heavy a load and must be separated from the tool by means of a boundary lubrication layer (3). Hydrostatic lubrication exists in a valley (2). At the highest peaks, even the boundary layer may fail, leading to intermetallic contact and cold welding (4). By continued relative movement, this contact has to deform too much, resulting in shearing off. The particle may remain on one of the surfaces (6), or become entrapped in a roughness valley (5).

2.3.2 Description

Roughness is almost always characterised by the R_a value, but it is generally accepted that this is not sufficient. For instance, profiles with the same R_a value can have different frictional behaviours because the shape of the profiles can be completely different. Emmens [2.10] notes that when surfaces have a comparable type of roughness, one parameter will be sufficient to describe the roughness and rank the surfaces for their frictional behaviour. Bello et al. [2.11] clearly demonstrate that different lubricants react differently with larger roughness. Even when the trend of the friction coefficient with increasing roughness is apparent, large scatter is observed. Some authors have proposed parameters to describe roughness, but no generally accepted standard has been reached. In general, the proposed parameters are aimed at evaluating the bearing possibilities of surfaces, because quite large agreement has been reached that a roughness with plateau-like peaks and adequately large profile valleys is regarded as giving the best frictional behaviour. Besides this bearing possibility of surfaces, the peak density is another parameter which is increasingly seen as important.

Furthermore, according to Overby [2.12] and Muller [2.13] roughness is generally oriented. As has been shown by Kumpulainen [2.7] with a strip drawing test, this orientation of roughness influences the friction coefficient. Patir and Cheng [2.14] analyse the effect of roughness on lubricant flow. They prove that the orientation of the roughness affects the lubricant flow, especially at low film thickness to roughness ratio. These observations lead to the conclusion that 3-dimensional descriptions of surfaces are necessary to identify a surface.

2.3.3 Feeding lubricant into the contact zone

According to Atala and Rowe [2.15] a matt surface retains lubricant better than a smooth one, and is less likely to suffer from lubricant breakdown. If both tooling and blank are smooth, the lubricant cannot be brought into the contact zone, leading to a high friction coefficient. If both are too rough, too many asperity peaks rise above the lubricant barrier and interact with each other, again creating a high coefficient of friction. An ideal situation according to Nine et al. [2.16] could be formed with one rough surface for carrying the lubricant and one smooth surface, so that the asperity peaks of the other surfaces can slide easily.

The acceptance of the idea that roughness with plateau-like peaks and adequately large valleys gives the best frictional behaviour for the sheet is based on the idea that the plateau-like peaks are less likely to break through the lubricant, and that the valleys of the roughness profile act as micro-pockets. For the subsequent process, various possibilities can be mentioned, after Kudo [2.17]:

- Firstly, where part of the load is supported by the hydrostatic pressure in the lubricant, the lubricant contacts the tool statically, resulting in wetting of the tool (hydrostatic boundary lubrication).
- Secondly, when these micro-pockets are compressed, the lubricant will be forced out, leading to a thin hydrodynamic film (hydrostatic micro-hydrodynamic lubrication), or supplying lubricant for the formation of a boundary layer (boundary plasto-hydrodynamic lubrication).

Whichever is the predominant mechanism, is determined by the lubricant in use. For the above mentioned, a remark has to be made that the valleys are connected together as channels, so that lubricant can also flow sideways through the channels. Montfort et al. [2.18] came to the conclusion that it is desirable to create roughness patterns with valleys that are not interconnected, to suppress the sideways flow.

2.3.4 Workpiece

Various mill roll surface treatments such as shot-blast, lasertex, Defourny [2.19] electrical discharge texture, Snaith [2.20] or electron beam texture are applied to give the sheet certain roughness characteristics. A review is given in Pankert [2.21]. Hilsen and Bernick [2.22] have noted that the roll surface smoothens as a result of wear, giving a smoother sheet surface.

For roughness changes during the process, Wilson [2.23] and Gosh et al. [2.24] state that the best performance is achieved with sufficient profile depth. Kumpulainen [2.7] recommends an arithmetical average roughness of R_a = 0.7 to 1.5 μm, with a peak density of 4 - 6 peaks/mm for the prevention of galling. Various authors have suggested that a roughness of about 1 μm leads to acceptable deep drawing results.

As indicated by others, Nine [2.25], Schey [2.26] and Anderson [2.27] there is an optimum condition of roughness in a certain situation. A certain bandwidth is present

around this optimum, in which the process will also perform. Critical processes will have narrow bandwidths.

These observations can be seen from the following perspective. A certain roughness will be necessary to hold the lubricant, which will lead to a minimum value for the roughness. Then, with high roughness, asperity peaks contact each other through the lubricant layer. This latter observation will lead to a maximum value for the roughness. A robust process will have a low sensitivity towards roughness changes, which leads to the conclusion that the range from the minimum towards the maximum value for the roughness should be relatively large.

Material transfer is a disturbance in the above mentioned; particles of the generally softer workpiece are transferred to the tools. Their effect on tool roughness can be two-fold. For example, particles can fill flaws on the tools, or concentrate at a certain spot.

Bragard et al. [2.28] showed that if the micro-hardness of the plateaus of the roughness profile is lower than that of the valleys, galling is likely to occur, while when this is the opposite, the sheet behaves well.

2.3.4.1 Roughening

Roughening in deep drawing occurs in the regions of the process where the material is not in contact with the tools, the socalled free surfaces. These regions are: the large (inner or central) part of the flange, the material under the flat part of the punch, and the material in the wall of the product.

In metal forming, a metal is roughened, and newly exposed, by bulk plastic deformation, which is a tribological feature experienced only in metal forming. Both Kienzle [2.29] and Osakada [2.30] revealed that the surface roughness of plastically deformed metal is in proportion to the equivalent strain, and the proportion modulus is in proportion to the grain size and increases as the number of slip systems in the crystal structure decreases. Kobayashi [2.31] revealed that such surface roughening depends on the strain paths, and the strain at which rapid roughening starts is similar to the limit strain which governs the forming limit of metal sheet. Wollrab et al. [2.32] concluded that the type of deformation is important for the amount of roughening. Kals and Dautzenberg [2.33] relate roughening to the stress state. Furthermore, the roughening is anisotropic to a lesser or greater extent. Streidl et al. [2.34] notify that the initial roughness is not sufficient to describe a sheet in a forming operation.

The type of deformation also has an important influence on the friction coefficient. Keeler finds that the results of a punch radius test are higher than those found with a draw-bead simulator [2.35]. Similarly, the results of a stretch forming test are found to be much higher than the results found in a radial drawing test Kaftanoglu [2.36]. Ghosh [2.37] and Duncan et al [2.38] state that this is caused by the area enlargement in stretch forming and the turning out of grains in this process by which new asperities are created each time. Guangnan et al. [2.39] have carried out an interesting research considering the effect of

effective strain and strain state in stretch forming of steel sheet. Three different surface damaging mechanisms are found:

- void nucleation and growth,
- slip stages and,
- surface grains rotation.

The latter has been found to be the most important.

Kaga and Yagi [2.40] found that the change in surface texture begins with translations of groups of grains as a whole, followed by rotational displacement of individual grains within each group. The roughening depends on the effective strain and the grain size.

Above a certain effective strain, the relationship between roughness and effective strain is found to be linear. In a tensile test, roughness increase is greater in the direction of the minor strain than in the direction of the major strain. If deformation is suppressed in one direction in the plane of the sheet and perpendicular to the tensile stress (plane strain), then the ratio of roughening is smaller than one. In equi-axial stretch, the ratio is approximately equal to one, Sengupta [2.39]. Sengupta et al. [2.24] found that a single step increase of the friction force occurred immediately after the yield point was reached in a tensile test with a simultaneously coupled flat die simulator. Roughening was found to increase with increasing strain. It was also found that the contour of the roughness became sharper and the peaks had a smaller radius.

Considering the grain size of the material, Kasuga et al. [2.41] have reported that friction is higher in the case of a material with a large grain size in simultaneous sliding and deforming than if the grain size is small. Furthermore, the grain size influences the roughening during the process, Wilson [2.23]. A larger grain size will lead to greater roughening.

Klimczak et al. [2.42] analysed roughness changes in sheet material by means of power density. They identified three different wavelengths that are of importance. The shortest wavelength is of the order of the grain size. The other two are approximately three and nine times larger. The largest one is connected with local necking, the remaining one is of the order of the mean spacing of profile irregularities. The largest wavelength has the largest influence on the roughening, especially after the beginning of local instabilities.

2.3.4.2 Flattening

Flattening in deep drawing occurs where the material is in contact with the tools, as at the outer rim of the flange, in the vicinity of the die shoulder, and the punch nose.

The asperities start to deform as a result of the contact pressure. Doege [2.43] arrives at the following: As long as the contact pressure is below the magnitude of the yield stress of the surface material, whether this is a coating or the raw material, only flattening of the asperities occurs. This results in decreasing roughness. If the contact pressure reaches the order of the yield stress, then macroscopic plastic deformation starts. In this, the valleys between the asperities are filled. A further increase in contact pressure will result in failure

of the coating, and roughness rises. If the surface, however, is raw material, this failure will not happen, and roughness remains at the same level.

Wilson [2.4] deduced that flattening of asperities increases monotonically with strain, in an idealised upper bound analysis, combined with similar experiments. Wilson and Sheu [2.44], Fog [2.45] and Avitzur and Nakamura [2.46] showed that the deformation resistance of asperities decreases when bulk deformation is present.

Ike and Makinouchi [2.47] analysed the deformation of asperities of the workpiece in contact with a flat die. They found that the state of stress in the underlying bulk material affects the asperity deformation. If the underlying bulk material is in compression, asperities bulge into the non-contacting valleys. If the bulk material is in tension, asperity material flows sideways with the bulk material. Also, with increasing hydrostatic pressure, the ratio of real contact area to apparent contact area increases.

Wang et al. [2.48] analysed the effect of filling valleys. They showed that large valleys are initially easily filled to a certain extent, but complete filling of small cavities is not likely to occur. They mention two different mechanisms in filling: centripetal flow and lifting up. The first is stated to be the most important.

2.3.5 Tooling

Quite large agreement has been reached considering the fact that the tooling should be as smooth as possible to achieve low friction. In general, increasing tool roughness increases friction, particularly when tool roughness equals workpiece roughness. However, a few opposing measurements exist; Nine [2.49] reports that equal roughness of tool and sheet gives the best lubrication results. According to experiments carried out by Lindsay et al. [2.25] using chromium plated draw-beads with varying degrees of roughness gives an optimum roughness. This conclusion can also be drawn from the work by Dalton and Schey [2.26]. They state that the asperities peak through the lubricant film at higher roughnesses, while the valleys of the tool surfaces do not serve as micropockets at low roughness values. This latter effect seems dubious while the tool valleys are not compressed, which will be necessary for forcing out lubricant. At low roughness, metal pick-up probably leads to immediate roughening of the tool, which might lead to increased friction.

2.4 Tool and workpiece material, lubricant, and interactions in the contact region

2.4.1 Introduction

A large amount of the frictional conditions to be observed is related to contributions which are made by material specific properties, for instance, crystal structure etc. Important properties of material combinations are the physical and chemical interactions which take place at their interface spots: workpiece & lubricant, tool & lubricant, and tool & workpiece.

2.4.2 Tool material

Die prototyping is used in the development of many sheet metal forming operations. This prototype is usually made from a relatively soft material. Because a different material results in a different friction coefficient, erroneous final equipment might be realised from this prototyping. This is noted by Brazier and Thompson [2.50] especially in cases when zinc coatings are applied on the workpiece material. In a following article [2.51], the same authors presented experimental evidence that a softer tool (kirksite, zinc-based alloy) produces lower friction coefficients than a harder one (D2 tool steel) for different zinc-based coatings except galvanealed steel sheet. The latter discrepancy could be eliminated by the use of a more effective lubricant. The most important conclusion that can be drawn from their work is that soft tool trials on zinc-coated sheet steels are likely to produce erroneous results when extrapolated to hard tool conditions unless frictional differences and speed effects are corrected by judicious lubricant selection. They advise draw-bead simulation tests when selecting lubricants for soft tool trials on a coated product [2.51].

In contrast to the remark made by Brazier and Thompson that a softer tool will result in lower friction, Meuleman and Zoldak [2.52] mention that a softer tool of a zinc-based alloy combined with the same type of coatings produces higher friction. Meuleman and Zoldak [2.52] mention that, to simulate the frictional behaviour more accurately, it is better to replace zinc-based sheets with uncoated bare sheets in the soft tooling stage. Note that they used a zinc-based soft tool material. Keeler et al. [2.16] state that two different features are desirable in prototyping with soft tooling. The first is having a lubricant performing identically on both hard and soft tools. The second is to have a lubricant A which, combined with a soft tool, acts as lubricant B does with a hard tool. Gross [2.53] gives an overview of different zinc alloys in use for soft tooling.

Montfort et al. [2.54] divide the tool materials (or coatings) into three classes, based on the mutual solubility between die and sheet: High affinity, low affinity and inert. The lower the mutual solubility, the lower the friction appears to be. This is a necessary but not sufficient condition for tool material selection.

2.4.3 Tools coating and surface treatment

The main purpose of a coating or surface treatment is to protect the underlying material in one way or another. For metal forming tools, coatings are used to reduce friction, wear, or galling. Of course, a coating cannot be seen independent from its substrate material, especially when high pressures are applied: The substrate material must have sufficient hardness because a coating will fail when the substrate material starts to deform, Ranta Eskola et al. [2.55].

The coating thickness is typically in the range of 2 - 20 μm. A thicker coating is chosen when the main problem is formed by chemical reactions (attacks) or abrasive wear. To minimise chipping or spalling, a thinner coating is chosen when the tool is subjected to repeated impact loading, or high compressive pressures.

A coating that acts as a panacea for all different tribological problems does not exist (at the moment). A coating should be chosen that depends on the type of problem observed. Important properties of a coating (or tool material) are, after Schmoeckel and Frontzek [2.56]:

- Adhesion ability
- Sliding performance
- Elastic properties
- Hardness
- Ductility
- Coating tool material strength.

Besides the well-known carburising and nitriding techniques, etc., Chemical Vapour Deposition (CVD) and Physical Vapour Deposition (PVD) have also found application on metal forming tools.

Publications by Schmoeckel and Frontzek [2.56], Kawai and Dohda [2.57], Cocks and Fisher [2.58], Lindsay, Nine and Mickalich [2.25], Meuleman and Dwyer [2.59] and Keeler and Nine [2.16] review coating applications.

When compared with the bare situation, the effect of a coating on the friction coefficient can hardly be predicted beforehand. From research by Vijgen and Sniekers [2.60], it has become evident that, as a result of varying surface morphology, the production circumstances of a coating have a major influence on the frictional characteristics. This then implies that a coating should be characterised by more than just its chemical composition.

2.4.4 Workpiece material

Even when the workpiece material is of the same class, frictional properties can vary significantly. Wojtowicz [2.61] uses silicon-killed 1010 CR steel (obtained from four different suppliers) in a flat die simulator. The resulting friction values differ by a factor of two. Similar research has been carried out by Davies and Stewart [2.62], who observe variations of a factor of three. In a round robin test by the BDDRG, in which the author participated, a test was carried out with two materials from two different suppliers. The materials are expected to be similar, and compete on the market. In the tests, performed in various laboratories in the Benelux, one material proved to be inferior to the other. Not only was a higher friction coefficient observed, but also stick-slip behaviour. In order to explain the differences, various other aspects of the material were measured in the research. The only aspect that differed significantly was the peak count, 4 peaks/mm for the poor performing material, compared with 6 peaks/mm for the better performing material.

2.4.5 Coating

In recent years, many sheet materials have already been provided with a surface coating because it is generally more efficient to coat the raw sheet material in flow than the finished products separately. Mostly, the coating is applied to protect the underlying

material during the product life, or to achieve a certain surface finish. The coating is sometimes applied to improve the manufacturing process.

The bulk of the reported coatings are:

- Electrogalvanised [2.43, 2.55, 2.63, 2.64, 2.65, 2.66]
- Zinc Hot Dip [2.43, 2.55, 2.63, 2.64, 2.65, 2.66, 2.67, 2.68]
- Galvalume (Zn-Al) [2.55, 2.65, 2.66, 2.69]
- Galvanealed [2.43, 2.55, 2.64, 2.65, 2.66, 2.67, 2.70, 2.71]
- Zn-Ni [2.72, 2.73]
- Zn-Ni-Fe [2.43, 2.55, 2.74]
- PVC [2.74]
- Al [2.75]
- Sn [2.76]
- Al-Si [2.74, 2.75]

Few agreements have been reached about the influence of these various coatings on friction. A striking example is given by the following:

As reported by Overby et al. [2.12], the friction coefficient for galvanised material is about two times higher than the friction coefficient for uncoated material. These tests were carried out on a stretch forming apparatus. The same was observed by Brazier and Stevenson [2.77]. With the aid of a deep drawing test, Yamade [2.75] also confirmed that the galvanised coatings show higher friction coefficients. In a punch stretching test, this is also reported for hot dip zinc and galvanealing on soft tools (kirksite), Brazier et al. [2.50]. In contrast, Thompson [2.69] reports that no difference exists between the frictional behaviour of these coatings. Finally, Aoki et al. [2.78] and Doege [2.43] report that a lower friction coefficient was obtained with galvanised coatings. Both effects are reported by Keeler [2.35]. The authors are all employed by US car manufacturers, so they are focusing on similar problems.

Some of the differences can be explained by the following: Similar coatings from different suppliers have a different frictional behaviour, see Keeler and Dwyer [2.79]. Approval of this is found in Keeler [2.35]. Davies et al. [2.62] report that no two electrocoating lines are the same, leading to differences in the coatings produced. According to Nine et al. [2.80], temperature, current density, flow rate and pH determine the structure and texture of the electrocoated surface.

Nine [2.49] reports that the surface texture (including the crystal orientation of the coatings) can have a strong influence on friction. A coating results in another structure and morphology of the surface, when compared with bare cold rolled sheet, where a directional pattern of rolling marks is normally seen, Nine [2.80]. For zinc, for instance, it Nine [2.80] and Milian [2.82] noted that prismatic type texture enhances formability or reduces friction. It is observed that basal orientation of the zinc deposit results in higher friction coefficients. Good lubrication can eliminate this difference, Nine et al. [2.80]. Other aspects of coatings are deformation modes and bonding strength. The hardness is mentioned by [2.83].

The thickness is an important property of a coating, Yamada [2.75] and Rajagopal [2.76]. The thickness mainly determines the failing of a coating, not the frictional behaviour (prior to failing), Keeler [2.79]. There are various failure mechanisms for these coatings: scoring, galling, flaking, powdering, peeling, burnishing, crack formation and fracture [2.55, 2.84]. Doege [2.43] states that the contact pressure mainly determines the failure of the coating. If the contact pressure reaches the yield stress of the material, failure of the coating starts.

In conclusion, it becomes obvious that the frictional characteristics of a coated material compared with the bare material are not predictable beforehand. More research effort is required to understand the various mechanisms. Promising results may be found by studying the surface morphology and texture, Di Carlo et al. [2.85]. Kotchman [2.86] notes the differences in porosity. Another point might be the influence of material transfer.

2.4.6 Interaction of workpiece material and tool material

Figure 15 represents the diagram of Rothery. In this diagram, the atom radius is displayed against the atom number. Rothery's observation is that when the atom radii differ by less than 15%, the metals will be soluble in each other. The mutual solubility of metals can be easily checked with the aid of this diagram. The solubility of materials in each other is one thing, friction is another. However, if cold welding occurs, it will be easier to cold weld if the solubility is high.

This has already been mentioned by Montfort [2.54] in a slightly different form for deep drawing, see Paragraph 2.4.3.

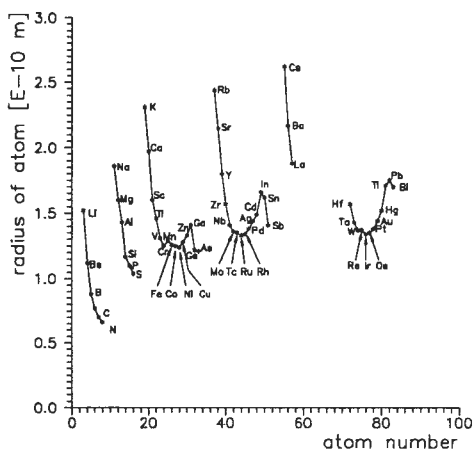

Fig. 15: Diagram of Rothery. Remake from [2.87]

2.4.7 Lubricant

The primary functions of a lubricant in metal forming are to minimise metallic contact, because this will eventually lead to material transfer and/or wear, and to reduce the frictional forces between the workpiece and tools. In most cases, mill oil is already present on the sheet applied by the steel manufacturer for rust prevention in metal forming. If, however, the steel manufacturer already applies drawability improving oils, these are called prelubes. In the actual production there are three possibilities:

- No additional lubricant is applied, only the mill oil or the prelube lubricates the metal forming operation.
- A special lubricant for the forming operation is added.
- The mill oil or prelube is removed from the sheet, followed by the application of a deep drawing lubricant for the forming operation.

Various types can serve as lubricants, for example, solids, greases, dry film, liquid oil, emulsion and gas, etc. Various subdivisions can be made within these classes of lubricants. Besides the type of the lubricant, the applied amount of lubricant, and the resulting film thickness, also play important roles, Nakamura [2.88].

Important aspects of lubricants are formed by the reactivity of the lubricant, which determines whether the lubricant can form a mono-layer in the case of boundary lubrication. With hydrodynamic lubrication, the most important factor is viscosity. Additives to the lubricant are used for most forming applications to meet the requirements for the lubricant. These additives can have various purposes, such as viscosity improvers, corrosion inhibitors, wetting agents and extreme pressure lubricants, etc., Horlacher [2.90].

Examination of a lubricant can be made with the following criteria, which have been compiled from the authors: Wilson [2.23], Kramer [2.89], Horlacher [2.90], Meuleman and Zoldak [2.52]:

- Ability to eliminate pick-up and scoring in the operation concerned.
- Promotion of the required surface finish.
- Corrosion protection
- Ability to build a boundary layer.
- Height of friction coefficient should promote formability.
- Ease of application: Cleanliness and freedom from harmful or objectional effect on operators, equipment or environment.
- Ease of removal: Freedom of staining and corrosive effects, freedom from a tendency to leave objectional residues on the surface.
- Stability in storage.
- Overall economy.

For reasons of economy and ease, most press shops aim at the application of one lubricant for all metal forming operations. The following steps are recommended by Keeler [2.16] when choosing such a press shop lubricant:

- The lubricant should not be used to control metal flow, this should be done by tooling geometry. i.e. draw-beads.
- The ideal press shop lubricant should then produce a low friction coefficient.
- Furthermore, it is required that this friction coefficient is robust, which means that it remains about the same value over a wide range of process variables.
- The selected lubricant should then be exhaustively tested to find the smallest influences of process parameters on the friction coefficient.

However, the most important observation that can be made from literature is the fact that lubricant performance depends on the substrate on which is tested; thus lubricant performance on one substrate cannot be used to predict performance on another substrate, see Keeler [2.79] and Meuleman [2.52].

Reviews of different lubricants are given in [2.91, 2.92, 2.93, 2.94].

2.4.8 Lubricant interaction with tool workpiece material

Various mechanisms are responsible for lubricant components to adhere to the tool or workpiece material:

- The first mechanism is surface chemistry, whether or not the lubricant or one of its components is able to react chemically with the material, EP lubrication. With an atmospheric oxide layer covering the material, boundary lubrication is easier to achieve with active materials such as copper, zinc, iron, magnesium and aluminium. With passive materials, such as nickel, chromium and platinum, boundary lubrication is difficult to achieve.
- The second mechanism is polarity. If polar components are present in the lubricant, these can be attracted electrically to either tool or workpiece material.
- The third mechanism is affinity. This relatively unknown mechanism is based on the solubility of a metal part of a metal soap in the base material of tool or workpiece material.

2.5 Various

2.5.1 Tooling aspects

2.5.1.1 Radii

Considering the punch radius, Wilson [2.23] reported that smaller radii result in more flattening of the asperities, because of the increased contact pressure. In a strip stretch test, Duncan et al. [2.95] found that a smaller radius leads to higher friction coefficients. This is also stated by Kotchman et al. [2.86]. Perpendicular to this, considering the radius geometry, Siegert [2.5] stated that a larger radius results in a decrease of the bending force, while the friction force is increased by lowering the contact pressure. Ramaekers and Sniekers [2.96] also found that a smaller radius generally leads to lower friction, but this effect might be altered for coated workpiece material because of damage to the coating layer. FEM research on pressure distributions on the die shoulder by Sniekers and Hoogenboom [2.97] has clearly shown that local bending is the cause of high contact pressures. From this, one might design a die with constantly increasing and decreasing radii, so that the local bending will be spread over a larger area, leading to lower pressures.

Generally, it can be concluded that the pressure peaks caused by bending and straightening are lower for larger radii. Also, the contact pressure originating from the tensile forces in the strip will be lower with a larger radius. Then, there are surface alterations dependent on both flattening as a result of the contact pressure and roughening caused by the bending. The combined effect on friction coefficient is hard to determine.

Nakamura [2.88] states that, in order to build up lubricant pressure, a narrow gap can be helpful. In designing a die, this could mean that dies will have to be made concave.

2.5.1.2 Draw-beads

Draw-beads are often used to control the metal flow or to prevent the material from wrinkling etc. in the deep drawing of large parts with an irregular form. These draw-beads increase stresses towards the punch centre (radial direction in simple cupping), which leads to an increase of the contact pressure.

2.5.1.3 Blank holder stiffness

It has generally been accepted that a rigid blank holder concentrates its force on the outer rim of the blank in the deep drawing of a circular cup. Because of the thickening behaviour of the flange, the size of the influenced part is about the outer third of the remaining flange, von Finckenstein [2.72]. This means that, for a rigid blank holder, a large part of the remaining flange is free of pressure normal to its plane, which will have a significant influence on the friction stress distribution. As a result of this behaviour, the lubricant becomes trapped between the outer rim of the flange and the entrance to the die shoulder, Nakamura [2.88].

With an elastic blank holder, contact between the blank holder and the sheet can be obtained over a larger area, depending on the stiffness. By doing so, the contact pressure will be lower in the outer rim of the flange region.

The effect on frictional conditions of a rigid blank holder are quite detrimental while the outer rim slides between blank holder and die with quite high contact pressures. It will be difficult to keep lubricant in action in the contact zone.

2.5.1.4 Blank holder force

The blank holder is the only possibility of influencing the pressure distribution to a little extent in production. The blank holder force and friction coefficient together determine whether or not the process under consideration will be an actual deep drawing operation or a stretching operation. Low or high friction can be exchanged for high or low blank holder force, as long as no wrinkling or tearing of the product occurs.

Apart from the magnitude of the blank holder force, which is of evident importance to sheet metal forming operations, its development with the punch stroke is important. In many cases, springs are used to achieve a blank holder force with the punch stroke. Now, the blank holder force/punch stroke relation is fixed. Another approach gaining interest in recent years is external blank holder force control, with which combined failures can in some cases be removed.

2.5.1.5 Punch stiffness, guidance and alignment

Because of the forces acting on the punch and the resulting deformations, in addition to errors in the alignment and guidance of the punch, contact conditions can be greatly altered, especially when the clearance changes such that ironing occurs locally, which can

lead to increased wear and changed friction. Only few investigations have been done on this subject, and even fewer were aimed at the resulting frictional changes, see for instance Siekirk [2.98]. This aspect should be carefully checked and avoided in the design stage.

2.5.1.6 Tools wear

Friction is not a static parameter, but can vary during the tool life. Explanations for this can be found within friction itself. As a result of the interactions of the tools with the workpiece material, micro- and macro-alterations of the tool geometry occur. At a micro-scale, asperities can break off and, at a macro-scale, measures can change, for instance tool radii. Furthermore, an important cause of friction variations is originated by material transfer. This is caused by particles being scraped from workpieces, which then adhere to the tools.

A well-known effect is that new dies have to run in, during which, for instance, the roughness perpendicular to the flow direction decreases.

2.5.2 Blank

2.5.2.1 Product dimensions

The blank's geometry is given by its original diameter and thickness. Considering friction, the ratio of punch diameter to sheet thickness is important, and is a characterisation for the size of the product. With increasing D_P/s_0 ratio, the frictional share in the stress distribution increases if the other parameters are kept constant. The radial stress will increase to higher values than with smaller products, resulting in higher contact pressures at tool curvatures.

In combination with a workpiece coating, a greater thickness of the sheet gives rise to increased powdering, flaking, and sticking, because of the enlarged bending strains.

Sheet material always varies in thickness, even within one coil. In normal production, spread in material thickness of the order of about 5% is observed for sheet thicknesses towards 1 mm, see Siekirk [2.98].

Another important aspect of the blank geometry is the finishing in the blanking operation, i.e. if burrs at the edge of the blank are formed by cutting out the blank for the forming operation, Siekirk [2.98] and the resulting flattness of the blank.

2.5.3 Environment

In the press shop, effects of the environment that can be mentioned are humidity, dust, and vibrations, Siekirk [2.98]. Fisher and Schey [2.99] report that low humidity leads to an increase of limiting dome height. They attribute this phenomenon to interference of moisture with the lubricant. Möllers and Fischer [2.100] showed that friction in deep drawing can be reduced by 90% with the aid of ultrasonic waves.

2.6 Conclusions

Friction is a complicated phenomenon. Even in a relatively restricted area such as deep drawing many, many variations can be found. Different friction conditions are found from position to position in the deep drawing process. As already outlined in Paragraph 1.4, friction has a major influence on the deep drawing process, especially with large products, so it will be necessary to have a valid means of accurately measuring friction coefficients.

The coefficient of friction which results is completely dependent on the specific combinations of parameters chosen, and cannot be predicted from any other combination, Keeler [2.16]. This explains the press shop experience of wide swings in the performance of the production tooling resulting from changes in the frictional characteristics caused by apparently small alterations in the process.

As shown by comparing various literature sources, contradictory results are reported by different researchers. Some of these effects can be explained, others cannot. In general, it can be stated that the transferability of experiments is low, and can lead to erroneous results.

To eliminate surprises originating from experiments not well fitted to the industrial application when testing the frictional behaviour of a certain combination of parameters, it is of major importance to simulate the deep drawing process that forms the basis for the experiments as well as possible.

In the papers reviewed, it was occasionally difficult (or impossible) to discover the circumstances under which the experiments were carried out. This might have troubled the author's view occasionally.

In this work, attention has been focused on the determination of the coefficient of friction. This has been done from the viewpoint of pre-production calculations to optimise the tooling and blank geometry. Of course, more aspects relate to the frictional behaviour of a given deep drawing system, for instance, surface quality and appearance after the deep drawing operation and subsequent production steps such as painting.

References

2.1 Hsu, T.C.
The internal variables approach in friction modelling of computer simulation in sheet metal forming processes.
Journal of Material Processing Technology, 37 (1993), p.95-114

2.2 Bongaerts, P.C.B.
Faalaspecten bij omvormende bewerkingen.
Eindhoven University of Technology
report WPA-120015 1994

2.3 Wilson, W.R.D
Friction models for metal forming in the boundary lubrication regime.
Trans. ASME
Journal of Engineering Materials and Technology, 113 (1991) 1 p.60-68

2.4 Sheu, S., Wilson, W.R.D.
Flattening of workpiece surface asperities in metal forming.
Proc. North American Metalworking Research Conf. XI, 1983, p.172-178

2.5 Siegert, K., Thomas, V.
Einsatz von Schmierstoffe zur Beeinflussung der Reibung beim Umformen von Karosserieteilen.
Use of lubricants to affect friction in the forming of auto body panels.
Aluminium, 63 (1987) 4, p.401-410.

2.6 Kumpulainen, J.O., Ranta-Eskola, A.J., Rintimaa, R.H.O.
Effect of temperature on deep drawing of sheet metals.
Journal of Engineering Materials and Technology, 105 (1983), p.119-127

2.7 Kumpulainen, J.O.
Factors influencing friction and galling behaviour of sheet metals.
Proc. 13th IDDRG conf., Melbourne, 1984, p.476-490

2.8 Lenard, J.G.
The effect of temperature on the coefficient of friction in flat rolling.
Annals of the CIRP, 40 (1991) 1

2.9 Emmens, W.C.
Some frictional aspects in deep drawing.
Publ. Hoogovens Group IJmuiden

2.10 Emmens, W.C.
The influence of surface roughness on friction.
15th Biennial congress IDDRG, Dearborn, Michigan, USA, 16-18 may 1988

2.11 Bello, D.O., Walton, S.
Surface topography and lubrication in sheet metal forming.
Tribology International, 20 (1987) 2, p.59-65

2.12 Ru, Z. Overby, D.
Strip friction experimental study on galvanized steel sheet.
15th Biennial congress IDDRG, Dearborn, Michigan, USA, 16-18 may 1988, p.85-90

2.13 Muller, R.
Evaluation of the properties of sheet with lasertex surface texture.
15th Biennial congress IDDRG, Dearborn, Michigan, USA, 16-18 may 1988, p.99-107

2.14 Patir, N., Cheng H.S.
An average flow model for determining Effects of three dimensional roughness on partial hydrodynamic lubrication.
Trans ASME,
Journal of Lubrication Technology, 100 (1978)

2.15 Atala, H.F., Rowe, G.F.
Surface roughness changes in rolling.
Wear, 32 (1975), p.249-269

2.16 Keeler, S.P., Nine, H.D., Siekirk, J.F.
Formability criteria for selecting sheet metal lubricants.
SAE Technical Paper 880366 (1988)

2.17 Kudo, H., Azushima, A.
Interaction of surface microstructure and lubricant in metal forming tribology.
Advanced Technology of Plasticity, 1 (1987), p.373-384

2.18 Montfort, G., Defourny, J., Bragard, A.
Progress in the roughness texture of cold rolled steel sheets related to deep drawing and forming.
15th Biennial congress IDDRG, Dearborn, Michigan, USA, 16-18 may 1988, p.91-98

2.19 Defourny, J.A., Leroy, V.M., Nilles, P.E.
Update of developments in lasertex technology.
Iron and Steel Engineer, aug. 1991, p.39-45

2.20 El-Menshawy, F., Snaith, B.
Advances in electro discharge texturing (EDT) for cold mill work rolls.
Iron and Steel Engineer, aug. 1991, p.57-59

2.21 Pankert, R.
Aufrauhen von Arbeitswalzen in Kaltwalswerken.
Stahl und Eisen, 110 (1990) 3, p.55-60

2.22 Hilsen, R.R., Bernick, R.M.
Relationship between surface characteristics and galling index of sheet steel.
Formability Topics-Metallic Materials, ASTM STP 647, 1978, p.220-237

2.23 Wilson, D.V.
Lubrication & formability in sheet metal working.
Sheet Metal Industries, dec. 1966, p.929-944

2.24 Sengupta, A.K., Fogg, B., Ghosh, S.K.
On the deformation behind the punch-blank surface conformation in stretch forming and deep drawing.
Journal of Mechanical Working Technology,
5 (1981), p.181-210

2.25 Lindsay, J.H., Nine, H.D., Mickalich, M.K.
Effect of surface finish on the drawing characteristics of chromium-plated sheet metal forming tools.
SAE Cong. and Exp. Detroit, MI, USA,
25 febr. - 1 mar. 1991
Autobody Stamping Technology Progress.
SAE Special Publications 865 (1991), Warrendale, PA, USA, p.15-27

2.26 Dalton, G.M., Schey, J.A.
Effects of bead surface preparation on friction in the draw-bead test.
SAE Cong. and exp. Detroit, MI, USA
25 febr. - 1 mar. 1991
Autobody stamping technology progress.
SAE Special Publications 865 (1991), Warrendale, PA, USA, p.29-39

2.27 Andersson, B.
The influence of surface topografy on the forming performance of aluminium.
Central Institute for Industrial Research Forknigsvn
1 Oslo 3, Norway, p.467-475

2.28 Bragard, A., Leroy, V., Bonnarens, H., Richelmi, J., Marique, C.
Proc. 10th IDDRG Congress, Warwick (1987) p.253

2.29 Kienzle, O.
Dictionary of Production Engineering, vol. 3,
Sheet Metal Forming 1965

2.30 Iwata, K., Osakada, K., Fujino, S.
Analysis of hydrostatic extrusion by the finite element method.
Journal of Engineering for Industry
Trans. B, 94 (1972), p.697-703

2.31 Kobayashi, T., Ishigaki, H.
Granulating behaviour of surface texture and deforming limit in press forming.
Journal Japan Society for Technology and Plasticity, 15 (1974) 158, p.197-205

2.32 Wollrab, P.M., Kopietz, J., Streidl, M.
Changes in the surface structure of deep drawing sheet steels subject to various forming stresses.
Publication BMW AG, Munchen, FRG

2.33 Dautzenberg J.H. Kals, J.A.G.
Surface roughness caused by metal forming.
Annals of the CIRP, 34 (1985) 1

2.34 Streidl, M., Kopietz, J., Breun, F.,
On the behaviour of the microsurface structure of sheets in free and constrained forming condition.
Blech Rohre Profile, 38 (1991) 3, p.211-217

2.35 Keeler, S.P.
Evaluating the lubricity of press shop lubricants on various types of galvanized steels.
28th Mechanical Working and Steel Processing Conf.
Pittsburg, Pennsylvania 26-28 oct. 1986
The Metallurgical Society of AIME,
Warrendale, Pennsylvania, 1986

2.36 Kaftanoglu, B.
Determination off coefficient of friction under condition of deep-drawing and stretch forming.
Wear, 25 (1973), p.177-188

2.37 Ghosh, A.K.
A method for determining the coefficient of friction in punch stretching of sheet metals.
International Journal of Mechanical Sciences,
19 (1977), p.457-470

2.38 Duncan, J.L., Shabel, B.S., Filho, J.G.
A tensile strip test for evaluating friction in sheet metal forming.
ASME Dearborn, MI, USA 1978
SME Paper nr.780391,

2.39 Sengputa, A.K., Fogg, B., Ghosh, S.K.
On the mechanism behind the punch-blank surface conformation in stretch-forming and deep-drawing.
Journal of Mechanical Working Technology,
5 (1981), p.181-210

2.40 Kaga, H., Yaji, S.
Microgeometric variation of surface profile in early stage of deep drawing process.
Proc. 12th Japan Cong. on Materials Research-Metallic Materials, 1969, p.181-210

2.41 Kasuga, Y., Yamaguchi, K., Kato, K.
Friction and lubrication in the deformation.
Processing of Metals.
Bulletin Japan Society of Mechanical Engineering 11 (1968), p.361-365

2.42 Klimczak, T., Dautzenberg, J.H., Kals J.A.G.
On the roughening of a free surface during sheet metal forming.
Annals of the CIRP, 37 (1988) 1

2.43 Doege, E.
Eigenschaften und Umformverhalten oberflächen veredelten Feinbleches beim Tiefziehen.
Blech Rohre Profile, 39 (1992) 1, p.25-30

2.44 Wilson, W.R.D., Sheu, S.
Real area of contact and boundary friction in metal forming.
International Journal of Mechanical Sciences,
30 (1988) 7, p.475-488

2.45 Fogg, B.
Preliminary study of the influence of stress and deformation in the substate on junction growth and friction.
Proc. of the Institute of Mechanical Engineers
(1967-1968) 182 (PT 3K) p.152-161

2.46 Avitzur, B., Nakamura, Y.
Analytical determination of friction resistance as a function of normal load and geometry of surface irregularities.
Wear, 107 (1986), p.367-383

2.47 Ike, H., Makinouchi, A.
Effect of lateral tension and compression on plane strain flattening processes of surface asperities lying over a plastically deformable bulk.
Wear, 140 (1990), p.17-38

2.48 Wang, Z., Kondo, K., Mori, T.
Optimum conditions for surface flattening by replication mechanisms in ironing process.
ASME 1992
Engineered Surfaces, PED 62 (1992)

2.49 Nine, H.D.
Friction measurement for forming of zinc-coated sheet steel.
Zinc-Based steel coating systems: Metallurgy and Performance Conf. Detroit, MI, USA,
1-3 Oct. 1990, p.233-243

2.50 Brazier,W.G., Thompson, R.W.
The effect of die materials and lubrication on punch stretching and drawing forces of cold-rolled and zinc-coated steels.
SAE Technical Paper 850274 (1985)

2.51 Brazier,W.G., Thompson, R.W.
The effect of zinc coatings, die materials, and lubricants on sheet metal formability.
SAE Technical Paper 860434 (1986)

2.52 Meuleman, D.J., Zoldak, J.J.
The interaction of coated steels, die material, and forming lubricants.
SAE Technical Paper 860432 (1986)

2.53 Gross,D.K
Zinc alloys:Specifications and processing.
SAE Technical Paper 871952 (1987)

2.54 Montfort, G., Defourny, J., Belliard, P., Thomas, B.
Coated steels in stamping: The interaction with tool material and its consequence on the galling behaviour.
Proc. 17th IDDRG Cong. Beijing 1992

2.55 Mäkitmattila, S., Ranta-Eskola, A.
Behaviour of galvanized coatings during forming.
Proc. 13th IDDRG Cong. Melbourne 1984,
p.293-304

2.56 Schmoeckel, D. Frontzek, H.
Reduction of wear on sheet metal forming tools.
Annals of the CIRP, 35 (1986) 1, p.195-198

2.57 Kawai, N., Dohda, K.
Tribology in metal forming processes.
ATPC Tokyo 1984
Japan Society for Technology and Plasticity,
1 (1984), p.145-156

2.58 Cocks, G.J., Fisher, P.
Application of the toyota (TD) process tooling for sheet metal forming.
Proc. 13th IDDRG Cong. Melbourne 1984,
p.515-520

2.59 Meuleman, D.J., Dwyer, T.E.
Die materials and treatments with electrogalvanized steels.
SAE Technical Paper 880369 (1988)

2.60 Vijgen, R.O.E., Sniekers, R.J.J.M.
Effects of coating parameters on frictional behaviour in deep drawing.
To be published.

2.61 Wojtowicz, W.J.
Sliding friction test for metalworking lubricants.
Lubrication Engineering, 11 (1955) 3, p.174-177

2.62 Davies,R.G., Stewart, W.S.
Influence of die material upon the coefficient of friction of zinc coated steels.
Zinc-based steel coating systems: Metallurgy and performance. Conf. Detroit, MI, USA,
1-3 oct. 1990, p.243-250

2.63 Lee, C.H., Shim, H.B., Yang, D.Y.
Determination of frictional coefficient for sheet metal working and its application to strecch forming.
VI International Cong. Experimental Mechanics
Conf. Portland, Oregon, USA, 6-10 June 1988
1 (1988), p.71-76

2.64 Blanchard, G.
Description of a friction test used for cold rolled sheets and examples of applications.
Bulletin Cercle d'Etudes des Metaux,
15 (1986) 12, p.19.1-19.12

2.65 Reitzle, W., Schlicht, H.P., Drecker, H., Fischer, F.
Tribologie vorbeschichteter Bleche beim Tiefziehen.
Stahl und Eisen, 103 (1983), p.41-46

2.66 Meuleman, D.J., Denner, S.G., Cheng, F.V.
The effect of zinc coatings on the formability of automotive sheet steels.
SAE Technical Paper 840370 (1984)

2.67 Sudoo, C., Hayashi, Y., Nishihara, M.
Behaviour of coated film in press forming of surface treated steel sheet.
Memoires et Etudes Scientifiques de la Revue de Metallurgie, 77 (1980), p.353-362

2.68 Chilaud, M., Mathieu, S., Pichant, P., Quinchon, G.
Hot dip galvanized steel - product of the future.
SAE Technical Paper 860271 (1986)

2.69 Kim, J.K., Thomson, P.F.
Friction and stress distribution in coated steel sheet during forming.
Journal of Materials of Materials Processing Technology, 21 (1990) 1, p.29-42

2.70 Numakura, Y., Nakayama, M., Yamada, M., Fukada, A., Konda, S.
Improvement on formability of galvannealed steel sheets with Fe rich-Zn alloy electrocated uppermost layer.
SAE Technical Paper 900509 (1990)

2.71 Toda, M., Kojima, H., Morishita, T.
Development of two-layered Zn-Fe alloy electroplated steel sheet - new coated steel sheet for automotive body.
SAE Technical Paper 840212 (1984)

2.72 Finckenstein, E. von, Lawrenz, K.J.
Beschichtete Bleche umformen.
Bänder Bleche Rorhe, 19 (1978) 3, p.130-136

2.73 Fukui, S., Yoshida, K.
Measurement of mean friction coefficient in sheet drawing.
International Journal of Machine Tool Design, 2 (1962), p.19-26

2.74 Pearce, R.
Sheet Metal Forming
Hilger, Bristol, 1991

2.75 Yamada, T., Kawase, H.
Formability of aluminium coated steel sheet.
Proceedings of the 13th International Deep Drawing Research Group
Melbourne 1984, p.329-338

2.76 Misra, S., Rajagopal, S.
Influence of tin coating thickness on the drawability and ironability of tin plate in D&I canmaking.
Lubrication and Challenges in Metalworking and Processing
Proceedings of the 2nd Conference ITT Research Institute, Chicago, 1979, p.85-93

2.77 Brazier, W.G., Stevenson, R.
Evaluation of a new dual phase, cold rolled steel formability.
SAE Reprints 780137 (1978)

2.78 Aoki, I., Horita, T., Herai, T.
Formability and application of galvanized sheet steels.
Technological Impact of Surfaces, ASM, Ohio, 1982, p.165-176

2.79 Keeler, S.P., Dwyer, T.E.
Frictional characteristics of galvanized steel sheet evaluated with a draw-bead simulator.
SAE Technical Paper 860433 (1986)

2.80 Lindsey, J.H., Paluch, R.F., Nine, H.D.
The interaction between electrogalvanized zinc deposit structure and the forming properties of sheet steel.
Plating and Surface Finishing, 76 (1989), p.62-69

2.82 Milian, J.L.
Effects of electrodeposited zinc coating on the formability of drawing quality aluminium killed steel.
JMEPEG 1992, p.275-284

2.83 Hashimoto, K., Ohwue, T., Takita, M.
Effect of temperature, die materials and lubricant on sliding behaviour of various coated steel sheets.
16th IDDRG Conf. Borlange 1990, p.153-160

2.84 Rault, D., Entringer, M.
Anti-galling roughness profile permitting reduction of the blank holder pressure and the required amount of lubricant during the forming of sheets.
Applications to the high yield strength steels.
Sheet Metal Forming and Energy Conservation
p.97-114

2.85 Di Carlo, S., Puozzo, L., Arrigoni, G., Marzari Chiesa, G., Rettagliata, M.
Parameters affecting the press formability of electrogalvanized steel sheets.
IDDRG Working Group Meeting, Budapest, april 1989

2.86 Kotchman, D.P., Kim, I.,Sa, C.Y., Lee, D.
Determination of frictional behaviour in sheet metals using orthogonal arrays.
JMEPEG 1992, p.555-564

2.87 IJpelaar, R., Berkelaar, L., Rijsewijk, A. van,
Hardmetaal is taaier dan U denkt. Aanladen en oplosslijtage zijn te reduceren.
Polytechnisch Tijdschrift Materialen
11-12 (1994), p.70-73

2.88 Nakamura, T., Kinpara, H.
Seizure initiation mechanism in cold metalworking processes. (Effect of tool surface roughness on the critical oil film thickness).
Engineering for Industry, 32 (1989) 3 p.484-490

2.89 Krämer,W
Untersuchung von Schmiermitteln für das Tiefziehen.
Industrie Anzeiger, 86 (1964) 12, p.2167-2170

2.90 Horlacher,U
Lubricants and lube additives for cold forming from the solid.
Wire, 40 (1990) 3, p.338-341

2.91 Schey, J.A.
Metal Deformation Processes: Friction and Lubrication.
Dekker, New York, 1970

2.92 Schey, J.A.
Tribology in Metalworking; Friction, Lubrication and Wear.
Dekker, New York, 1983

2.93 Wunsch, F.
Möglichkeiten und Grenzen der Feststoffschmierung.
Gesellschaft für Tribologie e.V., Deutsche Gesellschaft für Mineralölwissenschaft und Kohlenchemie, Fachgruppe Anwendungstechnik, Fachaussschuss Schmierstoffe: Tagung: Tribologie in Theorie und Praxis, Schmierstoffe und ihre Anwendung, 1981.

2.94 Nachtman, E.S., Kalpakjan, S.
Lubricants and lubrication in metalworking operations.
ISBN 0-8247-7401-9, Marcel Dekker Inc, New York

2.95 Wang, X.J., Duncan, J.L., Davenpeck, M.L.
Punch friction test for sheet metal working.
Journal of Applied Metalworking
3 (1983) 1, p.3-11

2.96 Ramaekers, J.A.H., Sniekers, R.J.J.M.
Experiments on stripdrawing with stationary bending an straightening.
Proc. 4th ICTP Beijing 1993, p.1716-1721

2.97 Sniekers, R.J.J.M., Hoogenboom S.M.
Analysis of stationary bending and straightening during stripdrawing.
Proc. 4th ICTP Beijing 1993, p.1722-1727

2.98 Siekirk, J.F.
Process variable effects on sheet metal quality.
Journal of Applied Metal Working
4 (1986) 3, p.262-269

2.99 Fischer, R.F., Schey, J.A.
Tribological factors affecting the LDH test.
SAE Technical Paper 920434 (1992)

2.100 Möllers, J., Fischer, F.
Über den Einfluss von Ultraschall auf die Reibung beim Tiefziehen.
Bänder Bleche Rohre, 16 (1975) 11, p.457-460

Chapter 3 Test methods for friction in deep drawing

3.1 Introduction

Various testing methods have been developed by research institutes all over the world. In order to make a valid choice from these test methods for application towards the deep drawing process, the requirements that they have to meet must be made clear.

The following paragraphs highlight the requirements that the author considers to be most important, with their advantages and disadvantages.

3.2 Demands on test methods

3.2.1 Applicability

The literature study described in Chapter 2 made evident that friction in deep drawing depends on many variables. For some variables (i.e. roughness) it is not even clear how they should be described accurately. It has also become clear that extrapolation of experimental data from one situation to another can lead to erroneous results. Therefore, to avoid as many problems as possible, the first requirement for testing is that **experiments have to be carried out with a high degree of similarity to the actual process**. For instance, this could imply that a test piece from the raw material must be tested with the same oil as used in production, against a test tool manufactured in the same way, and from the same material as the actual production tool.

3.2.2 Data evaluation

Friction tests can be divided into three groups:

- One step measurement, the friction coefficient can be calculated directly from the measurement of forces.
- Two step measurement, one test is carried out in the absence of friction, and then with the presence of friction; the friction coefficient is calculated from the difference.
- A process model for the test is available. The friction coefficient is then calculated by fitting the theory to the measurement.

Apart from the observation made in the previous paragraph, the friction coefficient derived from an experiment must at least be valid for the experiment itself.

The second requirement becomes evident if we consider the following: Suppose an experiment is carried out. When we assume a certain deformation pattern or a model of the material behaviour, and use these **models** to calculate a friction coefficient from the obtained punch load - punch travel diagram, an error is introduced, because models are always imperfect. The resulting error will then lead to an unknown error in the friction coefficient. Therefore, **testing must be free of deformation or material modelling**.

The third requirement arises from the fact that some experiments are carried out twice, once with friction present, the second time in (relative) absence of friction. The difference is hence stated to depend on the friction. This would be useful if a process could be realised that is not influenced by friction, but unfortunately most processes cannot. If the test in absence of friction still includes some friction, an error is introduced. This leads to the conclusion that **it must be possible to derive the friction coefficient from one single experiment.**

3.2.3 Conclusion

A valid friction test has to have the following characteristics:

- The test conditions must match the conditions in deep drawing as close as possible.
- No model is necessary for the plastic deformation and no assumptions have to be made about the material behaviour.
- The friction coefficient must be obtained in one single experiment.

3.2.4 Restrictions

If these requirements are fulfilled, then the friction coefficient observed in the test can be expected to be as close as possible to the actual friction coefficient in a production line. However, in order to have general purpose tests, it must be possible to manufacture the test pieces from the sheet material. Furthermore, for reasons of economy and ease of use, the testing would benefit from easy to manufacture workpieces and tooling parts. The latter two requirements apply to all the test methods mentioned in the following section.

3.3 Flat die simulator

One of the most widely used tests in simulating frictional effects is the flat die simulator, as originally developed by Wojtowicz [3.1, 3.2] see Figure 16. Various authors have done intensive research with the flat die simulator, including Emmens [3.3], Blümel [3.4], Blanchard [3.5], Schey [3.6], Stine [3.7] and Reitzle [3.8].

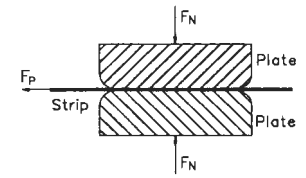

Fig. 16 : The flat die simulator

The advantage of this test is the apparent simplicity. The average friction coefficient is easy to calculate when the pulling force F_P and the normal force F_N are measured. Also, by means of this test, speed and contact pressure can be very well adjusted to desired levels.
A disadvantage that must be mentioned is that no bulk plastic deformation is present. In addition, the expected uniform conditions at each point are difficult to obtain, because the test surfaces are very unlikely to conform to each other, as already was mentioned by Witthuser [3.9] and Emmens [3.10].

Furthermore, it can be mentioned that the geometry of the die shoulder and the blank holder at the place where the strip enters the contact zone have quite an influence on the frictional behaviour, see for instance Wilson and Cazeault [3.11].

Considering the design of the flat die simulator, a complete review has been given by Emmens [3.10], who names misalignment of jaws, elastic deformation of the jaws, the squeezing effect of the jaws, and the limitation on the pulling force by the yield stress as limiting factors in the application of the flat die simulator. He proves that the avoidance of these problems leads to conflicting design requirements.

3.4 Radial strip drawing test

In a strip drawing test, a strip is pulled over a die shoulder, see Figure 17. The strip is pulled at a constant velocity ($\dot{u}$) over the die shoulder, which has a radius R, using a force F_P. At the other side of the strip, a back-pull force F_{Bp} is applied. Various methods are available to apply this back-pull force on the strip, for instance a draw-bead or a hydraulic system.

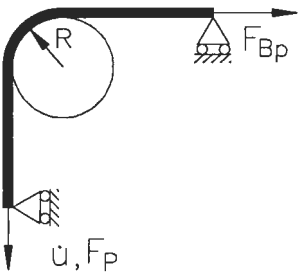

Fig. 17 : Basic radial strip drawing

Advantages of this test that can be mentioned are the one sided contact and subsequent good conformation to the die. Also, the friction coefficient can be derived from one experiment without using models for the deformation pattern or the material behaviour. The relative velocity between workpiece and tooling is quite constant and can be manipulated very well.

Disadvantages are that there is no bulk plastic flow in a large part of the strip, the local contact pressure in the contact area varies to a great extent, and the average contact pressure can only be controlled within a certain range.

3.5 Strip deep drawing test

This test, which is actually a combination of the strip drawing test and the flat die simulator, simulates the frictional effects in the die shoulder region and in the flange region, see Figure 18, the principle taken from Schmoeckel and Frontzek [3.12].

In general, the advantages and disadvantages are also inherited from those test methods. Additionally, it can be mentioned that the advantage of this type of testing is that bending effects around the die shoulder force the flange to release from the flat part of the die, as in real deep drawing circumstances.

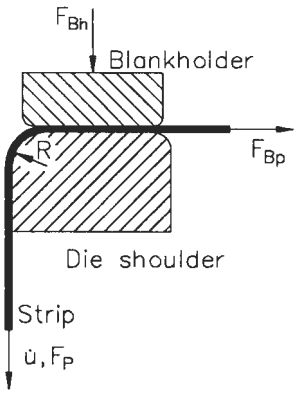

Fig. 18 : Strip deep drawing test, after Schmoeckel and Frontzek

A similar design based on the same principle is given in Figure 19. In this experimental set-up, (note that there is no flow in the direction perpendicular to the drawing) the actual deep drawing process is quite well simulated.

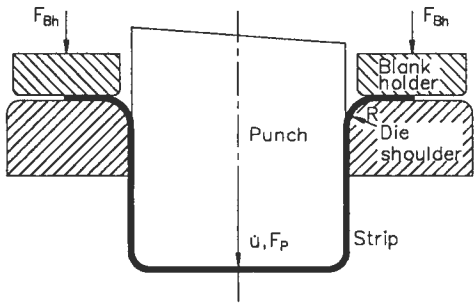

Fig. 19 : Strip deep drawing test EUT

3.6 Strip stretching test

In this test, which was first reported by Lee, Shim and Yang [3.13], a strip is wound around a radius, and then stretched over this radius by applying a velocity $\dot{u}$ at one side of the strip, while the other end remains fixed.

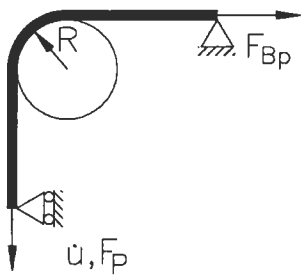

Fig. 20 : Strip stretching test

In the original apparatus it is possible to vary the contact angle between strip and radius, but Lee, Shim and Yang, as well as Fox, Maniatty and Lee [3.14] mention that satisfactory results were obtained only for the contact angle of 180 degrees. Based upon the same principle, Duncan and Wang [3.15] worked out a similar apparatus, which can deal with a contact angle of 90 degrees, rather than 180 degrees. In the author's view, however, if this test is slightly modified, it can be dealt with in a similar way as with the radial strip drawing test, and then this test fulfils the requirements made for data evaluation.

An advantage of this test is the fact that actual bulk deformation occurs in the contact zone. This type of deformation, stretching, is similar to the deformation at the punch nose. The disadvantages are: The normal pressure cannot be adjusted to desired levels, and the sliding velocity in the contact area varies and is hard to measure.

Work with this apparatus is reported by: Overby [3.16], Shi [3.17] Siegert [3.18] and Duncan [3.19].

3.7 Draw-bead simulator

Fig. 21 : The drawbead simulator, acc. to Nine

The draw-bead simulator, as originally developed by Nine [3.20], is probably the most used friction test, especially within Canada and the US based automotive industry.

Figure 21 gives the principle of this test. A strip of test material is drawn over three radii, which resemble closely a draw-bead in a production tool. The radii can be fixed or rotating. At point B, horizontal displacement is imposed on the strip, while at point A vertical displacement of the strip is suppressed. Because of the imposed displacement, the strip will start to slide along the radii when these are fixed. When the radii can rotate freely, it is assumed that the strip does not encompass friction. Unfortunately, as a result of the bending - unbending operations, thinning of the strip occurs, which leads to differences in velocity at the tool/strip interface.

Doublet experiments have to be carried out: once with fixed radii and once with rotating radii. The differences in the two experiments are then thought to originate from the difference in friction. In principle, however, this test can be regarded as a three-fold radial strip drawing test with contact angles of approximately 180 degrees; with some modifications, the test can be changed such that only a single experiment is necessary, similar to the radial strip drawing test.

Reported work with this test has been carried out by: Brazier [3.21, 3.22], Keeler [3.23, 3.24], Meuleman [3.25, 3.26], Siekirk [3.27] and Lindsay [3.28].

3.8 Other tests

Of course, more tests have been proposed on friction in forming. However, in the author's view, these tests fail in their applicability towards sheet metal forming, or because of reasons that the precise friction action is hard to determine.

Examples of the first type are the tests proposed by Pawelski [3.28], Sachs [3.29], Wiegand and Kloos [3.30], Shima and Yamamoto [3.31], Kawai and Dohda [3.32]. Examples of the second type are cupping tests and limiting dome height tests, as frequently used by the American automotive industry. Schey and Mclean [3.6] also arrive at the conclusion that these tests do not yield more information than a draw-bead test.

3.9 Review test principles

Various friction tests have been presented in the previous paragraphs, with a brief description of their specific properties. A more detailed analysis of these tests shows that there are two basic principles of which they all consist, namely sliding along a radius or between two flat surfaces.

Both types of sliding can be combined with bulk plastic deformation, local plastic deformation, or no plastic deformation (except possibly asperity peaks). Keeping this in mind, the following observations can be made:

- A combination of bulk or local deformation and sliding is difficult to obtain in a flat die simulator, but it is possible to pre-strain or pre-stress the test piece.
- A draw-bead simulator can be seen as a threefold radial strip drawing tester, with increasing back-pull forces. As a result of the increasing back-pull forces, the calculated friction coefficient will be an average over three different situations.

- A strip deep drawing test can be regarded as a radial strip draw test combined with a flat die simulator.
- A strip stretch test can be regarded as a radial strip draw test with the back-pull force as high as necessary to clamp the strip at the back-pull side.

3.10 Conclusions

Different types of deformation can be identified in deep drawing, and nothing seems more reasonable than choosing an appropiate friction test for a certain region in the deep drawing operation. In this way, it might be possible to include some of the effects of bulk deformation in the friction coefficient, leading to better simulations when these are used in pre-production simulations.

One of the starting-points in the search for good friction testing methods for deep drawing is the fact that it must be possible to determine the friction coefficient from one experiment only. Apart from reasons of economy, the main objection to be made against friction coefficients derived from more than one experiment is: When duplo experiments are used, once with and once without friction, the tests are not identical, the difference is not only friction, but also some changes arising from different deformation caused by different stress levels.

Another starting-point was the necessity to achieve tests that can be evaluated for the coefficient of friction without using models for the deformation that occurs. If a model is used to calculate deformation aspects in a measurement, this means that all errors in the model will be included in the friction coefficient, leading to erroneous results.

Summarising, useful friction tests for deep drawing have the following characteristics:
- Good resemblance with a certain region in the deep drawing process.
- The friction coefficient can be derived from one single experiment.
- It is not necessary to use a model for the deformation that occurs in the friction test, or to model material behaviour.

Nearly all the above-mentioned tests can meet these requirements, although some need modification when compared with the original proposition made by their "inventors". This, then, considers the tests with sliding along a radius.

It is shown that the friction tests aimed at simulating frictional aspects in deep drawing consist of sliding along a radius, or sliding along a flat surface. All the tests shown can be reduced to two tests, namely a radial strip drawing test with varying boundary conditions and a flat die simulator.

References

3.1 Wojtowicz, W.J.
Sliding friction test for metalworking lubricants.
Lubrication Engineering, 11 (1955) 3, p.174-177

3.2 Wojtowicz, W.J.
Properties and control of drawing compounds for deep drawing.
Porcelain Enamel Institute Forum,
22 (1960), p.26-30

3.3 Emmens, W.C.
The influence of surface roughness on friction.
15th Biennial Congress IDDRG, Dearborn, Michigan USA, 16-18 may 1988

3.4 Blümel, K.
Surface interactions during pressforming as simulated by the strip draw test.
10th IDDRG Cong. Warwick 1978, p.297-301

3.5 Blanchard, G.
Description of a friction test used for cold rolled sheets and examples of applications.
Bulletin Cercle d'Etudes des Metaux
15 (1986) 12, p.19.1-19.12

3.6 Schey, J.A. McLean, M.
Critical evaluation of test methods for sheet metal working lubrication.
Winter Annual Meeting of ASME on Friction and Material Characterizations
27 nov. - 2 dec. 1988, p.25-32

3.7 Stine, P.A., Seward, R.E., Beyerle, M.T., Luken, P.C.
CAE sheetmetal formability model-predictive capability improved with experimentally derived input data.
Computer modelling of sheet forming process-theory, verification and application.
Warrendale, PA, USA, TMS-AIME,
1986 p.107-220

3.8 Reitzle, W., Schlicht, H.P., Drecker, H., Fischer, F.
Tribologie vorbeschichteter Bleche beim Tiefziehen.
Stahl und Eisen, 103 (1983), p.41-46

3.9 Witthüser, K.P.
Untersuchung von Prüfverfahren zur Beurteilung der Reibungsverhältnisse beim Tiefziehen.
PhD. Dissertation Universität Hannover 1980

3.10 Emmens, W.C.
A novel design friction tester
Publication Hoogovens Group R&D IJmuiden

3.11 Wilson, W.R.D. Cazeault, P.
Measurement of frictional conditions in lubricated stripdrawing.
Proc. North American Metalworking Research Conf., Columbus, Batelle 1976

3.12 Schmoeckel, D., Frontzek, H.
Reduction of wear on sheet metal forming tools.
Annals of the CIRP, 35 (1986) 1, p.195-198

3.13 Lee, C.H., Shim, H.B., Yang, D.Y.
Determination of frictional coefficient for sheet metal working and its application to strecch forming.
VI International Conference on Experimental Mechanics. Portland, Oregon, USA,
6-10 june 1988, vol. I, p.71-76

3.14 Fox, R.T., Maniatty, A.M., Lee, D.
Determination of friction coefficient for sheet metal materials under stretchforming conditions.
Metallurgical Transactions A
20A (1989) 10, p.2179-2182

3.15 Wang, X.J., Duncan, J.L., Davenpeck, M.L.,
Punch friction test for sheet metal working.
Journal of Applied Metalworking
3 (1983) 1, p.3-11

3.16 Ru, Z., Overby, D.
Strip friction experimental study on galvanized steel sheet.
16th IDDRG conf, Dearborn, MI, USA,
16-18 may 1988, p.85-90

3.17 Shi, M.F., Gerdeen, J.C., Aifantis, E.C.
On the coupling of deformation heating and contact friction during strain localization: Application to the strip friction test.
Res Mechhanica, 31 (1991), p.365-390

3.18 Siegert, K. Thomas, V.
Einsatz von Schmierstoffe zur Beeinflussung der Reibung beim Umformen von Karosserieteilen.
Use of lubricants to affect friction in the forming of auto body panels.
Aluminium, 63 (1987) 4, p.401-410.

3.19 Duncan, J.L., Shabel, B.S., Filho, J.G.
A tensile strip test for evaluating friction in sheet metal forming.
SME Paper 780391, SME, Dearborn, MI, USA 1978

3.20 Nine, H.D.
Testing lubricants for sheet metal forming.
Novel techniques in metal deformation testing.
ED. R.H. Wagoner Warrendale, PA
The Metallurgical Society AIME 1983, p.31-46

3.21 Brazier, W.G., Thompson, R.W.
The effect of die materials and lubrication on punch stretching and drawing forces of cold-rolled and zinc-coated steels.
SAE Technical Paper 850274 (1985)

3.22 Brazier, W.G., Thompson, R.W.
The effect of zinc coatings, die materials, and lubricants on sheet metal formability.
SAE Technical Paper 860434 (1986)

3.23 Keeler, S.P. Dwyer, T.E.
Frictional characteristics of galvanized steel sheet evaluated with a draw bead simulator.
SAE Technical Paper 860433 (1986)

3.24 Keeler, S.P.
Evaluating the lubricity of press shop lubricants on various types of galvanized steels.
28th Mechanical working and steel processing conference, Pittsburg, Pennsylvania 26-28 oct. 1986
The Metallurgical Society of AIME, Warrendale, Pennsylvania 1986

3.25 Meuleman, D.J., Zoldak, J.J.
The interaction of coated steels, die material, and forming lubricants.
SAE Technical Paper 860432 (1986)

3.26 Meuleman, D.J., Dwyer, T.E.
Die materials and treatments with electrogalvanized steels.
SAE Technical Paper 880369 (1988)

3.27 Keeler, S.P., Nine, H.D., Siekirk, J.F.
Formability criteria for selecting sheet metal lubricants.
SAE Technical Paper 880366 (1988)

3.27 Lindsey, J.H., Paluch, R.F., Nine, H.D.
The interaction between electrogalvanized zinc deposit structure and the forming properties of sheet steel.
Plating and Surface Finishing, 76 (1989) 3 p.62-69

3.28 Pawelski, O.
Ein neues Gerät zum Messen des Reibungsbeiwertes bei plastischen Formänderungen.
Stahl und Eisen, 84 (1964) 20, p.1233-1243

3.29 Sachs, G.
Ein neues prüfgerät für tiefziehbleche.
Metallwirtschaft, 9 (1930) 10, p.213-218

3.30 Wiegand, H., Kloos, K.H.
Der reibungs- und schmierungsvorgang der kaltformgebung und möglichkeiten seiner messung.
Werkstatt und Betrieb, 93 (1960) 4, p.181-187

3.31 Shima, S., Yamamoto, N.
Effect of tool/workpiece contact length on friction coefficient in metal forming.
ATP Conf. Stuttgart, FRG 24-28 aug. 1987
vol.II, p. 901-908

3.32 Kawai, N., Nagoya, K.
New lubricity evaluation method for metal forming by a compression-twist type friction testing machine.
Trans. of the ASME, Journal of Tribology,
109 (1987) 109, p.343-350

Chapter 4 Friction test development

4.1 Introduction

In the previous chapter, the demands for a friction test have been elucidated, and it has been shown that the majority of the well-known friction tests for deep drawing can be reduced to two basic types, namely radial strip drawing and the flat die simulator. This chapter deals with the technical details of the test methods chosen: technical set-up, data processing, validation and reproducibility of the measurements.

4.2 Technical set-up of the radial strip drawing simulator

Figure 22 shows the experimental set-up in detail. Here, we have chosen to present the experimental set-up first, and then detail the experimental procedure.

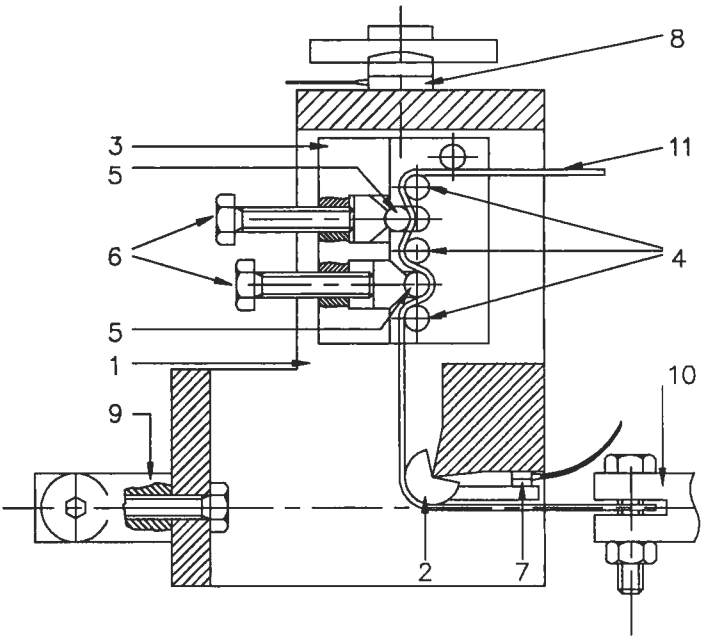

1 Housing
2 Radius
3 Braking mechanism
4 Fixed beads
5 Movable beads
6 Bolts
7 Piezo element
8 Piezo element
9 Fixed head
10 Moving head
11 Strip

Fig. 22 : The radial strip drawing apparatus

The set-up primarily consists of a housing (1), a braking device (3) to induce the back-pull force and the draw radius (2). The strip is numbered 11. The braking device is based on draw-bead action. The movable beads (5) can be adjusted by means of the bolts (6), forcing the strip to a certain deformation in this region. As a result of this, and the friction the strip encompasses while passing this braking device, a back-pull force is applied to the material currently being drawn over the radius. Material being drawn through the braking device is not allowed to enter the actual test zone.

In this set-up, three forces are measured by piezo elements 7 and 8, and the built-in dynamometer of the tensile tester.

The dynamometer of the tensile tester records the process force F_P required to draw the strip over the radius, see Figure 23. The back-pull force F_{Bp} is measured by piezo element 8. Finally, a third force is measured by piezo element 7. The radius can rotate freely around the knife edge on its mid-point. By simply evaluating the equilibrium of torque around this mid-point, the measured force can be worked out to the frictional induced torque by:

$$M_{Fr} = F_0 D \tag{4.1}$$

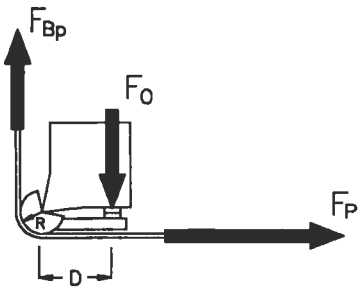

Fig. 23 : The measured forces

4.3 Data processing

4.3.1 Introduction

To work out this test method, the most common method is based on the pulley equation. This method is compared with a newly developed method in the following section. The derivation of the new method is similar to Sniekers and Ramaekers [4.1].

4.3.2 Integrative approach

Figure 24 shows the resulting force from the back-pull force and the process force. It can easily be seen that the resulting force imposed on the radius by the strip must equal:

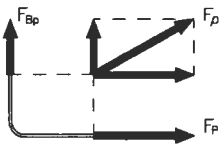

Fig. 24 : Resultant force imposed on the radius by the strip

$$F_\rho = \sqrt{F_P^2 + F_{Bp}^2} \tag{4.2}$$

Following this, this force is also imposed on the strip by the radius, see Figure 25. The resulting force can now also be split into the frictional part, along the surface of the cylinder in the virtual point of application, and a part perpendicular to the die surface, the contact force.

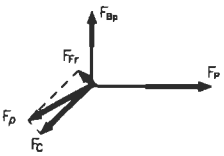

Fig. 25 : Equilibrium on the strip

$$F_\rho = \sqrt{F_C^2 + F_{Fr}^2} \tag{4.3}$$

or, rewritten:

$$F_C = \sqrt{F_\rho^2 - F_{Fr}^2} \tag{4.4}$$

combining (4.2) and (4.4):

$$F_C = \sqrt{F_P^2 + F_{Bp}^2 - F_{Fr}^2} \tag{4.5}$$

For the friction force, it is known from the equilibrium of torque on the radius element that:

$$F_{Fr} = \frac{M_{Fr}}{R} \tag{4.6}$$

with the assumption:

$$\mu = \frac{F_{Fr}}{F_C} \tag{4.7}$$

finally, to express μ in terms of the measured forces and geometrical quantities, this leads to:

$$\mu = \frac{\frac{M_{Fr}}{R}}{\sqrt{F_P^2 + F_{Bp}^2 - \left(\frac{M_{Fr}}{R}\right)^2}} \tag{4.8}$$

4.3.3 Pulley equation

This method is called the pulley equation after its original application, namely a means of calculating the pulley loss. Here, a swift derivation is presented. If the equilibrium of forces is taken along the sheet direction, the following is yielded, see Figure 26:

$$\sigma_\phi s b + \tau R b d\phi = (\sigma_\phi + d\sigma_\phi) s b \tag{4.9}$$

simplification leads to:

$$d\sigma_\phi = \frac{\tau R}{s} d\phi \tag{4.10}$$

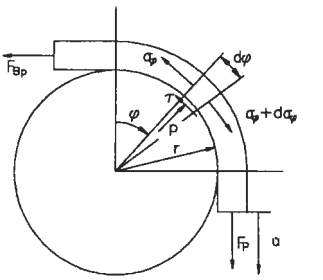

Fig. 26 : Equilibrium of forces

Perpendicular to the sheet, the equilibrium yields:

$$p R b d\phi = 2 \sigma_\phi s b \frac{d\phi}{2} \tag{4.11}$$

With the Coulomb friction rule:

$$\tau = \mu p \tag{4.12}$$

we can derive:

$$\frac{d\sigma_\phi}{\sigma_\phi} = \mu d\phi \tag{4.13}$$

Integration leads to:

$$Ln \frac{\sigma_{Bp}}{\sigma_P} = \mu \theta \tag{4.14}$$

A back pull force F_{Bp} is present at the entrance of the sheet to the die radius, while the process force F_p is active at the exit of the sheet from the radius. In the common pulley equation, the thickness is assumed to be constant, which implies that the ratio of stresses can be replaced by the ratio of the forces. Combined with rearranging, the following equation is obtained:

$$\mu = \frac{1}{\theta} Ln \frac{F_p}{F_{Bp}} \tag{4.15}$$

A disadvantage of this method is that the analysis assumes that the material behaves as a membrane, i.e. the material has no resistance to bending, which might be true for a rope, but is not generally true for sheet metal when being pulled over a relatively small radius. In literature [4.2], a review is given on modifications which have been proposed to improve the results achieved with this model; but a physical background is lacking.

4.3.4 Discussion

The pulley equation is valid for any contact angle. The integrative approach is only valid for a contact angle of 90 degrees, but can be easily extended. The validity of the methods is thoroughly investigated in the following paragraphs, but from a theoretical point of view, the integrative approach seems more valid than the pulley equation.

4.4 Radial strip drawing

4.4.1 FE Modelling

The FEM analysis was used to gain more insight into the mechanics of strip drawing. Figure 27 presents the problem studied, [4.3]. For this purpose, ABAQUS-implicit (4.9) was used. In the modelling of any metal forming process, the boundary conditions are of major importance, which is a reason for dealing with them first. The back-pull force is applied to the nodes forming the counter side, while a certain displacement (u) is prescribed at the nodes on the pulling side. Furthermore, node a is not allowed to move perpendicular to the direction of F_{Bp}, and similarly node b is not allowed to move perpendicular to the direction of u. Dimensions L_1 and L_2 have been chosen large enough so that local influences of the boundary conditions on the deformation in the bending and straightening zones are negligible. The tool itself is fixed in both rotation and translation.

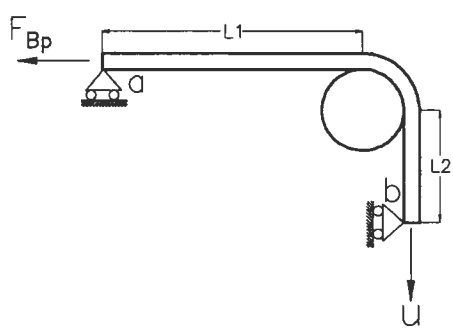

Fig. 27 : Boundary conditions

Except when explicitly remarked, all simulations in this paragraph (4.4) were carried out for Steel 15, with Youngs modulus (E) 210000 N/mm^2, Poisson constant (ν) 0.3, characteristic deformation resistance (C) 580 N/mm^2, pre-strain (ε_o) 0.006, and strain harden-

ing exponent (n) 0.23. The radius (R) of the tool was 5 mm and the thickness (t_o) of the strip 1 mm. The friction coefficient (μ) equalled zero. Finally, the back-pull stress (σ_o) was a quarter of the characteristic deformation resistance.

As stated, the strip drawing process is a plane strain problem, therefore plane strain elements were used. The assumption of plane strain has been checked with a 3D model, see Paragraph 4.5.1. The width strain appeared to be very small. The performance of both the 4-noded CPE4R and the 8-noded CPE8R was investigated. Both these plane strain elements use reduced integration to prevent locking phenomena caused by incompressibility constraints during plastic deformation. The matching interface elements (IRS21, IRS22) were used to describe the contact conditions.

The first step is now to investigate the influence of the element size. Principally, the use of square elements is preferred. Figure 28 gives the distribution of the strip thickness for 4-node and 8-node elements.

Note that larger element sizes are applied for 8 nodes than for the 4-node elements.

As can be seen, the thickness decreases in the bending and straightening zones, which emphasises the local character of the deformation process. On the roll, the thickness is constant. With decreasing element size, both sequences converge to approximately the same values for the thickness after bending and straightening. To reach the right solution with 4-node elements, the element size must be smaller than necessary for 8-node elements. This is because the quadratic order of 8-node elements makes them more efficient at describing bending. However, for the purpose of this study, the use of 8-node elements is disadvantageous. This can be explained if the contact pressure over the roll is considered, see Figure 29.

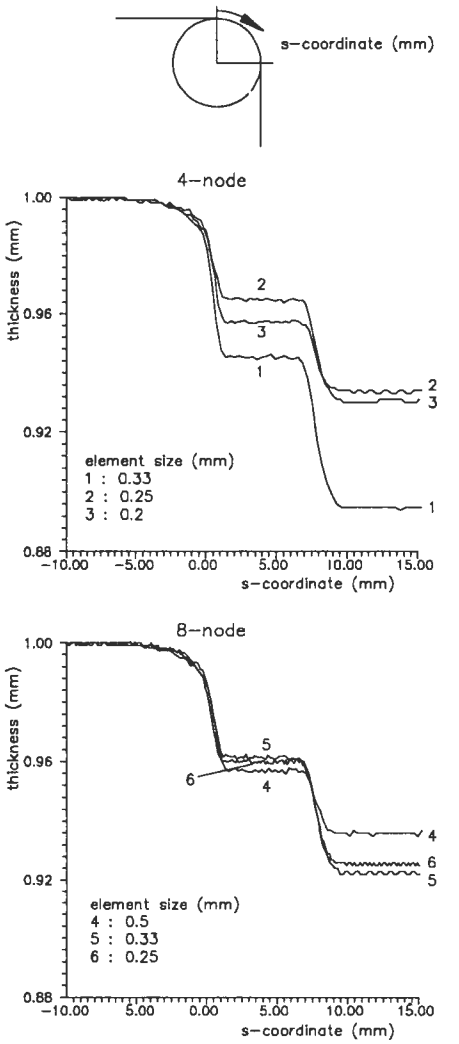

Fig. 28 : Influence of element size on calculated shape

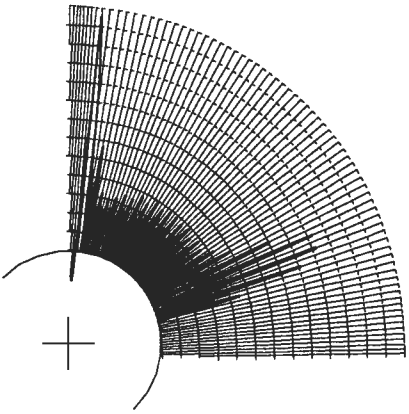

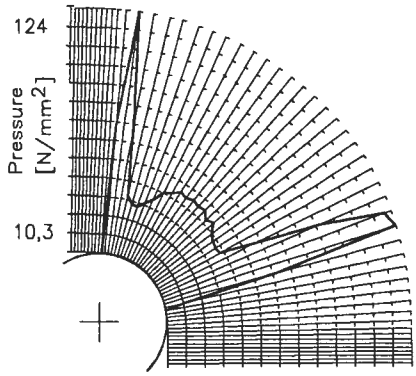

Fig. 29 : Contact pressure with 3-node interface element *Contact pressure with 2-node interface element*

The middle node of the 3-node element face does not contact the rigid surface of the roll, as often observed. If a complete element face is in contact with a rigid tool, the situation is comparable with a distributed pressure applied on the same element face [4.4]. This problem does not occur with the 2-node interface element. The contact pressure over the roll is characterised by high values at the beginning and end of the contact, and an approximately constant level in the middle. This again shows that the resistance to bending of the strip cannot be neglected.

Initially, the total strip in the FEM model is undeformed, contrary to the real physical process. This means that the pull side of the strip has to travel a certain distance before the process becomes stationary. First, the process force rises to a certain level, and becomes semi-stationary. After some further process travel, material already hardened in the bending zone, starts to pass the straightening zone, resulting in a second increase of the process force. After this the real stationary state has been achieved, see Figure 30.

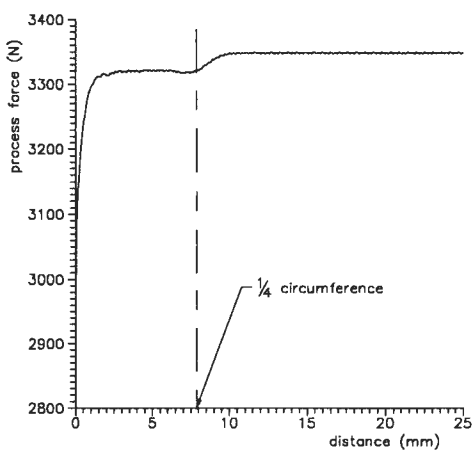

Fig. 30 : Process force in dependance of drawing distance

Comparison of several calculations and experiments in terms of total force, thickness after bending and straightening prove the model to be valid [4.5]. As an example, the thickness distribution on the strip is given in Figure 31, [4.5]. To be able to measure thickness differences, an experiment was performed on soft, relatively thick aluminium. Material data: Youngs modulus (E) 70000 N/mm^2, Poisson constant (ν) 0.3, characteristic deformation resistance 137 N/mm^2, pre-

strain (ε_0) 0.001, and strain hardening exponent (n) 0.033. The radius (R) of the tool was 5 mm and the thickness (t_0) of the strip 2.98 mm. The friction coefficient (μ) equalled zero. Finally, the back-pull stress (σ_0) was a quarter of the characteristic deformation resistance.

The distribution agrees well with the experimental data. From the previous explanation, it can be concluded that 4-node elements should be used. The element size used for further calculations was 0.25 mm. The strip has to travel more than a quarter of the circumference of the radius before the process is stationary.

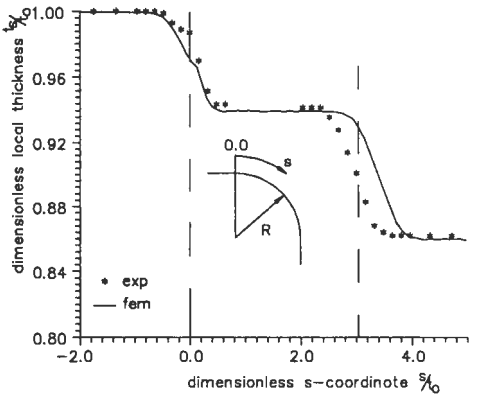

Fig. 31 : Thickness distribution

4.4.2 Comparison of methods of data processing by means of FEM model

As presented, the calculation of friction coefficients from the strip drawing experiment can be done in various ways. The next step is to determine which way is most appropiate. The previously-developed FEM model was used for this purpose.

To simulate strip drawing, a friction coefficient is needed as input for the FEM model. After the simulation, the strains and stresses are known in detail, anywhere in the process. The resulting forces can be calculated with the aid of the stress distribution. Except for these forces, the moment of force on the roll is needed to calculate the friction coefficient. This moment can be calculated with the pressure distribution on the roll.

$$M = R * b \sum_{i=1}^{i=last\ cont.element} \mu\, p\, l_i \tag{4.16}$$

Together with the known back-pull force, the quantities are known for the determination of the friction coefficient according to formula 4.8. Thus, what in fact is done is quite simple: An analysis is performed with a certain "input" friction coefficient, and then, after the simulation, the "output friction" coefficient is calculated from the resulting forces etc. In the ideal case, these two are identical: the straight line in Figure 32.

As stated, the simulations agree well in terms of process force and thickness distribution, the back-pull force is put into the model as a boundary condition. Here, the dimensionless back-pull stress σ_0 is given. If the 'input' friction coefficient agrees well with the calculated friction coefficient according to formula 4.8, that particular method proves to be valid for calculating friction coefficients from an experiment.

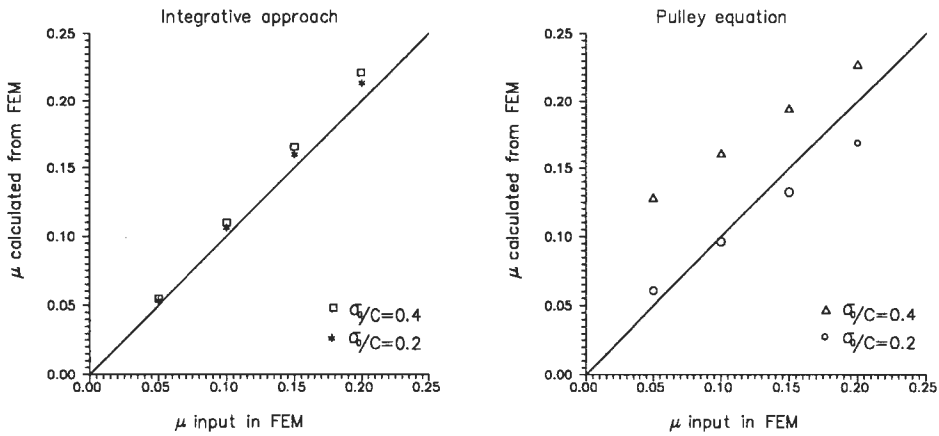

Fig. 32 : Comparison of input and output friction coefficient

Figure 32 gives the comparison of the 'input' and the calculated friction coefficients. As can be seen, the calculated friction coefficients tend to the ideal line for the integrative approach. The deviation is always of the order 6-7%. For the pulley equation, the results differ to a great extent, especially in the low friction regime. This means that the friction coefficients for strip drawing should be calculated according to the integrative approach.

4.4.3 Discussion

In the presentation of the experimental set-up and following the data processing, a constant μ value is used in the entire deformation zone, which does not necessarily need to be. It is possible, and also very likely, that different friction coefficients can be present because of, for instance, different contact pressures in the deformation and sliding zone, or because of the surface enlargement of the strip. This cannot be measured with the current method, so that local quantities therefore need to be measured.

Another point of consideration is the fact that lateral forces can also be present in the strip between the braking device and the radius, or between the radius and the moving head of the tensile tester. These forces are certainly present, as can be seen from Figure 29, because the strip does not contact the radius over the full 90°. Their influence seems to be relatively small, as can be seen in the comparison of input and output friction coefficients in Figure 32.

4.4.4 Conclusion

The experimental set-up and data processing have proven to be a step forward in obtaining valid (average) friction coefficients which do govern in the experiment itself, compared with experimental set-ups in which the frictional torque on the radius is not measured and, subsequently, data processing is done by means of the pulley equation.

4.5 Strip stretching

4.5.1 FE Modelling

Strip stretching is a special case of the common radial strip drawing test. The back-pull force is as high as necessary to prevent the back-pull side of the strip from moving. For the test set-up itself, this differs only little, but the material deforms in quite a different way. To describe this behaviour, another FEM analysis [4.6] was carried out with the Abaqus package, version 5.3.

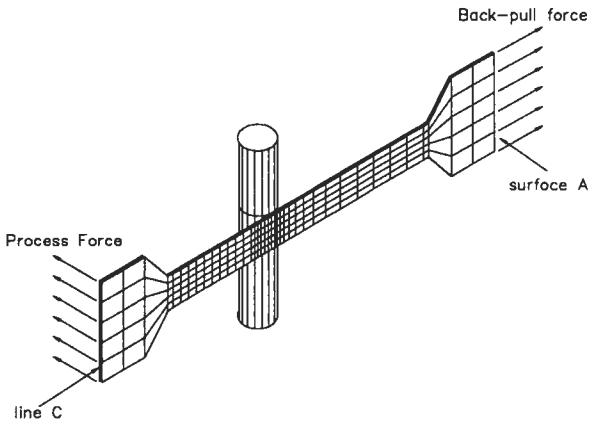

Fig. 33 : Bending the strip

The naming of the boundary conditions in Figures 33 and 34 is consistent with the radial strip drawing test. In the present analysis, however, this means that the back-pull force side, surface A, is not allowed to move in any direction.

The analysis was carried out as follows: First, the bending of the strip around the die radius was roughly modelled, by applying load to line C. This was actually performed in a number of steps by adjusting the direction of the force.

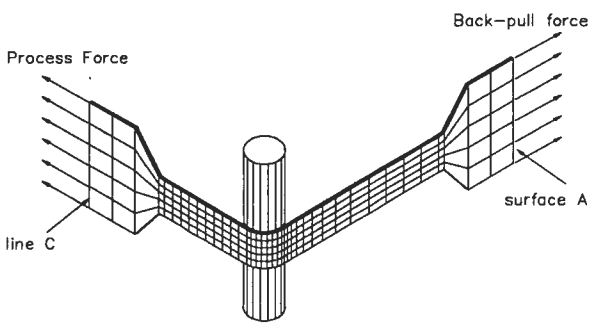

Fig. 34 : The actual strip stretching

After this, strip stretching was analysed carefully. Eight 8 nodes were used: 3-dimensional elements with reduced integration (C3D8R). The contact element was IRS4. Four layers of elements were applied over the thickness of the strip, while five elements were applied in the width direction of the strip. The region contacting the die radius has a higher density of elements. Figure 34 shows the element set-up for the beginning of the process.

Once the first step (bending along the radius) has been accomplished, the actual stretching of the strip can be carried out. Line C is given a certain displacement to start the stretching process. Surface A is still not allowed to move in any direction.

4.5.2 Comparison of methods of data processing by means of FEM model

Comparison of the data processing methods can be done in two different ways. First, the coefficient of friction can be calculated during the process. This gives two graphs for the calculated friction coefficients: according to the pulley equation, and according to the integrative approach. Following this, the average friction coefficients can be taken during a relevant period in the process for a number of calculations. If the latter is carried out for a number of input friction coefficients, insight is gained into the behaviour of the data processing methods for various values of the friction coefficient. Both these two evaluations are carried out in the next two paragraphs.

4.5.2.1 Evaluation of friction coefficients during FEM calculation

Figure 35 presents the evolution of the output friction coefficient with an input value of 0.025. The input value, calculations according to the integrative approach and the pulley equation are marked. As can be seen, the integrative approach is constant, slightly higher than the input value, while the pulley equation is quite unpredictable. The peak values are twice as high as the actual input value.

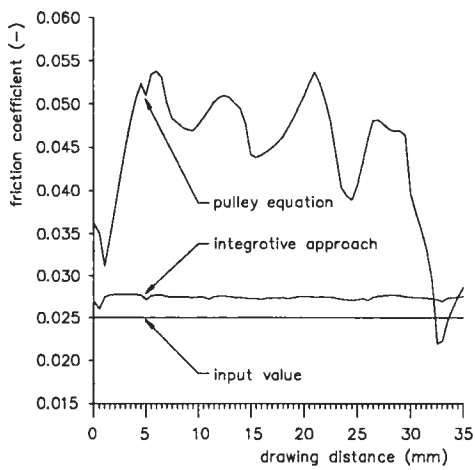

Fig. 35 : Evolution of the friction coefficient during FEM simulation, with input value μ=0.025

If an FEM simulation is performed with an input value of 0.2 for the friction coefficient, the behaviour of the pulley equation differs quite a bit, see Figure 36. The pulley equation now gives accurate results while the integrative approach shows a similar behaviour as shown in the previous graph. The simulation still results in friction coefficient values that are constant sligthly higher than the input value.

The small dimple in the friction coefficient at a drawing distance of 12 mm results from the fact that all material bent in the first stage of the modelling now has passed the radius.

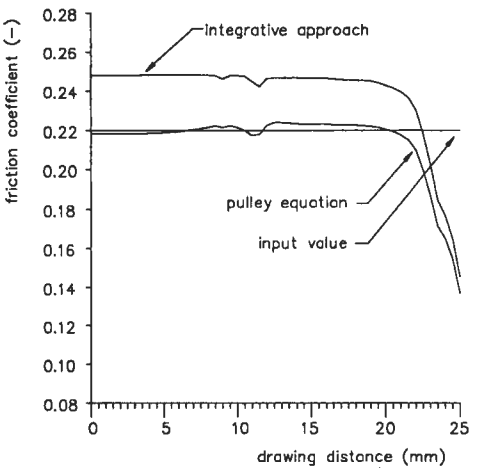

Fig. 36 : Evolution of the friction coefficient during FEM simulation, with input value μ=0.200

4.5.2.2 Comparison over a range of input friction coefficients

In the previous paragraph, we saw that the calculated friction coefficient according to the integrative approach is constant over a certain part of the strip stretching process. This part is now used to calculate an average friction coefficient for each numerical simulation. The results for radii of 6 and 8 mm are shown in Figures 37 and 38.

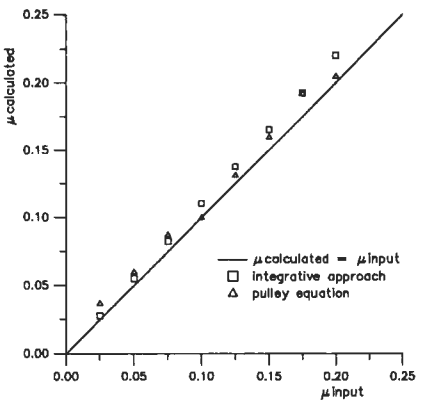

Fig. 37 : Comparison of input and output friction coefficient, in case of a radius of 6 mm

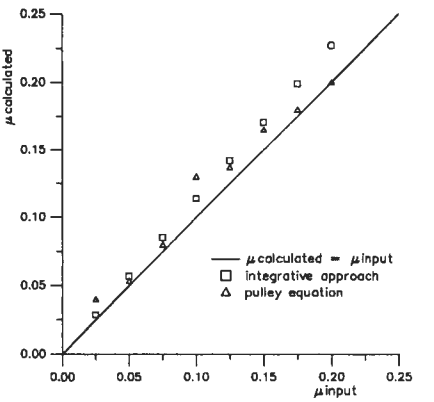

Fig. 38 : Comparison of input and output friction coefficient, in case of a radius of 8 mm

In figure 37, it can be seen that the integrative approach shows constantly 6-7% higher values than the input value. The pulley equation floats in a bandwith about 0.03 above the input value. If a die radius of 8 mm is taken, the constant deviation of the integrative approach is shown to be a little higher, while the pulley equation still moves within a certain bandwith.

4.5.3 Discussion

First, it has to be mentioned that the FE model has some disadvantages, because of the poor description of the bending part of the process. While considering strip stretching, the description of the process prior to the actual strip stretching is quite important. The material deformed in the bending operation will also be deformed in the stretching process.

However, if the effort is aimed at the comparison of data processing methods, this is of lesser importance, because the same data sets are used in the actual comparison. These data sets are both obtained from the FEM simulation, with the input value of the friction coefficient included. In the equations used for the evaluation of the friction coefficient from the calculated or measured forces, no model for the deformation of the material is included in the integrative approach. Some assumptions are included in the pulley equation, the major being the idealisation of the sheet material as a membrane.

In strip stretching, the pulley equation shows reasonable results, better than in radial strip drawing. The generally higher stress level in strip stretching will result in a lower gradient of the bending stress over the thickness of the sheet, so that the real world situation will be closer to the assumed behaviour.

4.5.4 Conclusions

To evaluate different data processing methods, strip stretching can be sufficiently described by FEM simulation.

In strip stretching, the pulley equation performs relatively well if the friction coefficient is not too small. If it is, large deviations are to be expected. The integrative approach gives a constant error of about 10 % over the whole range of friction coefficients. Research is being continued to reduce this.

4.6 Technical set-up of the flat die simulator

Again, the experimental set-up is given first.

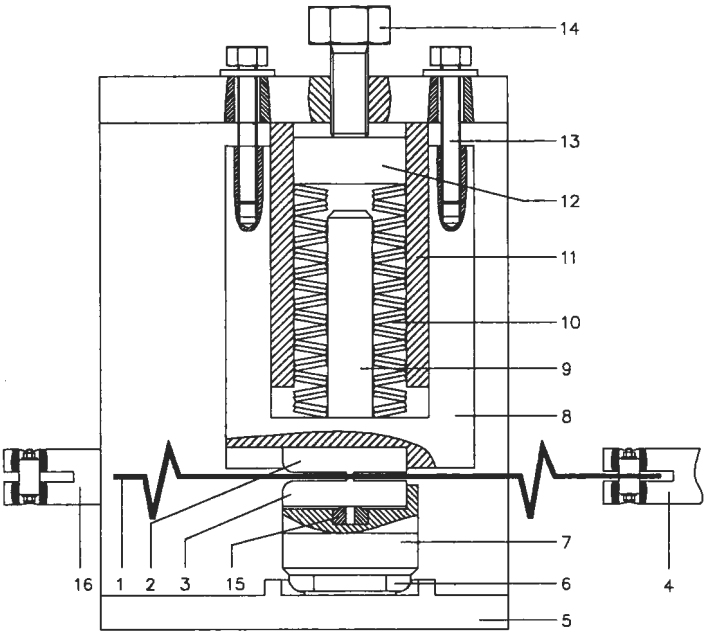

Fig. 39 : The flat die simulator

The strip (1) is pulled through the upper (2) and the lower (3) platens by the moving head (4) of the tensile tester. The lower platen is held by a block (7), which can rotate to some extent in the ball bearing (6). The ball bearing is mounted in the housing (5). The upper platen is mounted in a block (8), on which the spring package (10) exerts its force. The spring package is centred by a pin (9), and slides in a spring holder (11). The block (8) also slides over the spring holder. The spring package is compressed by the compression disc (12), which can be moved by a bolt (14). The bolts (13) are used to lift the entire block (8).

The process force F_P is measured in the fixed head (16) of the tensile tester by the built-in dynamometer, and the normal force F_N is measured by means of a piezo element (15), on which the lower platen rests.

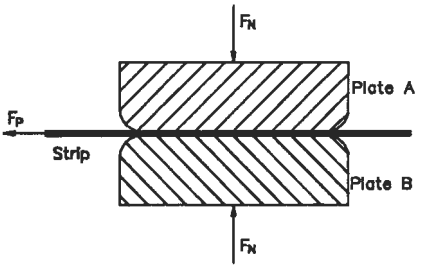

Fig. 40 : The measured forces

4.7 Data processing

With the flat die simulator, data processing is basically quite simple: it can easily be seen from Figure 40 that:

$$\mu = \frac{F_P}{2\,F_N} \tag{4.17}$$

Some normal force is lost in the measurement. The measured normal force relates to the actual normal force:

$$F_{Nm} = \left(1 - \mu\mu_T - \mu\mu_T \frac{e}{2L}\right) F_{Na} \tag{4.18}$$

Where μ is the friction coefficient present in the flat die drawing process, μ_T is the governing friction coefficient between the lower platen and the block. Furthermore, e equals the eccentricity of the middle of the strip from the middle of the test platens, and L represents the length of the test platens. The eccentricity of the strip will always be small in good experiments, while even a small eccentricity fast enlarges itself (which is easy to observe), leading to exclusion of the experiment. As far as the friction between the tool parts is concerned, measures have been taken to lower this friction coefficient. Furthermore, when performing a test, the normal force is applied first, before the strip is pulled through. As can be observed from the formula, the maximum error in the measurement of the normal force equals the friction coefficient present in the flat die drawing, times 100%. In this case, the friction coefficient between the tool parts has to equal 1, which will be highly unlikely.

4.8 FE modelling flat die simulator

To gain some insight into the distribution of the pressure in the flat die simulator, a short study has been made by means of FE. Again, Abaqus implicit, version 5.3 was used. Figure 41 shows the FE model, [4.7].

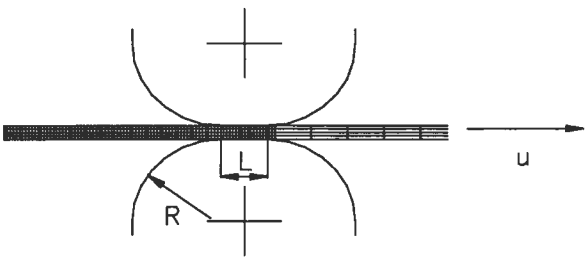

Fig. 41 : FE model flat die simulator

Four layers of elements CAX4R were used over the thickness of the strip. In the zone that may contact the die during the process, 400 small elements have been used. In the non-contacting regions at the left and at the right, 40 and 80 larger elements are used respectively. The contact element used is IRS22A. The upper and lower toolings have a flat part of size L. Tools are rounded off at both sides to a radius R.

By means of this model, it was first studied whether or not the radius R influences the pressure distribution to some extent.

In order to study this, three calculations were carried out, of which the resulting pressure distributions are shown in Figure 42. The calculations only differed with respect to the size of the radius R. This was varied at 0.5 mm, 3.0 mm, and 20 mm. L was always 1.57 mm. The strip thickness was 0.5 mm. The average normal pressure was 150 N/mm^2.

As can be seen in figure 42, the effect on the pressure distribution is small. The maximum pressures are all at the same level: 170 N/mm^2. The pressure only appears to be built up over a slightly smaller distance for R = 20 mm, which will be the result of the elastic deformation of the strip, which causes some thinning in the contact zone, leading to an enlarged contact, especially for larger radii.

The pressure distribution has a characteristic profile. At the left (right) the quick increase (decrease), where the strip comes into (leaves the) contact zone. Just beside this, a small peak can be observed, which might be caused by some local shear, which takes place locally. In the middle part of the graphs, a slightly declining pressure can be observed. The pressure decreases about 15%. This is because of the momentum induced by the frictional shear stresses, which must be compensated for by an uneven pressure distribution.

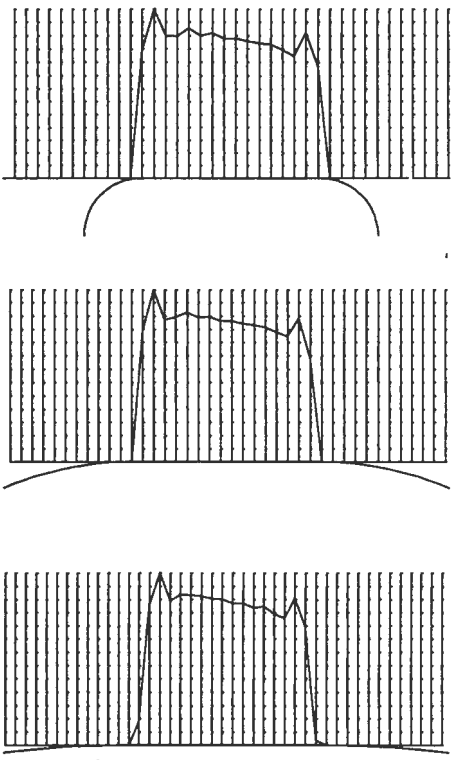

Fig. 42 : The pressure distribution, for R = 0.5 mm, R = 3.0 mm, and R = 20 mm, top - down.

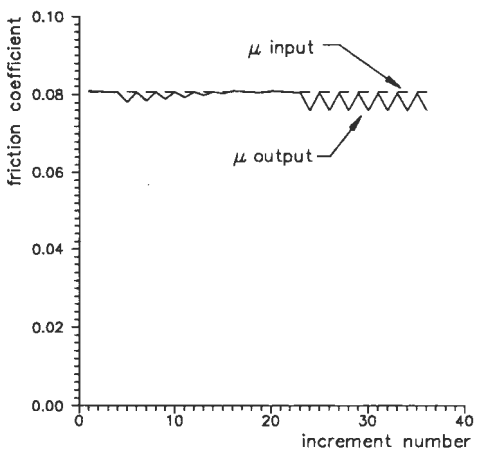

Fig. 43 : Evolution of the friction coefficient during FEM simulation

4.9 Validation of data processing

The previously-mentioned model was also used to compare the input friction coefficient with the output friction coefficient, calculated from the forces obtained from the FE simulation. Here, it is chosen to present the evolution of the friction coefficient during one process, see Figure 43. Conditions are identical to those mentioned in the previous paragraph, with R = 3 mm.

It appears that the output friction coefficient is close to the input friction coefficient. The maximum deviation is in the order of 5%.

4.10 Discussion

Although the flat die simulator seems relatively simple, on second thoughts, some problems arise. As shown, pressure decreases in the sliding direction. Emmens [4.8] already mentioned this problem, and shows that the pressure drop Δp related to the average pressure p is:

$$\frac{\Delta p}{p} = 6\,\mu\,\frac{d}{l} \tag{4.19}$$

Where l is the sliding length, and d the distance between the contact surface and the point of rotation. The problem can be solved by attaching both tooling parts to the fixed world, such that momentum can be absorbed. However, this will lead to problems when the strip thickness is unevenly distributed.

4.11 Conclusions

By using the FE model developed, the drawing of a strip through the flat die simulator can be simulated very well. The data processing method proves to be valid.

In the design of a flat die simulator, dimensions have to be chosen with great care if a tooling part can rotate freely. If dimensions are incorrectly chosen, the assumed uniform pressure distribution is not present. With tooling parts that are not allowed to rotate, great care must be taken to avoid local thinning.

4.12 Experimental practice

4.12.1 Test set-up

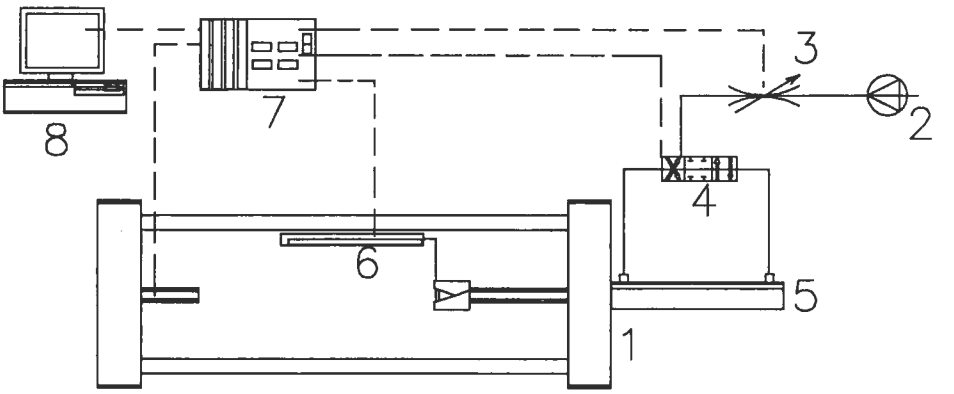

Fig. 44 : Overview of the test set-up

Figure 44 shows the main components of the test set-up. The main part of the system is a hydraulically driven tensile tester (1). This tensile tester was specially built for this research, because of the large variation in speed that can easily be obtained with hydraulically driven components.

The hydraulic power is achieved by means of a hydraulic pump unit (2), which delivers oil to the flow control valve (3). The flow control valve can be adjusted to regulate the flow, which is a necessary feature to control the speed of the cylinder (5). The oil not required by the cylinder is returned to the reservoir.

Switch (4) is placed between the cylinder (5) and the valve (3) to move the cylinder backwards or forwards, or let it remain stationary by returning the oil to the reservoir. The current position of the cylinder head is measured by means of a linear potentiometer (6). This device gives a signal to the control and measurement rack (7), which in turn is controlled by the computer with labcard (8). Signal lines are drawn dashed.

The speed is measured from the subsequent positions of the cylinder head and, if necessary, the flow regulator, valve V, is adjusted. The measurement also provides the signals from the piezo elements built into the test units, and the signal from the dynamometer built into the fixed head of the tensile tester. For this purpose, the measurement and control rack is equipped with two capacity - voltage transducers, one bridge amplifier, one connection channel for the potentiometer, and the control card of the flow regulating valve. The latter is also connected to some microswitches, which limit the stroke of the process, or detect unallowable movements of the cylinder before they become harmful. A tailor-made program has been developed for the control and evaluation of the tests.

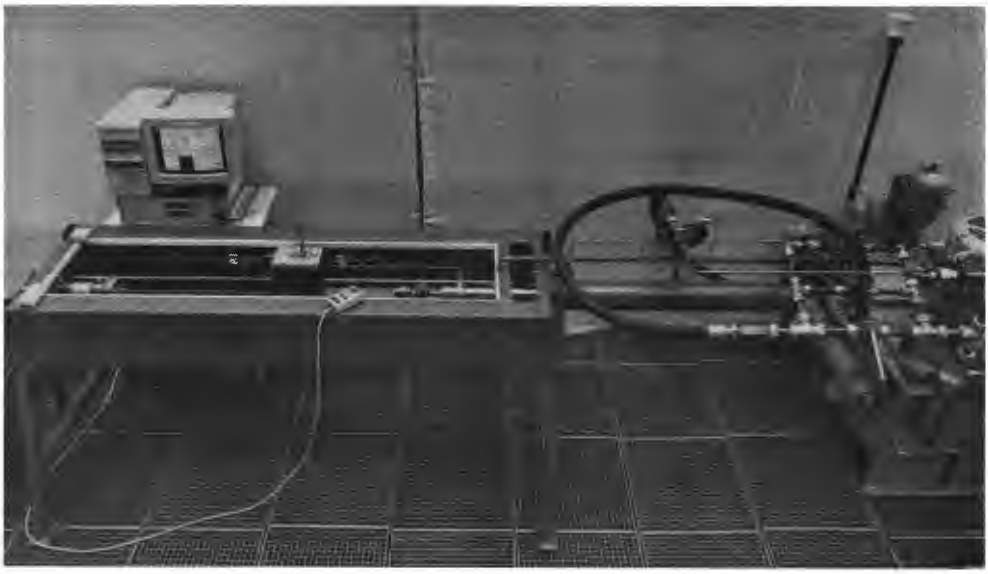

Fig. 45 : Test set-up

Figure 45 shows a photograph of the test set-up. The two previously-mentioned test units are mounted in the tensile tester. Figure 46 shows the radial strip drawing simulator in total, while Figure 47 shows the friction element in detail.

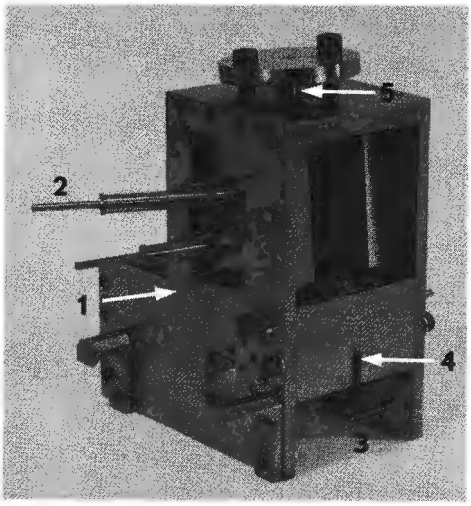

Fig. 46 : The radial strip drawing simulator

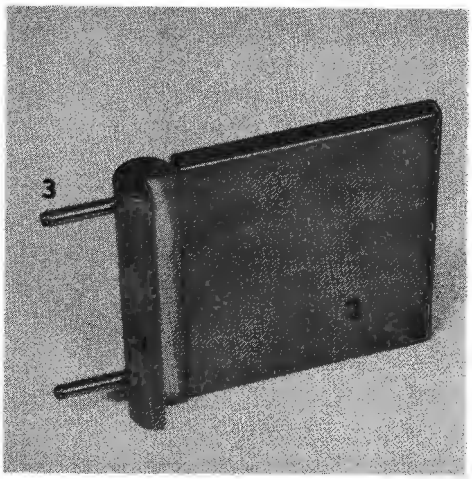

Fig. 47 : The friction element connected to the rocker

Figure 46 shows the fixed (1) and movable (2) beads, the rocker (3) to which the friction element is connected, and the piezo-elements for the measurement of the frictional torque (4) and the back-pull force (5). In Figure 47, the construction of the friction element (1) to the rocker (2) by means of two pins (3) is given in detail.

The flat die simulator is similarly shown in Figure 48, and both parts of its friction element in Figure 49.

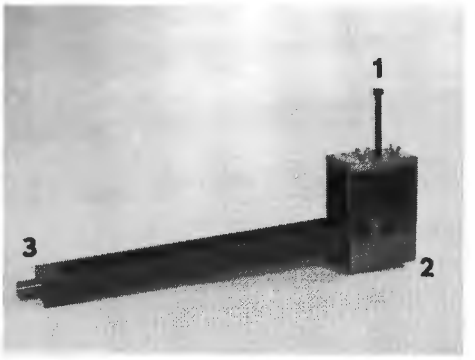

Fig. 48 : The flat die simulator

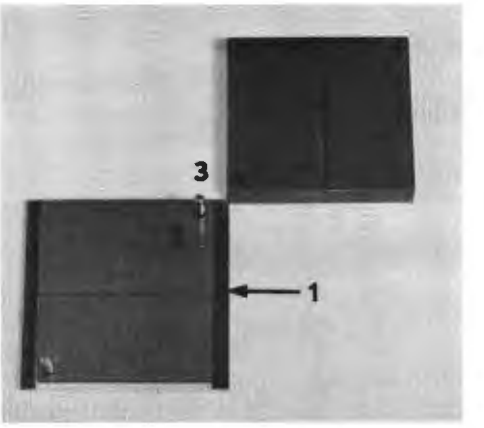

Fig. 49 : Both parts of the friction element

Figure 48 shows the screw (1) by which the spring package is compressed inside the housing (2). At (3) the die simulator is connected to the fixed head of the tensile tester. The friction element for the flat die simulator, as shown in Figure 49, has a contact surface (1) which is slightly higher than the base surface (2). If alignment problems are present, it is possible to use two sliders (3) to achieve better alignment.

4.12.2 Preparation of test strips

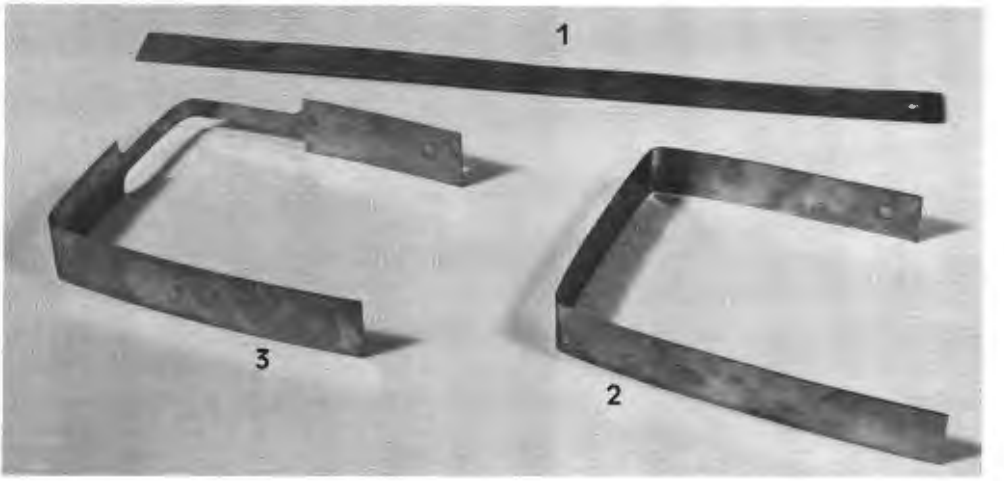

Fig. 50 : Test pieces: 1 flat die simulator, 2 radial strip drawing, 3 strip stretching

Test pieces are generally made of strip, or cut from sheet to strip. The maximum strip thickness is about 2 mm, depending on the yield strength of the material. The width of the

strip is a maximum of 40 mm. The length of the strip is about 400 mm. Figure 50 shows the strips. To mount the strips, a hole of 8 mm diameter was used.
Note that the strips for radial strip drawing and strip stretching are pre-bent. For thinner strips, this is not necessary. Furthermore, the strips used for strip stretching have reduced width in the tested part of the strip. To achieve sufficient force for keeping the strip fixed in this case, the width of the strip must be one third of the width of the strip in the draw-bead part of the braking device. The strips must be deburred after cutting and/or milling.

For lubricant suppliance on the strip, a small tool has been made, see Figure 51. This tool basically consists of two rollers (1), which can be made of various materials such as teflon, tool steel or even soft cloth.

To achieve similar squeezing at each point when the strip is pulled through it, the upper roller can adjust itself to a certain extent as a result of a flexible connection of the upper holder (2) with the lower holder (3). The upper holder can be made heavier by means of extra weigths (4) which can be mounted on top of the holder.

Different techniques are available to achieve reproducible amounts of lubricant on the strip. These techniques are also applied in industrial practice, and vary from no additional lubrication to rolling or spraying lubricant. Here, we chose to use a rolling lubricant suppliance, directly prior to the test. Spraying in a reproducible manner is difficult and costly. Commonly applied laboratorium techniques such as dip, drip and dry suffer from both ageing of lubricant and influences of environmental conditions such as humidity.

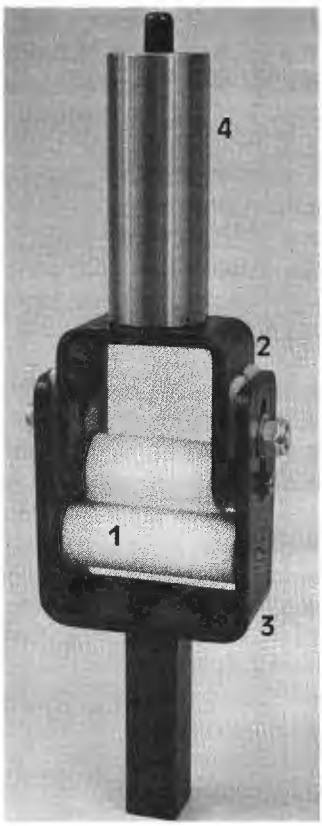

Fig. 51 : Oiling device

4.12.3 Running the test

When the strip is mounted in the test unit, the contact pressure must be adjusted. With the flat die simulator, this is done by compressing the spring package. The maximum total force to be supplied by the spring package is 20 kN. Division by the contact area then gives the contact pressure. For the radial strip drawing test, the back-pull force is controlled by adjusting the movable beads. The desired speed of the cylinder is input to the computer program, which starts to adjust the flow controlling valve until the desired speed is achieved after the process is started. For this adjustment, a preliminary (loose) stroke of 50 mm is used.

4.12.4 Reproducibility

Reproducibility measurements have been carried out. Typical results are shown in Figure 52, for radial strip drawing experiments.

As can be seen, reproducibility is approximately 0.01. As more experiments were carried out, the reproducibility appeared to be approximately 10% of the nominal value, as a rule of thumb.

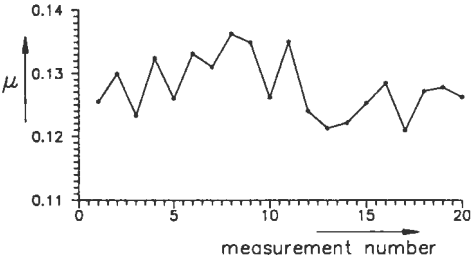

Fig. 52 : 20 repeated experiments

4.13 Conclusions

Three typical test methods have been under investigation, considering their design and data processing. It as been shown by means of FEM analysis that:

- The data processing for the radial strip drawing simulator and the strip stretch test according to the pulley equation gives poorer results than according to the integrative approach.
- The data processing for the flat die simulator holds well.
- When sufficient care is given to the geometrical construction, pressure distribution is quite uniform for the flat die simulator.
- Pressure distribution for the radial strip drawing simulator and the strip stretch test is characterised by two peaks because of bending and straightening.

In this chapter, friction coefficients are derived for the test methods, no information is yet present to determine the validity of these friction coefficients for the actual deep drawing.

References

4.1 Sniekers, R.J.J.M., Ramaekers, J.A.H.
Experiments on strip drawing with stationary bending and straightening.
Proc. 4th ICTP, 1993, Beijing

4.2 Vallance, D.W., Matlock, D.K.,
Application of the bending-under-tension test to coated sheet steels.
Journal of Materials Engineering and Performance, 1 (1192) 5

4.3 Smits, H.A.A
Striptrekken. Onderzoek naar lokale effecten.
Eindhoven University of Technology
report WPA-1556 (1993)

4.4 MARC Analysis and Research Company
Volume A: User information.
Rev. K.6, page 40.

4.5 Hoogenboom, S.M., Sniekers, R.J.J.M.
Analysis of stationary bending and straigtening during strip drawing.
Proc. 4th ICTP, 1993, Beijing.

4.6 Barten, P.L.W.M.
Stripstrekken. Onderzoek naar de wrijvingscoefficient met EEM.
Eindhoven University of Technology
report WPA-120006 (1994)

4.7 Barten, P.L.W.M.
Toepasbaarheid van variabele wrijving bij dieptrek-simulaties.
Eindhoven University of Technology
report WPA-120033 (1995)

4.8 Emmens, W.C.
A novel design friction tester.
Publication Hoogovens Group R&D, IJmuiden, The Netherlands.

Chapter 5 Local friction coefficients

5.1 Introduction

The previous chapter describes research that was aimed at obtaining valid coefficients of friction. This validity has only been proved for the friction test itself. The question that now arises is: **To what extent is a value for the friction coefficient, obtained in a certain experiment, valid as input for the simulation of a comparable process?**

To tackle this question, the most difficult problem to deal with is the difference in circumstances between the experiment and the process to be simulated. Differences exist in contact pressure distribution, velocity distribution and surface roughening, etc.

As an example, one can consider the comparison of the flat die simulator test and the radial strip drawing test. Both these tests are commonly used to determine friction coefficients for the deep drawing process. If both tests are compared (see also Chapter 4), the differences (except geometry) include those mentioned in the previous paragraph.

As stated before, the coefficient of friction is currently seen as a constant in most FEM simulations. In order to improve this, a method will be developed in which the friction coefficient is pressure dependent. This pressure dependency is chosen to compare the flat die simulator test with the radial strip drawing test.

The aim of the research was to develop a method by which dependencies of the coefficient of friction on local quantities can be described, as already mentioned by von Stebut [5.1], and Lenard [5.2]. The starting-point is that the effect of contact pressure on the friction coefficient can be measured by means of flat die simulator experiments. Note that this is actually only possible with the flat die simulator.

Following this, the values for the friction coefficient obtained from these measurements are interpreted by means of statistical software, which leads to an expression of the friction coefficient as a function of pressure.

Finally, this equation is incorporated in the Abaqus package, and some comparative analyses are carried out for radial strip drawing.

5.2 Coulomb friction in Abaqus

5.2.1 Coulomb friction in a user subroutine

5.2.1.1 Introduction

To implement a non-constant coefficient of friction in FEM package ABAQUS, the user subroutine UFRIC must be supplied to redefine the Abaqus command FRICTION.

This sub-routine is called for each contacting node at every iteration. In this work, the shear stress is taken to be dependent on local contact pressure (p) and the total slip. The user must specify the shear stress τ and its partial derivatives with respect to p and γ. The latter are required to compute a consistent tangent stiffness matrix.

5.2.1.2 UFRIC with Coulomb friction

For Coulomb friction in a situation shown in Figure 53, the relation between friction shear stress τ in relation to slip γ is characterised by the graph represented in Figure 54. In this graph, $\tau_{max}=\mu p$.

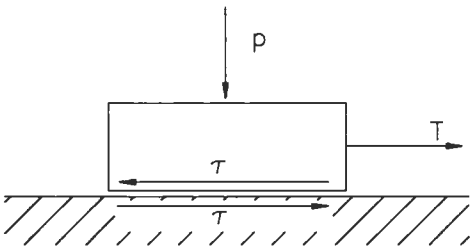

Fig. 53 : Common friction situation

As stated in the previous paragraph, one of the variables to be evaluated in a call to the subroutine is the partial derivative of friction shear stress to slip.

As can be observed, this value will cause problems in the region of slip equal to zero (γ = 0). When slip equals zero, the value of the partial derivative of friction shear stress to slip equals infinity. When this is the case, the FEM calculation becomes unstable and the simulation fails.

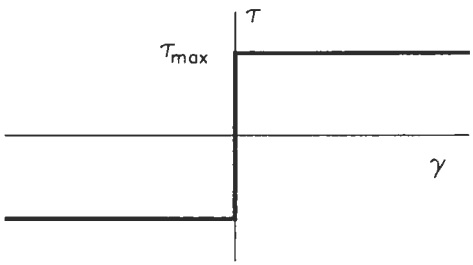

Fig. 54 : Ideal relationship between slip and friction shear stress

A common solution to this problem, also implemented in standard ABAQUS, is the introduction of a so-called elastic stiffness.

As can be seen in Figure 55, the value of the partial derivative is now limited because the "ramp" function at γ = 0 is replaced by a linear function in the region $-\gamma_{crit} \leq \gamma \leq \gamma_{crit}$. The physical implication of this is that relative movement will exist in the absence of a fully developed friction shear stress.

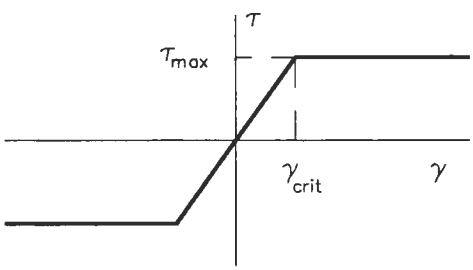

Fig. 55 : Stiff elastic behaviour

Still, some discontinuities in the value of the partial derivative of friction shear stress to slip exist. While these do not cause large problems in standard Abaqus, they do cause problems in some cases in the implementation of variable friction coefficients.

5.2.2 A continuous dependence of shear stress to slip

In this work, it was chosen to describe the friction-induced shear stress as a function of the slip as a hyperbolic tangent, Barten [5.3], see Figure 56:

$$\tau = \mu p \tanh\left(\frac{\gamma}{\alpha}\right) \qquad (5.1)$$

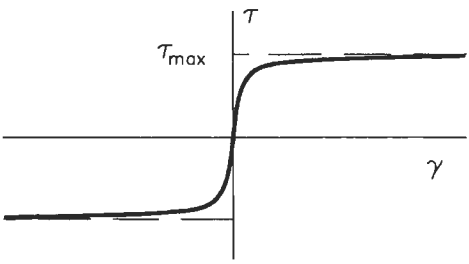

Fig. 56 : Friction shear stress described by hyperbolic tangent

In this equation, there is no longer a specified elastic slip boundary. The parameter α controls the elastic stiffness and typically has a value of approximately 10% of the element length. The maximum shear stress is a limit never reached, but closely approximated (less than 1% error when γ equals 3α).

One advantage of this method is the continuous partial derivatives, resulting in a more stable, and therefore faster simulation. The disadvantage is of course the absence of a sharp boundary between elastic slip and maximum friction.

A more fundamental aspect is that this is only allowed in cases where there is no reversal in the slip direction, while otherwise wrong frictional behaviour is implemented. In Appendix A, proof is given that the application of Formula 5.1 is allowed in the case of deep drawing [5.4].

5.2.3 Checking the effects of 'tanh'

To check the two disadvantages mentioned in the previous paragraph, a normal deep drawing simulation was carried out first with standard Abaqus Coulomb friction, and then with Abaqus and the user subroutine Ufric, in which equation 5.1 was incorporated. The reason why we chose to check this with deep drawing simulation instead of the relatively simple radial strip drawing simulation was to check if any effects of a reversal of the slip direction would be present and have a large influence.

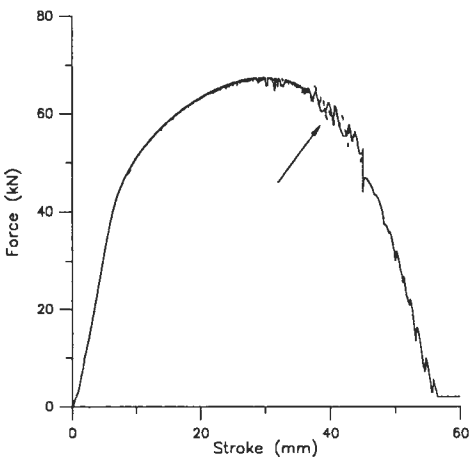

Fig. 57 : Punch force - punch stroke diagram for both user subroutine (drawn line) and standard Abaqus (dashed line).

The situation analysed is given in subparagraphs 6.2.2 and 6.3.1. Figure 57 presents both the punch force - punch stroke graphs. As can be seen, the differ-

ences between the two methods are negligible; the graphs virtually coincide with each other. Differences can only be observed at the place marked with an arrow. However, at this stage of the process, the elements passing the curvature are quite large, which causes the sawtooth shape of the curve. The differences here are merely because of this effect.
Subsequently, the contact pressure distributions were evaluated. Figure 58 gives the overall picture. In general, with a transition from a flat to a curved surface, peaks can be expected in the contact pressure distribution. The absolute height of these peaks cannot be calculated accurately [5.3].

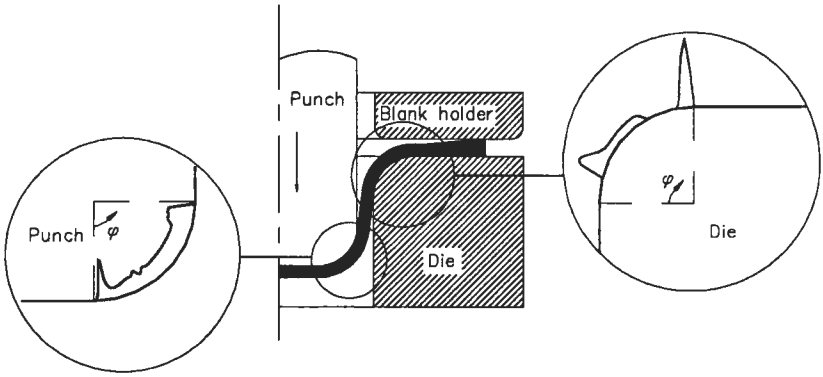

Fig. 58 : Calculated contact pressure distribution

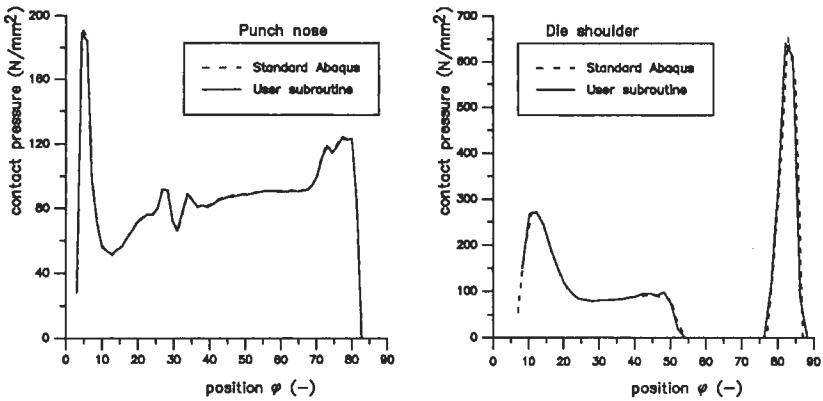

Fig. 59 : Calculated pressure distributions on tool curvatures in detail.

Figure 59 gives the contact pressure distributions in more detail. As can be seen, even on a local basis, the difference between standard Abaqus and the User subroutine is small. In general, it can be stated that the influence on the pressure distribution and the punch force - punch stroke diagram is small; the effect of the implementation of a smooth dependence of friction shear stress on the slip is negligible.

5.3 Flat die simulator

5.3.1 Introduction

Because the flat die simulator is the only experiment in which both contact pressure and sliding speed can be adjusted independently, it is very useful for determining the effect of these local quantities on the friction coefficient.

Experimental results from this test were used as a first step in applying variable coefficients of friction in FEM simulations for deep drawing. This was done by using the contact pressure distribution calculated in paragraph 4.8 with standard FEM. Because the slip velocity is constant, the dependence of friction on velocity does not need to be taken into account, providing all experiments are carried out at the same speed.

When the expected minimum and maximum contact pressures are known, flat die simulator experiments are carried out which comprise the entire range of average contact pressures. Then, by means of regression analysis, a relationship can be derived in which the friction coefficient is given as a function of the contact pressure. Subsequently, this is incorporated in the user subroutine Ufric, and a new FEM simulation is made, now including variable friction coefficients. From this FEM analysis, the average friction coefficient is obtained, as shown in Chapter 4.

5.3.2 Experiments

All experiments were carried out with a workpiece material 18 12 Cr Ni, tool material Philips N1019, and a lubricant mix of 70 % Ipro 484 and 30 % Tellus R10. This combination of materials and lubricant is according to industrial practice. Lubrication was according to paragraph 4.12.2.2. The drawing speed in all experiments was 65 mm/s. Dimensions R and L of the test tool (see Figure 41) were 1 mm and 1.57 mm. Material data is given in paragraph 6.2.2.

From a preliminary FEM simulation, it was learned that the contact pressure is roughly in the range of 0-200 N/mm^2. Using this as a starting-point, flat die simulator experiments were carried out that covered the range of 50 to 250 N/mm^2. With the contact tools specified, a pressure lower than 50 N/mm^2 could not be realised reproducibly. At contact

Table I: Flat die simulator friction coefficients, average value of three experiments

contact pressure p [N/mm^2]	friction coefficient μ [-]
54	0.016
56	0.023
109	0.060
111	0.061
143	0.078
147	0.080
218	0.098
220	0.099
247	0.099
250	0.099

pressures higher than 275 N/mm^2 (in flat die simulator experiments), the material is compressed between the contacting tools. The resulting experiments are given in Table I.

Subsequently, these measurements have been processed by means of multiple regression analysis. The following relationship was derived for the friction coefficient in dependence of the contact pressure.

$$\mu = 0.036 + 0.00114p - 2.4E\text{-}06p^2 \quad (5.2)$$

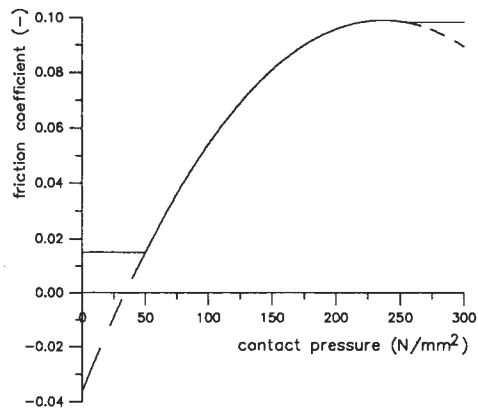

Fig. 60 : Coefficient of friction in relation to the contact pressure

Comparing values calculated with this formula and the experimentally obtained values, the maximum error appears to be 0.004. The above formula is plotted in figure 60. The fitted function is drawn dashed outside the experimentally covered area. The values for the friction coefficient are then taken as at the boundary.

According to the formula presented, the friction coefficient becomes negative at contact pressures below 50 N/mm^2, which is of course unrealistic.

5.3.2.1 Correctness of implementation of regression function

The relationship between the friction coefficient and the contact pressure is determined by means of flat die simulator experiments. However, a certain contact pressure distribution is also present in the flat die simulator. To evaluate the correctness of the implementation, a similar FEM simulation as shown in paragraph 4.8 was used, with both a 'smoothed' relationship between slip and frictional shear stress and dependency of the friction coefficient on the contact pressure.

As can be seen, the implemented method is close to the simulated experiment, with an average contact pressure of 147 N/mm^2 and a friction coefficient of 0.080.

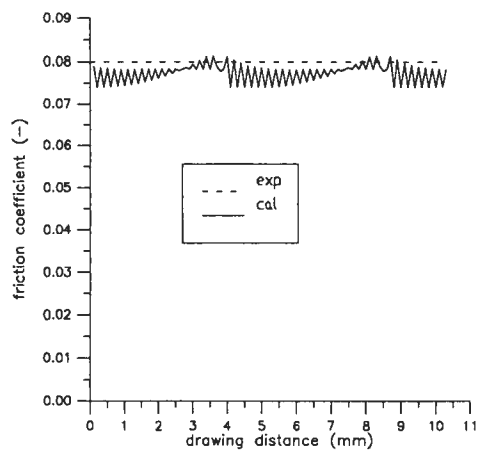

Fig. 61 : Friction coefficient in flat die simulator experiment

5.4 Comparing radial strip drawing experiments with flat die simulator experiments

It is known from experiments that flat die experiments generally produce lower friction coefficients than radial strip drawing experiments. By means of the methods presented here, it will be possible to eliminate one source of difference, namely the different contact conditions.

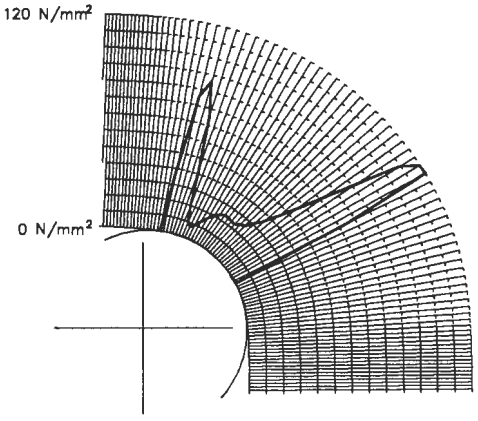

Fig. 62 : Contact pressure distribution in radial strip drawing

The radius of the tool in the analysis is 3 mm, and the strip thickness equals 0.5 mm. Material properties are listed in paragraph 6.2.2.

Figure 62 gives the contact pressure distribution for a radial strip drawing simulation that was carried out in the same conditions as the experiments in Paragraph 5.2, considering workpiece material, tool material, tool surface finishing and lubrication. The difference exists in the fact that one-sided contact between tool and workpiece is present. As can be seen in the graph, contact pressures are in the range 0 to 120 N/mm^2. These conditions were also realised in an experiment, carried out three times, from which an average friction coefficient of 0.135 was obtained. This value for the friction coefficient was also used in the simulation presented in figure 62.

At first glance, it can easily be observed that this friction coefficient is generally higher than the friction coefficients obtained from Figure 60, which are derived from the similar flat die simulator experiments.

However, the question that remains is how much the resulting friction coefficient will differ from the experimental one.

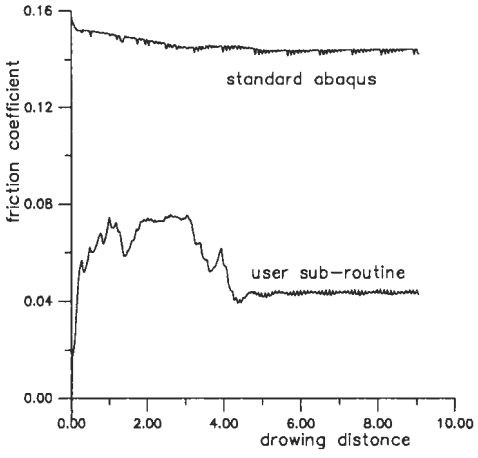

Fig. 63 : Comparison of friction coefficients from two simulations

Figure 63 plots the simulation as described. As can be seen, the average value for the simulation with the user subroutine is approximately 0.045. This is clearly lower than the average value of the experiment, 0.135. The standard Abaqus simulation, with input 0.135, results in an output friction coefficient of 0.148.

5.5 Discussion

With respect to friction coefficients obtained from the radial strip drawing tester, it must be noted that the calculated value of the friction coefficient is generally too high, see Figure 32 in Chapter 4. From the construction of the flat die simulator, it can be noted that some frictional signal will be lost as a result of construction properties, but this effect is generally only a few percent, as known from initial testing. Although both notes have a contributing effect to the gap in friction coefficient, they do not cause the entire difference. With respect to the flat die simulator experiments, it has to be noted that the contact length between tool and test piece was only 1.5 mm in these tests. This small contact length was necessary to achieve the maximum contact pressure of 250 N/mm^2. The small contact length did, however, lead to problems at low contact pressures, because the total clamping force cannot be controlled accurately enough at low values.

5.6 Conclusions

As shown, it is possible to implement a friction coefficient that depends on a certain number of variables. When this method is applied to simulate the same process (as also used for the experiments to obtain the friction coefficients), the results agree well.

When friction coefficients measured in dependence of the contact pressure by means of a flat die simulator are used in the simulation of the radial strip drawing process, it appears that the resulting output friction coefficient calculated from this simulation is too low, i.e. differs too much.

As a final conclusion, it can be stated that the applicability of friction coefficients obtained from flat die simulator experiments to other processes is low.

References

5.1 Stebut, J. von, Roizard, X.
Influence of test conditions on friction and sheet surface micro-mechanical response in strip drawing of uncoated mild steel sheets.
IDDRG WG Meeting, Linz, Austria, 1989

5.2 Lenard, J.G.
The effect of temperature on the coefficient of friction in flat rolling.
Annals of the CIRP, 40 (1991) 1

5.3 Barten, P.L.W.M.
Toepasbaarheid van variabele wrijving bij dieptrek-simulaties.
Eindhoven University of Technology
report WPA-120033 (1995)

5.4 Habraken, F.A.C.M.
Personal communication

Chapter 6 Friction coefficients for deep drawing

6.1 Introduction

In FEM simulations of deep drawing, the current methods of achieving friction coefficients that serve as input data are quite different. The most simple practice is the application of rough guidelines or figures from literature. A more accurate method is to carry out one or more experiments on a single test device, under conditions similar to the deep drawing circumstances, such as material pairing, surface finish and lubricant.

Currently, the most valid method is to perform one or more tests on various testing devices. The variety in testing devices is then aimed at achieving better similarity between tests and certain regions in the deep drawing process.

Finally, friction coefficients derived from experiments can be processed by means of the method developed in the previous chapter. Although it was shown that the applicability of this method is low for the radial strip drawing simulator, it is questionable whether or not the local approach can give advantages in the description of frictional behaviour for deep drawing. Apart from local alterations which are originated by the contact pressure distribution, the alterations in sliding velocity can also be taken into account in the friction coefficient.

The question that now arises is how to determine the most efficient way of aquiring friction coefficients that lead to the best possible deep drawing simulation. For this, we must define which item serves as the criterion for the quality of the simulation. Considering this, various items can be proposed, such as resemblances of punch force - punch stroke curve, or strain distribution.

Considering the latter, for instance, it is known that a rough punch, i.e. a punch with a high friction coefficient is beneficial for the deep drawability of a certain product. The reason for this is the reduction of the tensile stress along the punch nose [6.1]. Because of this, the stress state alters, and the strain path in the forming limit diagram rotates such that it enters the second quadrant in which failure occurs at higher strains. Aiming at improving the prediction of the strain distribution will lead to improved prediction of the manufacturability at the bearing side of the process, i.e. improving the accuracy of the prediction of the critical deep drawing force.

If major attention is paid to improving the accuracy of the punch force - punch stroke relation, more items can be chosen within this, such as maximum punch force or length of stroke before finishing the product. The latter again mainly concentrates on estimating the strain distribution in the tearing zone, because the amount of tearing mainly causes differences, besides anisotropy. The maximum punch force is chosen here as the criterion, because it determines the asking side of the manufacturability question; the maximum force is mainly determined by the force necessary to draw in the flange.

6.2 Experiments

6.2.1 Common conditions

All experiments were carried out with 18 12 Cr Ni steel, as workpiece material. The material behaviour according to Nadai Ludwik was:

$C = 1384$ [N/mm^2]
$n = 0.54$ [-]
$\varepsilon_o = 0.057$ [-]

In addition, the normal anisotropy is given:

$R = 1$ [-]

All tool materials consist of N1019. Lubrication was as described previous, with lubricant Ipro 484 70% - Tellus R10 30 %

6.2.2 Deep drawing

Ten experiments were carried out on Erichsen deep drawing test equipment to register the punch force punch stroke relationship.

The geometry shown in Figure 64 was used for the experiments, [6.2]. The dimensions were:

Blank	Punch
$D_o = 148$ mm	$D_P = 75$ mm
$s_o = 0.5$ mm	$\rho_P = 3$ mm

Die	Blank holder
D_{Di}=76.5 mm	$D_{Hi} = 75.5$ mm
D_{Du}=175 mm	$D_{Hu} = 150$ mm
ρ_D =3 mm	

Deep drawing characteristics
Deep drawing ratio = $D_o/D_P = 1.97$
Product size = D_o/s_o

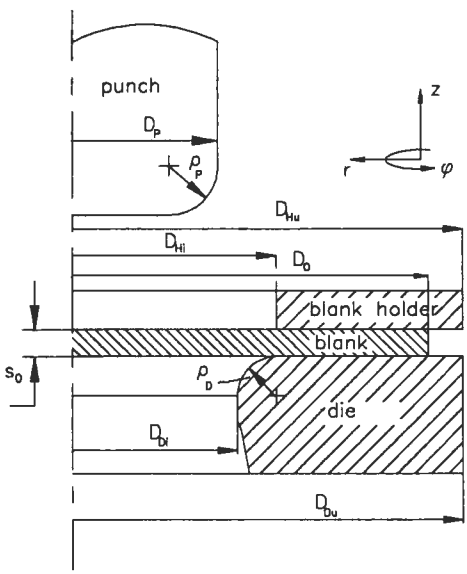

Fig. 64 : Geometry of deep drawing process

The maximum punch force obtained from these experiments was an average of 77.57 kN, with a standard deviation of 0.35 kN. The punch stroke at which the force achieves its maximum was an average of 30.1 mm, with a standard deviation of 0.62 mm. These values were measured in the presence of a blank holder force of 20 kN.

6.2.3 Determining global friction coefficients

The global friction coefficients for punch nose, die shoulder and flange friction region are determined by means of strip stretch, radial strip drawing and the flat die simulator respectively. As a result, the following data was achieved as an average of three measurements:

***Tabel II** : friction data*

Test method	Region	friction coefficient μ
flat die simulator	flange-die & flange-blank holder	0.131
strip stretch test	punch nose	0.152
radial strip drawing	die shoulder	0.177

6.2.4 Determining local friction coefficients

The local friction coefficients are derived similarly to that in the previous chapter. The range that needed to be covered with experiments was determined by means of an analysis with standard Abaqus. It appeared that the maximum values of speed and pressure are:

***Tabel III** : Contact conditions*

Region	Maximum sliding speed [mm/s]	Maximum contact pressure [N/mm^2]
die/blank/holder	8	100
die shoulder	9	275
punch nose	0.15	200

The following remarks have to be made:

- At first, the contact pressure for the die shoulder region in the simulations is sometimes higher than the flow stress in one node. When this is the case, it must be false.
- Secondly, the maximum speed at the punch nose is very sensitive to the process conditions, although it always remains small, magnitude differences of a factor two are likely.
- The minimum values of both speed and pressure are zero.
- All the above values are calculated with a blank holder load of 20 kN.

For the range mentioned above, several flat die simulator experiments were carried out, covering the speed range of 1 mm/s to 10 mm/s. Lower speeds could not be realised in the experimental set-up; higher speeds were not necessary because the Erichsen test machine has a maximum punch speed of 10 mm/s. The pressure range covered was 50 N/mm^2 to 250 N/mm^2. Lower contact pressures could not be realised in the test set-up with the same contacting tools. Higher contact pressure led to compression of the specimen. The experiments were evaluated by means of regression analysis, which finally resulted in:

$$\mu = 0.1886 - 0.000677 \times p - 0.134 \times \left(\frac{v}{p}\right) + 1.86E\text{-}6 \times p^2 \qquad (6.1)$$

This function expresses the local friction coefficient as a function of local contact pressure and sliding speed.

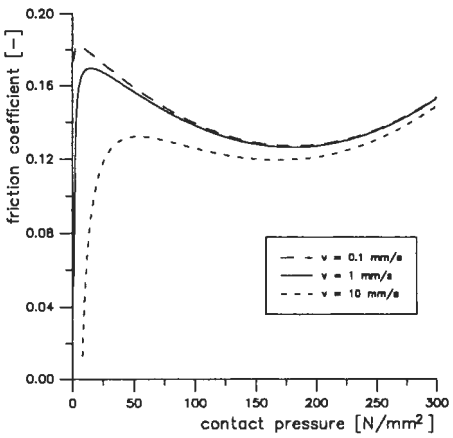

Fig. 65 : Friction coefficient as a function of contact pressure with sliding speed as a parameter

Tabel IV : Experimental data

Pressure [N/mm^2]	Speed [mm/s]	Friction coefficient [-]
49.9	3.32	0.157
50.5	1.86	0.156
51.3	5.55	0.146
52.0	3.58	0.140
52.0	9.07	0.138
54.3	14.98	0.117
98.4	5.40	0.133
103.9	1.07	0.144
107.6	8.13	0.125
108.1	10.75	0.118
110.3	5.35	0.126
148.2	2.93	0.122
149.5	12.42	0.128
149.5	6.37	0.123
151.1	6.25	0.127
151.3	2.87	0.124
151.4	8.99	0.118
153.5	3.32	0.118
155.3	7.74	0.125
193.6	2.93	0.116
197.1	7.11	0.120
200.8	4.82	0.126
202.2	11.23	0.129
211.8	8.72	0.131
229.4	0.29	0.140
241.1	10.26	0.126
247.4	5.73	0.132
248.0	6.88	0.124
250.5	3.13	0.134

In Figure 65, the above formula is plotted as a function of the contact pressure with the sliding speed as parameter. Note that the relation is determined in the pressure range of 50 to 250 N/mm^2. Actually, this formula may only be used on this range. However, for this research, extrapolation is used to 25 N/mm^2 downwards. At pressures lower than this, the

friction coefficient corresponding with a pressure of 25 N/mm^2 is used. It can also be seen that the difference between sliding speeds 0.1 mm/s and 1 mm/s is small on the range valid for use. At the higher contact pressures, the friction coefficient for contact pressures higher than $R_{P0.2}$, the tensile stress at 0.2% plastic strain, is taken as the contact pressure for contact pressure equal to $R_{P0.2}$.

Considering the velocity range, it should be noted that only one experiment was carried out in the range 0-1 mm/s. This is included in the data analysis and fits well. The extrapolated friction coefficient as a function of the contact pressure for a velocity of 0.1 mm/s is very similar to the function at a speed of 1 mm/s.

6.3 FEM simulations

6.3.1 Common conditions

The geometry of the modelled process was identical to the previously-mentioned experiments. The material behaviour was according to paragraph 6.2.1.

Analysis was carried out axisymmetrically. The element type used for this simulation is CAX4R, (Continuous AXisymmetric element with 4 nodes and Reduced integration). Four layers are necessary to describe the bending effects.

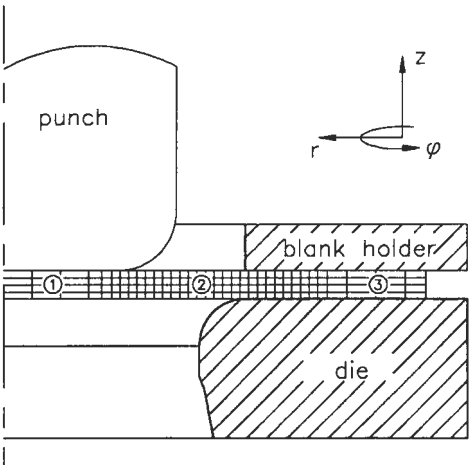

Fig. 66 : Meshing of blank

The elements do not have an equal length in the radial direction. In region 1, only a minor amount of biaxial stretching occurs, which is why few elements are used here. The material in region 2 will be in contact with the punch nose or die shoulder, or will be drawn inwards in the stage of the process prior to the maximum punch force. Finally, region three will be drawn over the die shoulder after the maximum punch force has been achieved. This stage of the process is of less interest, so again, few elements are used in this region.

Type IRS21A contact elements were used to describe the contact between the deforming workpiece and the rigid tool surface.

6.3.2 Calculation characteristics

The deep drawing process as modelled by means of Abaqus (see the previous paragraph) is now simulated with the following characteristics:

1 One global friction coefficient, determined with the flat die simulator.
$\mu = 0.131$

2 One global friction coefficient, determined with the strip stretch test.
$\mu = 0.152$

3 One global friction coefficient, determined with the radial strip drawing simulator.
$\mu = 0.177$

4 For each contact region, its own friction coefficient; for the flange-die and flange-holder, contact determined with the flat die simulator:
$\mu = 0.131$.
For the die shoulder region, the friction coefficient determined with the radial strip drawing test:
$\mu = 0.177$.
For the punch nose region, the friction coefficient determined with the strip stretch test:
$\mu = 0.152$

5 A local friction coefficient, determined by the flat die simulator for all contacting regions:

$$\mu = 0.1886 - 0.000677 \times p - 0.134 \times \left(\frac{v}{p}\right) + 1.86E\text{-}6 \times p^2 \qquad (6.1)$$

The first three simulations were all made with standard Abaqus. The fourth simulation used the smoothed shear stress - slip relation "tanh". This was done because standard Abaqus failed in this case; too many attempts were necessary to achieve a convergent solution. The fifth simulation was carried out as described in chapter 5. In addition, the user subroutine was programmed such that the velocity along the tool can be calculated. While recalculation of the speed in every increment proved to be very unstable, it was chosen to update the sliding speed every ten increments. The local speed will be up to date, the punch displacement in 10 increments is less than 0.5 mm.

6.4 Results

6.4.1 One versus three global friction coefficients

Figure 67 gives the resulting punch force - punch stroke graphs from the FEM simulations, together with the experimentally measured punch force - punch stroke relation.

Because of the scatter in the FEM graphs, the most interesting part of the graphs is given in more detail below. As can be seen, the friction coefficient obtained from the flat die simulator experiment (1) clearly predicts a punch force - punch stroke graph which is too low. The same can be said of the simulation carried out with the friction coefficient obtained from the strip stretch experiment (2).

Finally, considering FEM simulations carried out with one friction coefficient, the value obtained from the radial strip drawing simulator (3) appears to be too high.

The application of three different friction coefficients (4) appears to be very good, on a basis of comparing the force maxima.

Punch position was not measured accurately enough if we indirectly multiply punch speed by time. Although this method is quite reproducible, some error will be included when the speed is not exactly equal to the set point.

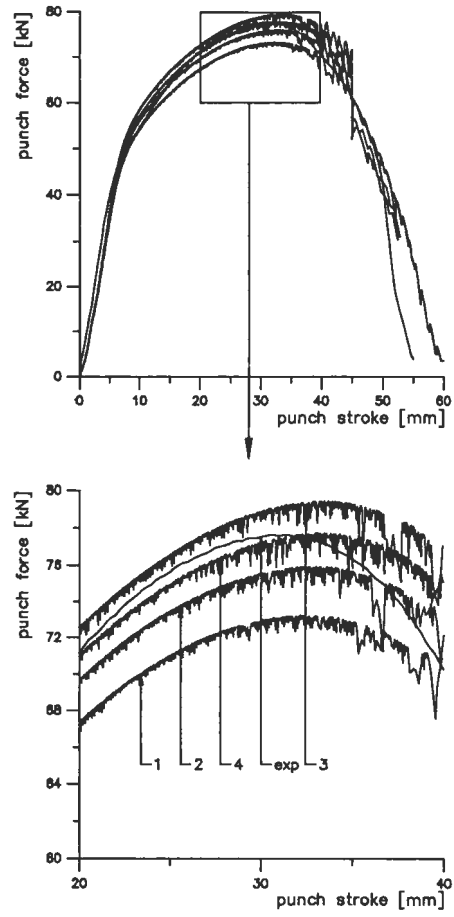

Fig. 67 : Comparison of various inputs for the friction coefficient with the experiment

6.4.2 Three global friction coefficients versus the local approach

Figure 68 again gives the experimental curve (exp), as well as the calculated curve for the case of three global friction coefficients (4). Finally, the curve calculated with local friction coefficients (5) is given.

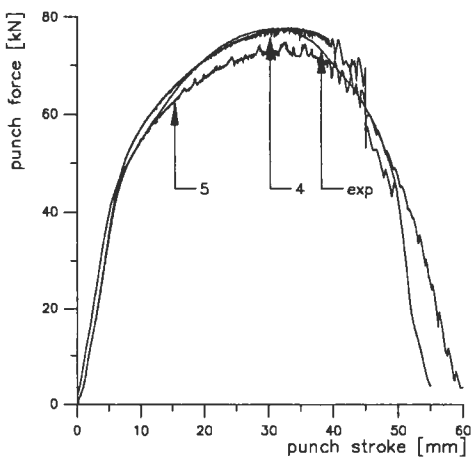

Fig. 68 : Comparison of local approach and three global friction coefficients as input for FEM simulations to the experiment

Similar to the observation made in paragraph 5.5, the calculated maximum punch force is too low, leading to the conclusion that the local friction coefficient generally calculates too low values for the friction coefficients in deep drawing.

6.5 Discussion

Using one value for the friction coefficient (as was done for simulations 1, 2 and 3) seems to be a rough method. By doing so, one actually states that only the chemistry in the contact zone is of importance, because the chemistry is the only similarity between the process and the experiments used to determine the friction coefficients. Other circumstances, such as contact pressure, sliding speed, surface enlargement and surface roughening will have some similarity to a certain region in the process, but will not apply for the entire process.

By using different friction coefficients for each contact region in the deep drawing process, an improvement is made with respect to the similarity of strain states in the experiments, the strip stretch test and the radial strip drawing test, which are applied to a certain region, namely punch nose and die shoulder. Also, in these cases, a similar contact pressure distribution is observed.

In the application of local friction coefficients, which are basically determined by means of flat die simulator experiments, two items having an important effect on frictional conditions (namely contact pressure and sliding speed) can be very well taken into account. Because no bulk plastic deformation occurs in flat die simulator experiments, effects of surface enlargement and surface roughening are not included.

Considering these observations and the results in paragraph 6.4, these lead to the conclusion that, in the case simulated here, effects of surface enlargement and roughening are more important than the inclusion of the effects of local pressure and sliding speed.

6.6 Conclusions

As appears from the experiments and simulations carried out here, the determination of three different friction coefficients (one for each region in the deep drawing process) is a sufficient method of achieving input considering the frictional conditions.

The application of local friction coefficients as a function of sliding speed and contact pressure fails, because these two quantities are not the most important ones. Effects of surface alterations seem to be more important. The test method used to determine a friction coefficient needs to have a high degree of similarity with the process.

6.7 Recommendations

An extension of the flat die experiments can be made to include the dependence of the friction coefficient with effective strains. This can at first be done by using pre-strained strips for flat die simulator experiments. A further extension can be made by tensile stretching of the test piece in the flat die simulator.

References

6.1 Bongaerts, P.C.B.
Faalaspecten bij omvormende bewerkingen.
Eindhoven University of Technology
report WPA-120015 (1994)

6.2 Barten, P.L.W.M.
Toepasbaarheid van variabele wrijving bij dieptrek-simulaties.
Eindhoven University of Technology
report WPA-120033 (1995)

Chapter 7 Evolution of the friction coefficient

7.1 Introduction

Besides the actual value of the friction coefficient, its evolution in time is also of importance in the deep drawing process. The friction coefficient will change as a result of the gradual alterations of the tool surface. Generally, the expected behaviour of the friction coefficient during tool life can be represented by Figure 69.

At first, a steep decrease in the friction coefficient can be observed. This decrease is caused by running-in phenomena, whereby, for example, the directional manufacturing patterns are flattened by wear, the highest asperity peaks (or even ridges) on the tool surface are sheared off.

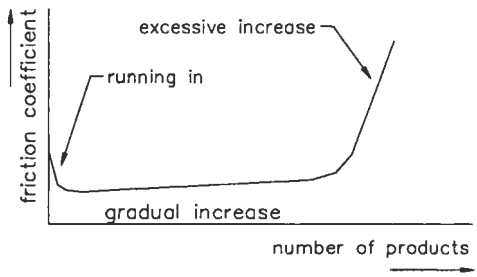

Fig. 69 : Expected behaviour of friction coefficient during tool life

After this, the friction coefficient remains more or less stable for a certain period, in which the wear of the tool increases, together with material transfer from the workpiece to the tool surface. During this period, transfer of material will either fill flaws on the tool or be in a stable condition. Particles that are transferred remain on the tool for a certain time, and are then sheared off again.

At a certain moment, however, the friction coefficient increases sharply; the more or less stable condition has ended. The tool surface modifications have overcome a certain critical condition, and the continuous building-up and shearing-off of workpiece material particles on the tool surfaces shifts such that more hills are built up than are sheared off.

Normally, the running-in period is short, approximately less than 1 metre of sliding length. The stable period is mainly determined by the combination of lubricant, workpiece material and tool material. The quality of the lubricant for the specific application determines the delay between running in, wear and excessive galling.

This chapter describes the development and initial testing of an experimental device, aimed at measuring friction coefficient evolution.

Similar work is reported by Huis in 't Veld [7.1], Schmoeckel et al. [7.2], and Shedin et al. [7.3].

7.2 Basic requirements

The aim of this research is to realise test equipment that can be used to evaluate long-term effects, by which we mean the gradual detoriation of the tool caused by the workpiece material passing by. By realising such test equipment, it becomes possible to rank lubricants on their effect on tool life, without having to use production tooling.

For ease of testing, it was chosen to base the test on coil material. These coils have typical dimensions of approximately 1 m outer diameter, and a core diameter of 0.5 m. The sheet thickness is typically in the range of 0.1 to 1 mm. The coil width is between 10 and 50 mm. The test equipment must allow the inclusion of various testing principles, such as the already described flat die simulator principle, the radial strip drawing simulator and, in addition, an ironing test. It is also required that the contacting tools are both easy to manufacture and easy to exchange.

The following characteristic forces can be identified on the basis of the types of test: The process force will be at maximum 8000 N. At the back of the process, a back-pull force of a maximum of 5000 N will be required. The required speed of the test will be between 10 and 100 mm/s.

7.3 Schematic design

A schematic design has been worked out on the basis of the requirements, see Figure 70, [7.4].

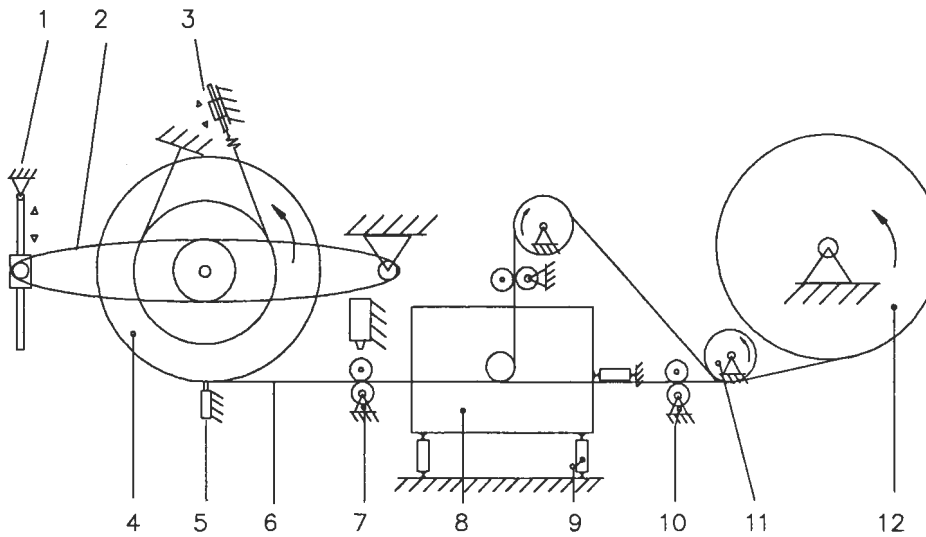

Fig. 70 : Schematic design of long-term test

Basically, the test equipment consists of a frame with two coil holders, 4 and 12. Coil holder 12 is driven. Coil holder 4 has a braking unit based on a belt principle (3) connected to it.

In order to properly supply the test unit with material, coil holder 4 can be adjusted vertically by means of a spindle (1), which moves the rocker (2) on which the coil holder (4) is placed. The measurement device (5) determines the current position of the strip (6), which can be lubricated by means of the lubricating device (7) before entering the test equipment, which is mounted on the test table (8). The test table (8) is connected by means of force transducers (9) to the frame.

Immediately after the test, the speed of the strip is measured by means of a tacho (10). To roll up the strip independently of the type of test, a bending roller (11) is present, which guides the strip properly to the driven coil holder (12). Figure 71 is a photograph in which the listed items are easy to recognise.

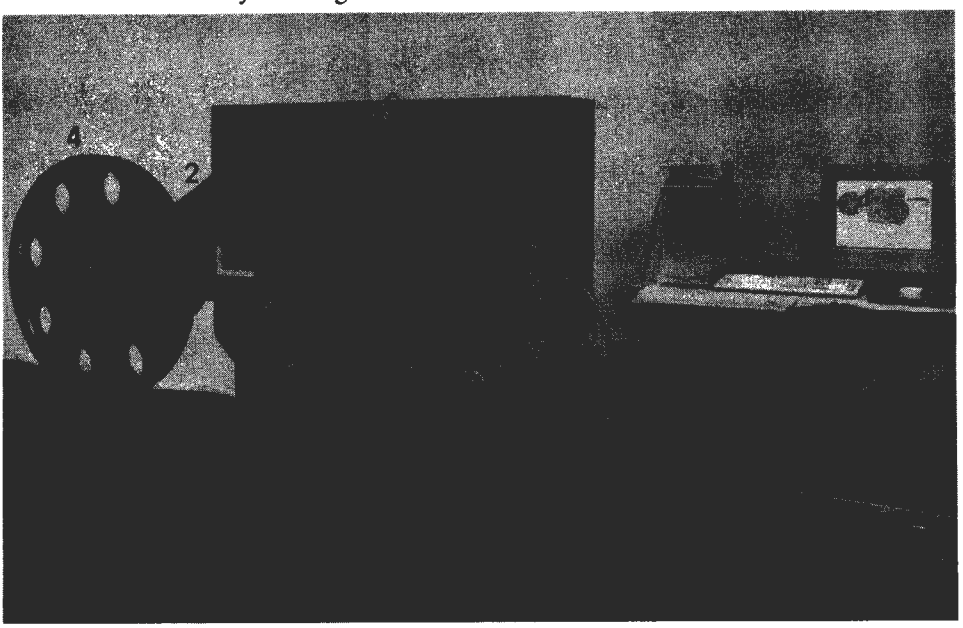

Fig. 71 : Overview of the test equipment

The entire experimental device is controlled by a special purpose computer program.

7.4 The radial strip drawing simulator

The radial strip drawing test was slightly modified for the development of the actual test units for this friction tester. The testing device includes a ground plate which is connected to the frame by means of strain gauge sensors. On this plate a simplified version of the radial strip drawing simulator is mounted, see Figure 72, where the strip, tool radius and ground plate are drawn with the reactions from the outside.
Equilibrium of horizontal forces:

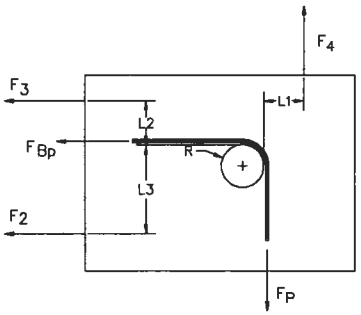

Fig. 72 : Equilibrium

$$F_{Bp} = -F_3 - F_2 \tag{7.1}$$

Equilibrium of vertical forces:

$$F_P = -F_4 \tag{7.2}$$

For the equilibrium of torque, only the tool and ground plate are used, for the frictional force it can be deduced:

$$F_{Fr} = \frac{-F_2\,(L_3 - R) + F_4\,(L_1 + R) + F_3\,(L_2 + R)}{R} \tag{7.3}$$

This again can be substituted in formula 4.8. Apart from a somewhat different data processing, little has been changed.

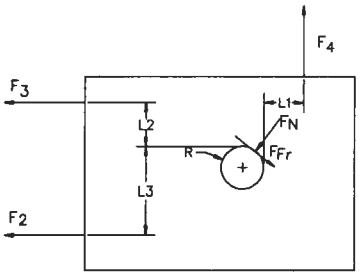

Fig. 73 : Equilibrium of torque

7.5 Experimental work

For this research on determining the manufacturability of products, it is interesting to know how various lubricants act in a certain process. Besides the actual value of the friction coefficient, measured by means of a radial strip drawing test as described in chapter 4, it is also questionable how long this friction coefficient will remain the same. By determining this at a given combination of workpiece material and tool material, combined with certain process conditions for a few lubricants, the most robust production can be identified. Such a robust production is profitable, not only because of producing few bad products, but also because of low tooling maintenance costs.

A stainless steel was chosen for the initial trials on this testing device. The lubricants used consisted of:

A Chlorine parafinic oil
B Mineral oil with solvents
C Mineral oil with boundary lubrication additives

The workpiece material consisted of X35CrMo13. The material behaviour is characterised by a characteristic deformation resistance (C) of 1145 N/mm^2, a strain hardening exponent n of 0.19, a pre-strain (ε_0) of 0.001, a Young's modulus (E) of 210000 N/mm^2, and the Poisson constant (ν) of 0.3. The thickness of the strip equalled 0.5 mm.

The test conditions were:

- Tooling radius: R = 4 mm
- Back-pull stress: σ_0= 30 N/mm^2
- Sliding velocity: v_0= 100 mm/s

Figure 74 gives the resulting friction coefficients as a function of the sliding length. Because of a failure of one strain gauge force transducer, the pulley equation (4.15) had to be used, which will introduce some error. As can be seen, lubricant A performs well; its friction coefficient shows little noise, an increase only now and then, followed by a similar decrease. With lubricant C, the friction coefficient increases slightly during the experiment. Also, it can be seen that more noise is present. Observing the strip during the test, it appeared that some scratches could be observed on the strip for lubricant C soon after the start of the experiment. These scratches started to develop within 10 metres sliding length, but then remained quite stable for a long period. Lubricant B, however, performs very poorly.

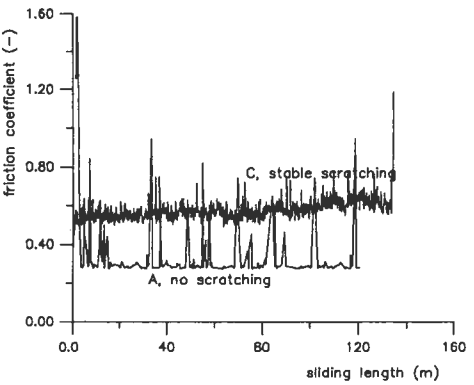

Fig. 74 : Three oils tested on their effect on the galling behaviour

Because the graph will not be identified in Figure 74, the graph for lubricant B is given in Figure 75. High values of the friction coefficient were observed. Observing the experiment, it appeared that almost immediately severe scratching could be observed on the strip (within 1 metre of sliding). This scratching becomes so excessive that it finally leads to failure of the strip. The strips sticks to the tool and remains fixed. Following this, the strip between the tool and the driven coil holder is elongated until failure.

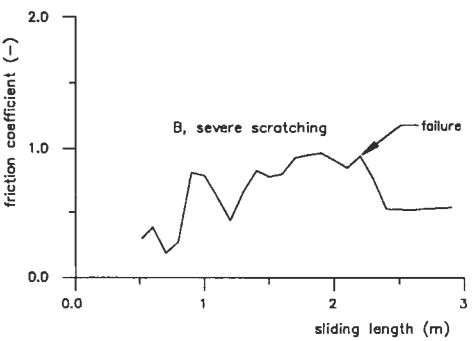

Fig. 75 : Effect of lubricant B on the friction coefficient

Figure 76 gives photographs that represent the damaged surface of the strip at the end of the tests. It can clearly be seen that with lubricant B the strip is severely damaged. For lubricant C, damage can also be clearly observed, but definitely less than with lubricant B. With lubricant A, damage of the strip material is nearly absent. The sliding direction of the strip is given by the arrow.

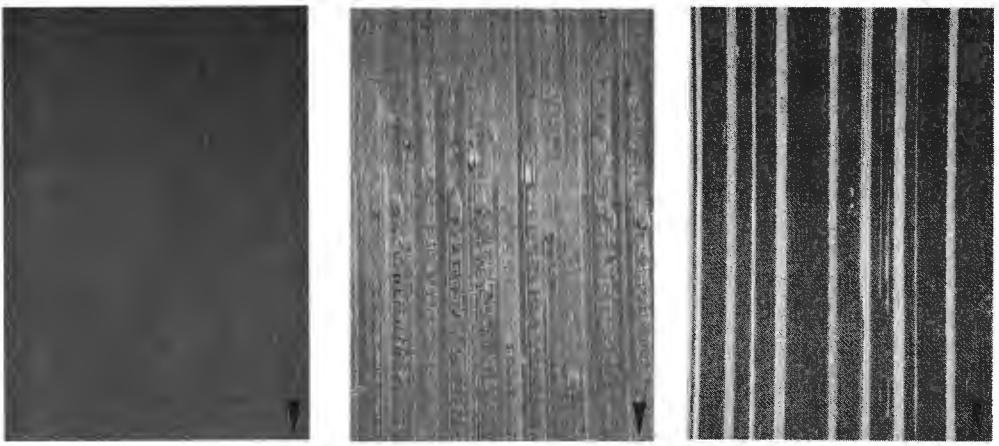

Fig. 76 : Damaged surfaces of strip. Lubricant A, B, C from left to right

Figure 77 gives the photographs of the contacting spots of the tools. Here also, it can be seen that lubricant A shows less damage than lubricant C, which in turn shows less damage than lubricant B. Again the sliding direction of the strip is given by the arrow.

Fig. 77 : Damaged surfaces of tool. Lubricant A, B, C from left to right

7.6 Discussion

The research presented here consists of first results. As noted in the text, the test device is not fully operational. Despite these remarks, the first results correspond with industrial practice. Lubricant A is typically used in cases such as heavy deep drawing or collar drawing operations for this type of materials. Because of environmental issues, this type of lubricant will need to be replaced. A typical lubricant which can sometimes serve as a

substitute for lubricant A is lubricant C. The experiments shown here prove that in the situation as present in this test (process conditions, material pairing), lubricant C will not be an effective substitute. Finally, lubricant B is known for its poor quality in deep drawing operations of high alloyed steels. The sole fact that it behaves so poorly under test conditions used already proves that the proposed type of testing is discriminating enough.

7.7 Conclusion

Although the test for the time being still in its engineering phase, it has proved its worth as a test method for determining so-called long-term effects in deep drawing.

References

[7.1] Huis in't Veld, A. J., Mens, J.W.M., Heide, E. v.d.
Coatings op omvormgereedschappen
TNO report 94P/09049/MEN (1994)

[7.2] Schmoeckel, D., Hohl, F., Stock, H-R., Mayr, D.
Tribological properties and wear behaviour of sputtered Titanium based hard coatings under seet metal forming conditions.
Materials science and engineering
A140, (1991), p. 593-601

[7.3] Shedin, E., Lehtinen, B.
Galling mechanisms in lubricated systems: a study of sheet metal forming.
Wear, 170 (1993) p. 119-130

[7.4] Tol, M.H.J. van,
Vooronderzoek. Het ontwerpen van een testopstelling voor het meten van aanladen.
Eindhoven University of Technology
report WPA 120040 (1995)

Chapter 8 Review

8.1 Conclusions

The primary goal of this work was to determine valid methods for the measurement of frictional phenomena, and thus to improve the predictability of deep drawing operations. The starting-point in this work was formed by the increasing use of numerical modelling in the pre-production stage of deep drawing operations. As already seen at the VDI conference "FE simulation of 3D sheet metal forming processes in the automotive industry" [8.1], the accurate descriptions of both material behaviour and contact conditions are increasingly becoming the most limiting factors in the simulation of deep drawing processes.

Friction is a complicated phenomenon. Even in a restricted area such as deep drawing, many variations are found. The friction coefficient is completely dependent on the specific parameters chosen. Even when apparently similar conditions have been reached in their experiments, different researchers will come to different conclusions. This inevitably leads to the conclusion that the transferability of friction coefficients is restricted when not determined under conditions close enough to the simulated process.

For deep drawing, various test methods have been proposed in literature. In this work, three of these have been chosen for further work. For these three tests, measurement set-ups, together with known or new data processing methods have been evaluated. As a result, test equipment is available that will provide friction coefficients which are in any case valid for the experiment itself.

From this point onwards, it becomes necessary to determine the transferability of these friction coefficient values, or, putting it in another way, how can these values be used in the simulation of deep drawing processes? Although the experiments are chosen such that they have a large similarity with at least one region in the deep drawing process, differences do still exist. To make use of local friction coefficients obtained from experiments carried out under varying conditions, a user subroutine was implemented in an FEM package, which, in the first instance, enables analysis with the friction coefficient of a function of pressure and speed.

Comparison of flat die simulator experiments on one hand, and of radial strip drawing and deep drawing on the other showed that the calculated friction coefficients are too small and deviate too much in comparison with the experiment.

For deep drawing, it was found in this research that the best practice for obtaining friction coefficients for deep drawing simulations was the determination of three different values, with three different tests, each applicable for a certain region in the deep drawing process.

For studying the evolution of the friction coefficient because of wear and galling during deep drawing, a test-apparatus has been designed and built. The first experiments on this device show to accord well with industrial practice.

8.2 Discussion

The conclusion that it will be sufficient for deep drawing to measure three different friction coefficients is in itself a practical one; relatively small effort is required. However, the fact that a fitted function of values obtained from a flat die simulator shows poorer results is unfortunate. This implies that the parameters included were insufficient to guarantee the desired similarity of the process to be simulated. In the work presented in Chapters 5 and 6, the main attention was paid to including the pressure and speed dependency of the friction coefficient.

Returning to the observations made in chapter 3, all friction tests can in principle be divided into 2 classes, namely one-sided curved contact or double-sided flat contact. Each class can subsequently be divided into three sub-classes, depending on the degree of deformation present in the substrate, no plastic deformation, local plastic deformation or bulk deformation. The radial strip drawing test and the strip stretching test both have one-sided curved contact. The radial strip drawing test contains local deformation, while the strip stretch test is carried out with bulk deformation. The flat die simulator presented here is a test with double-sided contact with no substrate deformation.

Regarding the fact that the radial strip drawing test and the strip stretch test appear to perform well, the conclusion that the absence of substrate deformation in the flat die simulator is one of the limiting factors in its application is readily made.

The question that now arises is how can the flat die simulator be modified such that influences of deformation on the friction coefficient can be measured? The problem that arises is that we do not know which of the deformation-related topics influences the friction coefficient the most. For example, does roughening cause an increase or decrease of the friction coefficient, or are asperities flattened more easily because of the higher stress level in the substrate? Depending on the answer to this question, different testing conditions are necessary to improve the prediction made by flat die simulator experiments.

Roughening caused by deformation as the sole contributor to the observed difference can be easily checked. An experiment can be carried out in which several tensile specimens are tested. Next, these test pieces can be elongated by a certain amount on a tensile tester, e.g. 1 to 20 % elongation. Measurement of the roughness will give the relationship between roughness and plastic strain. Subsequently, these test pieces can be used in flat die simulator experiments. From the results of this test, the relationship between plastic strain and friction coefficient can be found, within the margins of this test set-up. When the friction coefficient significantly increases with strain (roughness), we can globally check if the comparison between, for instance, the radial strip drawing simulator and the radial strip drawing test will now perform better. However, when roughening itself is not the main source of deviation, but the fact that bulk plastic deformation is present, additional experiments to explain the deviation will become more difficult. Now, it will be necessary to extend the flat die simulator such that bulk plastic deformation can be implied to the substrate in combination with the sliding of the strip between the two plates.

In practice, this will mean that the strip will be mounted on a tensile tester, combined with the simultaneous sliding of the flat die simulator, see Figure 78.

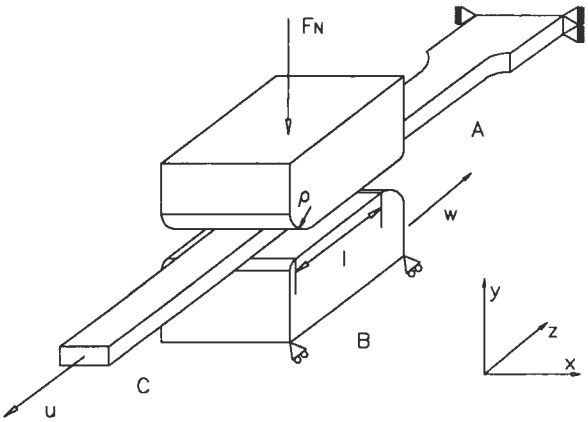

Fig. 78 : Schematic design of a flat die simulator with simultaneous stretching of te substrate material

The strip is clamped at one side in the fixed head of a tensile tester. At the other side of the strip, a displacement (u) is imposed. As a result, a tensile stress will be present in part C of the strip. The flat die simulator exhibits its pressure to the strip over a length l. The tensile stress in part A of the strip will be reduced as a result of this pressure, the length over which it is applied and, depending on the friction coefficient. The flat die simulator slides a distance w over the strip.

We can therefore distinguish three different regions in the strip: one region (A), in which a common tensile "test" is carried out; one region (B) between the two plates of the flat die simulator, in which the material is also subjected to a compressive stress; and one region (C), in which the stress is tensile, but the material thickness is not constant.

FEM simulations show that it is possible to build a test as described above. The main difficulties that become apparent from the FEM simulation are the achievement of a stable rotation of the upper tool along the Z-axis, required to achieve a uniform pressure distribution on one hand. On the other hand, the compressive stress must be chosen low enough to avoid compression as the only deformation mode. Also, to avoid plastic strain in part A, the reduction in tensile stress in part B of the strip, caused by the frictional shear stress, may not be too high.

Important items in the determination of the test conditions are the sliding length l related to the thickness of the strip, the contact pressure in part B of the strip related to the flow stress of the strip, the friction coefficient itself, and the strain hardening behaviour of the strip material.

8.3 Recommendations

In accordance with the last part of the discussion, it will be useful to extend the flat die simulator such that it will allow bulk deformation. By doing so, the compatibility between deep drawing and the experiment is improved.

Except for the use of the flat die simulator, whose main advantage is the possibility of good control of the contact pressure, it is also possible to design a type of radial strip drawing test in which the contact pressure can be controlled. The present radial strip drawing simulator cannot be used to determine the pressure dependency of the friction coefficient, which is merely caused by the pressure peaks at the bending and unbending zones. These pressure peaks are largely based on the "abrupt" transition from a strip with curvature zero to a curvature equal to the tool radius. If we now have a tool contour with a more continuous transition from curvature zero to a specific curvature, the peaks at the entrance and exit zones of the contact are spread out over the entire contact zone, i.e. bending and unbending becomes a continuous process.

Figure 79 gives an example of a new shape of a friction element, suitable for use in the radial strip drawing test, see Figure 22. This friction element replaces the radius (2) in the set-up. Point M is now the point of rotation around the knife edge. This shape is generated by assuming that the curvature increases and decreases linearly with the angle (ϕ), from value 0 towards an assumed value (1/R). With this assumption, it is possible to generate such a tool with dimensions small enough to be able to fit into the existing test equipment.

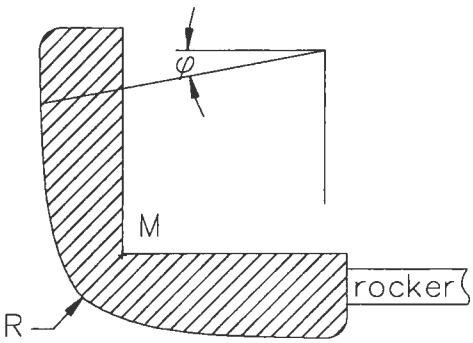

Fig. 79 : Friction element for the radial strip drawing test with continuous curvature

The question that arises is whether such a shape will lead to a uniform pressure distribution. A simulation by means of FEM of this shape can give an insight into the expected behaviour of such an element.

Another important item in the use of the flat die simulator is the achievement of carefully aligned contact surfaces. At the moment, two options are in use in the flat die simulator at the EUT. The first is the sole use of a ball bearing, see Figure 39, item 6. The second is the addition of two sliders, which align the upper and lower platens, items 2 and 3.

The first option is only sufficient with a large contact area. The second method must be applied with a small contact area, but influences the measurement. With the application of an elastic foundation as given in Figure 80, the rotational stiffness of the ball bearing caused by friction, which is the limiting factor in the application of the ball bearing can be avoided [8.2]. When the virtual point of rotation is in the contact surface, this type of foundation is capable of adjusting to small alignment errors.

The draw-bead simulator is a commonly used friction test for deep drawing, especially in the American automotive industry. The current data processing of this test is of the pulley equation type. By modifying the draw-bead simulator in such a way that the torque of the rolls can also be measured, the validity of this test can be improved to a large extent, especially at low friction.

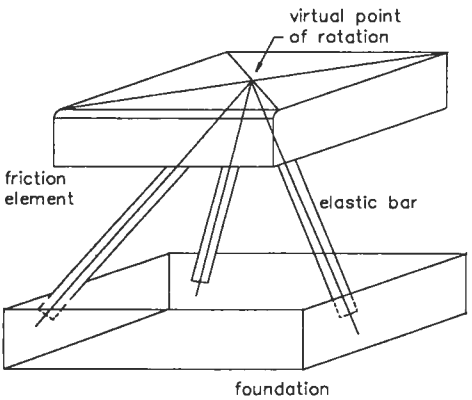

Fig. 80 : An elastic foundation of the friction element

8.4 Friction coefficients

During this PhD work, many experiments have been carried out. Although the author has stated several times that the transferability of friction coefficients, measured in a certain situation, to another situation is low, some data is presented here as a first impression. Only radial strip drawing experiments are included, with lubrication.

Table V : Friction coefficient ranges

Material	Range of Friction coefficients
Steel 15	0.05 - 0.20
Steel 15, hot dip Zinc	0.05 - 0.30
Steel 15, EG Zinc	0.05 - 0.30
Steel 15, polyuretane coating	0.01 - 0.16
Stainless Steel	0.10 - 0.50
Stainless Steel, polyurethane coating	0.01 - 0.15
Aluminium	0.15 - 0.35
Aluminium, prepainted	0.10 - 0.25
Aluminium C4S	0.15 - 0.30
Aluminium C4S prepainted	0.10 - 0.25

It can genuinely be stated that non-metallic coatings have a decreasing effect on the friction coefficient. With metallic coatings, the range to be measured is normally enlarged. Please note that the figures represented are rough guidelines, and do represent conditions such as lubrication, tool coating or tool finishing etc., as used in industrial practice.

References

[8.1] VDI Berichte 894
FE simulation of 3D sheet metal forming processes in automotive industry.
VDI Verlag 1991

[8.2] Tol, M.H.J. van,
Vooronderzoek: Het ontwerpen van een testopstelling voor het meten van aanladen.
Eindhoven University of Technology
report WPA-120040 (1995)

Appendix A Effects of slip reversal

A.1 Introduction

In Paragraph 5.2.2, it is stated that the hyperbolic tangent is only allowed in cases where there is no reversal of slip direction. In the case of slip reversal, all the previous slip is regarded as elastic slip, see Figure A1.

It can clearly be seen that, if there is sliding from position 0 to position 1, the increase in the slip leads to an increase in shear stress. The same applies when the slip increases from position 1 to 2 and from position 2 to 3. When a slip direction reversal occurs, from position 3 to position 4, the shear stress must become negative very quickly. In the figure, however, it is apparent that the entire "previous" positive slip must firstly be overcome before the shear stress becomes negative.

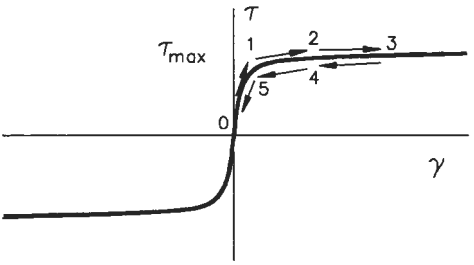

Fig. A1 : Effect of reversal of slip in case of formula 5.1 is applied

In this appendix, it is proved that this neglection of reversal of slip does not affect our deep drawing simulations.

A.2 Approach to the problem

In this paragraph, the same deep drawing simulation as given in detail in Paragraphs 6.2.2 and 6.3.1 is analysed. All the friction coefficients are set to 0.1. Following this, several user sub-routines were written [A.1].
Figure A2 gives three types of dependence of shear stress to slip. All of these consider all slip as elastic. Type A in the figure is the same dependence as given in Chapter 5, Formula 5.1. Type B consists of a sinoid around slip is zero, and a straight line elsewhere.

$$\begin{aligned} \tau &= -\tau_{max} & \gamma &< -\gamma_{crit} \\ \tau &= \tau_{max}\sin\left(\frac{\gamma\pi}{2\gamma_{crit}}\right) & -\gamma_{crit} &\le \gamma \le \gamma_{crit} \\ \tau &= \tau_{max} & \gamma &> \gamma_{crit} \end{aligned} \qquad \text{(A1)}$$

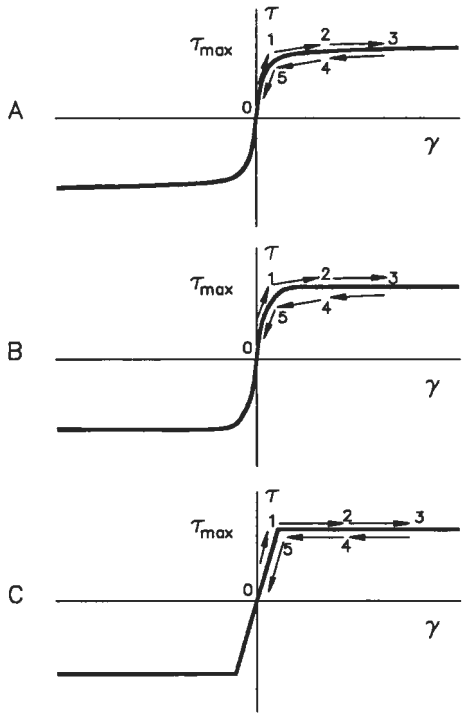

Fig A2 : Shear stress slip dependence with only elastic slip

Type C consists of the same approach as used in ABAQUS standard, except that the slip is also seen as totally elastic.

$$\tau = -\tau_{max} \qquad \gamma<\gamma_{crit}$$
$$\tau = \frac{\gamma}{\gamma_{crit}}\tau_{max} \qquad -\gamma_{crit}\leq\gamma\leq\gamma_{crit} \tag{A.2}$$
$$\tau = \tau_{max} \qquad \gamma>\gamma_{crit}$$

Figure A3 shows two methods when the slip is non-recoverable in the case of slip reversal. This was carried out for the sinoid type D and the standard ABAQUS method type E.

These methods have all been implemented in ABAQUS 5.4, and used in co-operation with the same deep drawing input as used in Chapters 5 and 6.

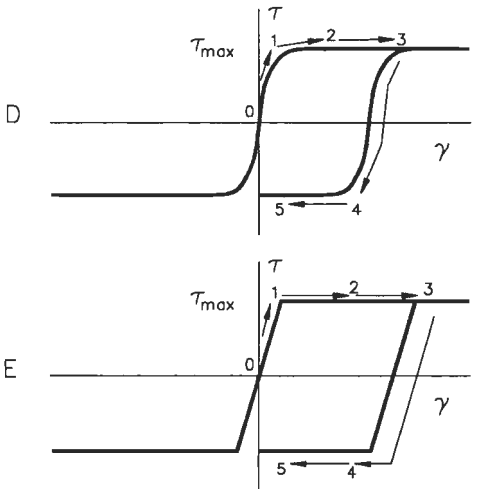

Figure A3 : Dependence between shear stress and slip in case of non-recoverable slip

Figure A4 gives the punch force punch stroke relations upto the moment of force maximum. As can be seen in the graph, the differences are small, especially at the beginning of the process. At a later stage in the process, the differences will be larger, but still relatively small.

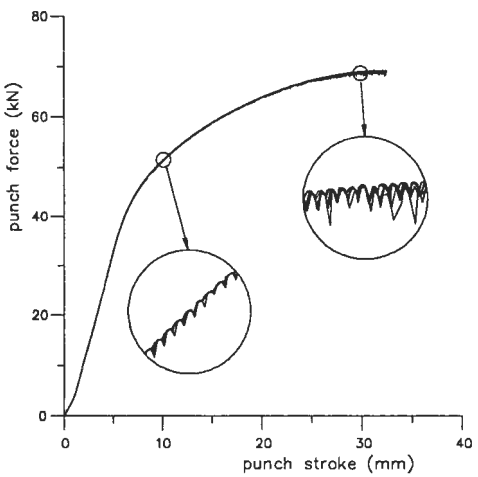

Fig A4 : Punch force - punch stroke graphs for different shear stress to slip dependencies

Figure A5 gives the calculated pressure distributions. The minima and maxima of the contact pressure are given next to the graphs in N/mm^2

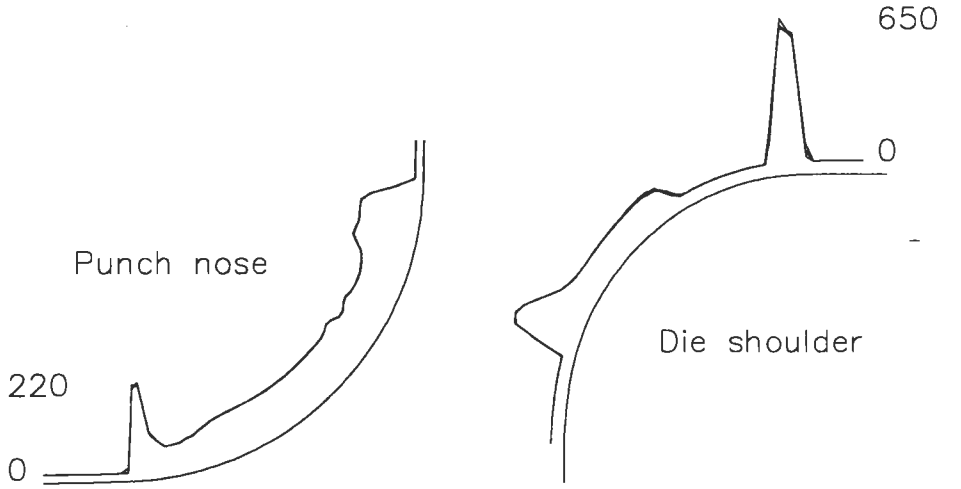

Fig A5 : Resulting pressure distribution

Although the pressure distributions differ to a small extent, the difference is negligible as far as this research is considered.

A.3 Conclusions

Although the simulations are different in their constitutive equations for friction, the results obtained from these simulations show that the effect of slip reversal problems in the analysis of the described deep drawing process is negligible. Intuitively, this can be understood. Once a particle in the flange moves inwards, it will always remain moving inwards. Also, a particle in contact with the punch will also remain moving outwards once it has started to move outwards, until the punch force maximum.

However, to avoid problems with slip reversal, it will be useful to implement the sinusoid type behaviour of shear stress dependence to slip, including the slip reversal option. By doing so, the advantage of a continuous derivative can still be maintained.

Nawoord

Het werk dat thans voor U ligt is niet het werk van een enkeling. Veel mensen hebben hieraan een bijdrage geleverd, ook al is die in de meeste gevallen niet terug te herkennen in de tekst. Bij deze wil ik iedereen die aan de totstandkoming van dit proefschrift heeft bijgedragen van harte bedanken. Alle studenten in de periode september 1990 tot 1996 die mijn nukken moesten verduren, de collega's van de sectie waarvan ik altijd veel moest lenen, de mensen van de CTD, die altijd met spoed veel werk moesten doen, de promotie-commissie welke het proefschrift van onleesbaarheden moest ontdoen, de collega's bij Philips, welke zich vooral de laatste tijd vaak afvroegen waar ik was tijdens de (reguliere) werktijd, en tenslotte mijn ouders en vriendin welke dezelfde vraag weleens gesteld hebben over de vrije tijd.

Terugblikkend moet mij van het hart dat het een prachtige tijd is geweest.

Curriculum Vitae

Roland Sniekers was born on November 30, 1966, in Maasbracht, the Netherlands. He attended the Scholengemeenschap St. Ursula in Horn, where he obtained his Atheneum-B diploma in 1985. In September of the same year, he entered Eindhoven University of Technology, where he began his study of Mechanical Engineering. This was finished in August 1990. Immediately afterwards, he was engaged by the Faculty of Mechanical Engineering to start a PhD study. Since November 1993, he has worked part time at the Eindhoven University of Technology and at the Philips Centre for Manufacturing Technology.

Stellingen
Behorende bij het proefschrift van Roland Sniekers
Friction in deep drawing

1 Bij het ontwerp van meetmethoden en de verwerking van de gegevens vormen numerieke methoden waardevolle gereedschappen.
- Dit proefschrift, hoofdstuk 4
- Frans Starmans, On friction in forming, 1990

2 Door de geheimzinnigheid waarmee smeermiddelleveranciers hun produkt omhullen, blijft de voorspelling van het wrijvingsgedrag bij toepassing van een smeermiddel zwarte kunst.

3 Het onderling vergelijken van experimenten uit de literatuur komt overeen met het vergelijken van appels en peren.

4 Bij het plannen van experimenteel werk op het gebied van wrijving dient een flinke bovenmarge op de benodigde tijd genomen te worden.

5 Het verschil tussen de japanse en nederlandse onderzoekscultuur wordt treffend geïllustreerd door de volgende anekdote:
Ooh, said the japanese researcher, in Japan everything is perfectly arranged if you are doing research, we have even got a separate ministry for friction. Well I said, in Holland we have got friction in every ministry.

6 Vegetariërs denken dat ze ouder worden. Dat is niet zo, ze zien er alleen ouder uit.
- R. Tazelaar, Produktschap Vee en Vlees

7 Op de TUE veranderingen doorvoeren is onmogelijk. De verhouding tussen het aantal inspraakorganen en tijd om inspraak te behandelen is te groot.

8 Het beste anti-conceptie middel is naar je collega's luisteren tijdens de koffiepauze.

9 De strategische positie van een vakgebied tussen de andere vakgebieden wordt voornamelijk bepaald door de achtergrond van de spreker die het onderwerp aanroert.

N.a.v. stelling 8, R.O.E. Vijgen, Quality control of protective PVD coatings, EUT thesis 1995

10 Het naderende afscheid van de dienstplicht heeft de laatste jaren een verhoogde belangstelling voor promoties veroorzaakt, met name onder mannen.

11 De veronderstelling dat arbeidsduurverkorting kosten neutraal kan is niet reëel.

12 Naar schatting is ongeveer één miljoen mensen lid van een vakbond. Aan dit soort minderheidsgroeperingen zou minder aandacht besteed moeten worden.

13 Als iedereen regelmatig uit zijn bol zou gaan, zou de psychiatrie in Nederland aanmerkelijk minder te doen hebben.